Mapping, Path Following, and Perception with Long Range Passive UHF RFID for Mobile Robots

Mapping, Path Following, and Perception with Long Range Passive UHF RFID for Mobile Robots

Dissertation

der Mathematisch-Naturwissenschaftlichen Fakultät

der Eberhard-Karls-Universität Tübingen

zur Erlangung des Grades eines

Doktors der Naturwissenschaften

(Dr. rer. nat.)

vorgelegt von

M. Sc. Ran Liu

aus Anhui, China

Tübingen

2014

Tag der mündlichen Qualifikation:	26.11.2014
Dekan:	Prof. Dr. Wolfgang Rosenstiel
1. Berichterstatter:	Prof. Dr. Andreas Zell
2. Berichterstatter:	Prof. Dr. Andreas Schilling

For my family

Abstract

Service robots have shown an impressive potential in providing assistance and guidance in various environments, such as supermarkets, shopping malls, homes, airports, and libraries. Due to the low-cost and contactless way of communication, radio-frequency identification (RFID) technology provides a solution to overcome the difficulties (e.g. occlusions) that the traditional line of sight sensors (e.g. cameras and laser range finders) face. In this thesis, we address the applications of using passive ultra high frequency (UHF) RFID as a sensing technology for mobile robots in three fundamental tasks, namely mapping, path following, and tracking.

An important task in the field of RFID is mapping, which aims at inferring the positions of RFID tags based on the measurements (i.e. the detections as well as the received signal strength) received by the RFID reader. The robot, which serves as an intelligent mobile carrier, is able to localize itself in a known environment based on the existing positioning techniques, such as laser-based Monte Carlo localization. The mapping process requires a probabilistic sensor model, which characterizes the likelihood of receiving a measurement, given the relative pose of the antenna and the tag.

In this thesis, we address the problem of recovering from mapping failures of static RFID tags and localizing non-static RFID tags which do not move frequently using a particle filter. The usefulness of negative information (e.g. non-detections) is also examined in the context of mapping RFID tags. Moreover, we present a novel three dimensional (3D) sensor model to improve the mapping accuracy of RFID tags. In particular, using this new sensor model, we are able to localize the 3D position of an RFID tag by mounting two antennas at different heights on the robot. We additionally utilize negative information to improve the mapping accuracy, especially for the height estimation in our stereo antenna configuration.

The model-based localization approach, which works as a dual to the mapping process, estimates the pose of the robot based on the sensor model as well as the given positions of RFID tags. The fingerprinting-based approach was shown to be superior to the model-based approach, since it is able to better capture the unpredictable radio frequency characteristics in the existing infrastructure. Here, we present a novel approach that combines RFID fingerprints and odometry information as an input of the motion control of a mobile robot for the purpose of path following in unknown environments. More precisely, we apply the teaching and playback scheme to perform this task. During the teaching stage, the robot is manually steered to move along a desired path. RFID measurements and the associated motion information are recorded in an online-fashion as reference data. In the second stage (i.e. playback stage), the robot follows this path

autonomously by adjusting its pose according to the difference between the current RFID measurements and the previously recorded reference measurements. Particularly, our approach needs no prior information about the distribution and positions of the tags, nor does it require a map of the environment. The proposed approach features a cost-effective alternative for mobile robot navigation if the robot is equipped with an RFID reader for inventory in RFID-tagged environments.

The capability of a mobile robot to track dynamic objects is vital for efficiently interacting with its environment. Although a large number of researchers focus on the mapping of RFID tags, most of them only assume a static configuration of RFID tags and too little attention has been paid to dynamic ones. Therefore, we address the problem of tracking dynamic objects for mobile robots using RFID tags. In contrast to mapping of RFID tags, which aims at achieving a minimum mapping error, tracking does not only need a robust tracking performance, but also requires a fast reaction to the movement of the objects. To achieve this, we combine a two stage dynamic motion model with the dual particle filter, to capture the dynamic motion of the object and to quickly recover from failures in tracking. The state estimation from the particle filter is used in a combination with the VFH+ (Vector Field Histogram), which serves as a local path planner for obstacle avoidance, to guide the robot towards the target. This is then integrated into a framework, which allows the robot to search for both static and dynamic tags, follow it, and maintain the distance between them.

Kurzfassung

Service-Roboter bergen ein großes Potential bei der Unterstützung, Beratung und Führung von Kunden oder Personal in verschiedenen Umgebungen wie zum Beispiel Supermärkten, Einkaufszentren, Wohnungen, Flughäfen und Bibliotheken. Durch die geringen Kosten und die kontaktlose Kommunikation ist die RFID Technologie in der Lage vorhandene Herausforderungen traditioneller sichtlinienbasierter Sensoren (z.B. Verdeckung beim Einsatz von Kameras oder Laser-Entfernungsmessern) zu lösen. In dieser Arbeit beschäftigen wir uns mit dem Einsatz von passivem Ultrahochfrequenz (UHF) RFID als Sensortechnologie für mobile Roboter hinsichtlich drei grundlegender Aufgabenstellungen Kartierung, Pfadverfolgung und Tracking.

Kartierung nimmt eine wesentliche Rolle im Bereich der Robotik als auch beim Einsatz von RFID Sensoren ein. Hierbei ist das Ziel die Positionen von RFID-Tags anhand von Messungen (die Erfassung der Tags als solche und die Signalstärke) zu schätzen. Der Roboter, der als intelligenter mobiler Träger dient, ist in der Lage, sich selbst in einer bekannten Umgebung auf Grundlage der bestehenden Positionierungsverfahren, wie Laser-basierter Monte-Carlo Lokalisierung zurechtzufinden. Der Kartierungsprozess erfordert ein probabilistisches Sensormodell, das die Wahrscheinlichkeit beschreibt, ein Tag an einer gegebenen Position relativ zur RFID-Antenne (ggf. mit einer bestimmten Signalstärke) zu erkennen.

Zentrale Aspekte dieser Arbeit sind die Regeneration bei fehlerhafter Kartierung statischer RFID-Tags und die Lokalisierung von nicht-statischen RFID-Tags. Auch wird die Verwendbarkeit negativer Informationen, wie z.B. das Nichterkennen von Transpondern, im Rahmen der RFID Kartierung untersucht. Darüber hinaus schlagen wir ein neues 3D-Sensormodell vor, welches die Genauigkeit der Kartierung von RFID-Tags verbessert. Durch die Montage von zwei Antennen auf verschiedenen Höhen des eingesetzten Roboters, erlaubt es dieses Modell im Besonderen, die 3D Positionen von Tags zu bestimmen. Dabei nutzen wir zusätzlich negative Informationen um die Genauigkeit der Kartierung zu erhöhen.

Dank der Eindeutigkeit von RFID-Tags, ist es möglich die Lokalisierung eines mobilen Roboters ohne Mehrdeutigkeit zu bestimmen. Der modellbasierte Ansatz zur Lokalisierung schätzt die Pose des Roboters auf Basis des Sensormodells und den angegebenen Positionen der RFID-Tags. Es wurde gezeigt, dass der Fingerprinting-Ansatz dem modellbasierten Ansatz überlegen ist, da ersterer in der Lage ist, die unvorhersehbaren Funkfrequenzeigenschaften in der vorhandenen Infrastruktur zu erfassen. Hierfür präsentieren wir einen neuen Ansatz, der RFID Fingerprints und Odometrieinformationen für die Zwecke der Pfadverfolgung in unbekannten Umgebungen kombiniert. Dieser basiert auf

dem Teaching-and-Playback-Schema. Während der Teaching-Phase wird der Roboter manuell gelenkt, um ihn entlang eines gewünschten Pfades zu bewegen. RFID-Messungen und die damit verbundenen Bewegungsinformationen werden als Referenzdaten aufgezeichnet. In der zweiten Phase, der Playback-Phase, folgt der Roboter diesem Pfad autonom. Der vorgeschlagene Ansatz bietet eine kostengünstige Alternative für die mobile Roboternavigation bei der Bestandsaufnahme in RFID-gekennzeichneten Umgebungen, wenn der Roboter mit einem RFID-Lesegerät ausgestattet ist.

Die Fähigkeit eines mobilen Roboters dynamische Objekte zu verfolgen ist entscheidend für eine effiziente Interaktion mit der Umgebung. Obwohl sich viele Forscher mit der Kartierung von RFID-Tags befassen, nehmen die meisten eine statische Konfiguration der RFID-Tags an, nur wenige berücksichtigen dabei dynamische RFID-Tags. Wir wenden uns daher dem Problem der RFID basierten Verfolgung dynamischer Objekte mit mobilen Robotern zu. Im Gegensatz zur Kartierung von RFID-Tags, ist für die Verfolgung nicht nur eine stabile Erkennung notwendig, es ist zudem erforderlich schnell auf die Bewegung der Objekte reagieren zu können. Um dies zu erreichen, kombinieren wir ein zweistufiges dynamisches Bewegungsmodell mit einem Dual-Partikelfilter. Die Zustandsschätzung des Partikelfilters wird in Kombination mit dem VFH+ (Vektorfeld Histogramm) verwendet, um den Roboter in Richtung des Ziels zu leiten. Hierdurch ist es dem Roboter möglich nach statischen und dynamischen Tags zu suchen, ihnen zu folgen und dabei einen gewissen Abstand zu halten.

Acknowledgments

This thesis would never have been done without the support of many colleagues, friends, and my family. First, I would like to thank my advisor Prof. Dr. Andreas Zell sincerely for giving me the opportunity to work in his group. He provided a great environment with state-of-the-art equipment for performing practical experiments. He gave me a high degree of freedom in conducting my own research and also taught me to critically and scientifically deal with the theoretical and the practical issues in research.

I also would like to thank Prof. Dr. Andreas Schilling, who is my second advisor, for reading my thesis.

It is a great pleasure to work with my colleagues at the Department of Cognitive Systems in Tübingen. I would like to thank Dr. Philipp Vorst for his several years of contribution to the software for our indoor robots. Also he taught me how to operate our Scitos robot and helped me with my first publication during my first year here. I also want to thank Artur Koch for correcting my papers for IROS and Softcom. Many thanks to Goran Huskić, Nedim Šrndić, Jacobo Jimenez, Richard Hanten, Duc My Vo, Anna Górska, Prateek Katiyar, and Kushal Kumar Das for proof reading of my thesis. Moreover, I would like to acknowledge Dr. Travis Deyle from Georgia Institute of Technology and Kirti Chawla from University of Virginia for their discussions about the behavior of our Impinj RFID reader.

Many thanks to Klaus Beyreuther for solving the hardware problems and Vita Serbakova for taking care of our official documentations. I also would like to thank the China Scholarship Council (CSC) for financing my studies in Germany.

Last, I would like to thank my family and my friends for their support, especially my parents and my wife for their unconditioned love and trust.

Contents

Chapter 1

Introduction

1.1 Motivation

Over the past few decades, service robots with the capability of providing assistance and guidance have been widely developed and applied in many fields, such as shopping assistance, health care, environmental monitoring, and entertainment. During the operation, the robots have to deal with various types of objects in order to effectively interact with their environments. The traditional ways of identifying objects with line of sight sensors (e.g. cameras or range-based sensors) face the problem of occlusions from the environment and are usually computationally expensive. Radio-frequency identification (RFID) technology, which exchanges the information between the reader and the tags without contact, provides a solution to overcome these difficulties.

Recent documents show an increasing application of employing passive UHF RFID tags in various industrial environments as well as everyday life. The prices of these tags are very low, for example the cost of one passive tag is between 0.07 $ and 0.15 $ depending on the volume of one's order. RFID tags can be attached to goods or items easily and thus further automate the traditional way of object identification. In the field of robotics, the RFID technology brings both opportunities and challenges. On the one hand, the mobile robot which carries an on-board RFID reader is able to traverse the environment and collect RFID measurements autonomously. In this case, the positions of RFID tags can be inferred by the detections of a mobile robot at different positions. Moreover, each RFID tag provides a unique ID, which can be used as a landmark for the robot localization or navigation. On the other hand, RFID does not provide any information about the position of the tag, i.e. neither distance nor bearing of the tag is reported by the reader. The reader only gives a positive detection and potentially the signal strength if the tag is detected. Moreover, the propagation of the radio signal is hard to predict. There are many factors that have high influence on the signal propagation, such as materials nearby, occlusions, and interferences from other radio devices. From this point of view, employing RFID as a sensing technology for mobile robots is challenging.

This thesis addresses three fundamental problems for mobile robots using RFID, namely mapping, path following, and tracking. A common setup, which is employed in many industrial environments, is to use a static configuration of RFID readers. In contrast, the

scenario considered in this thesis aims at exploring the mobility of the mobile robot for the perception of the environment (i.e. mapping of RFID tags) and improving the autonomy as well as the efficiency of the mobile robot to interact with the environment (i.e. path following and object tracking). For these purposes, we built up a mobile robot platform with the on-board RFID reader based on a commercial robot platform to perceive the RFID measurements in the environment.

The robot is able to localize itself in a known environment based on a laser-based Monte Carlo localization approach. Based on the measurements (the detections and the signal strength) perceived by the RFID reader equipped on the robot, we are able to infer the positions of the RFID tags. Although RFID-based mapping is a well studied topic, little attention has been paid to the particle deprivation problem, due to the impact of many environmental factors on the radio signal propagation. Therefore, this thesis addresses the problem of recovering from mapping failures of static RFID tags and localizing non-static RFID tags which do not move frequently. Moreover, we present a novel 3D sensor model to improve the mapping accuracy and localize RFID tags in 3D by mounting two RFID antennas at different heights on the robot.

Each RFID tag provides a unique ID, which can serve as the landmark for the robot localization or navigation. The fingerprinting-based approach achieves superior accuracy as compared to the model-based approach, since it can capture the unpredicted features of the existing RFID-equipped infrastructures. Therefore, we present a novel approach that combines RFID fingerprints and odometry information into the motion control of a mobile robot for the purpose of path following in unknown environments. Particularly, our approach needs no prior information about the distribution of the tags nor does it require a map of the environment. Our approach features a cost-effective alternative for the navigation of mobile robots in RFID-equipped infrastructures.

Previous research mainly focused on a static configuration of RFID tags, whereas the tags can be dynamic in some applications. For example, in the human robot interaction scenario, the tags are affixed to human beings for the purpose of identification or tracking. Therefore, we address the problem of tracking dynamic objects for mobile robots using RFID tags. In contrast to mapping of RFID tags, which aims at achieving a minimum mapping error, tracking does not only need a satisfactory and robust pose estimation, but also requires a fast reaction to the movements of the objects.

1.2 Contributions

In this thesis, we exploit the applications of the UHF RFID using mobile robots, especially in the field of mapping and path following as well as tracking. More precisely, we highlight the contributions of this thesis as follows:

- We present the adaptive particle filter, which is able to recover from mapping failures of static RFID tags and localize non-static RFID tags. Furthermore, although

negative information is usually considered to be less informative than positive information, we exploit the usefulness of negative information for RFID-based mapping. We show that a careful examination of the negative information improves the mapping accuracy and helps to recover from mapping failures, and may relocalize non-static RFID tags. Additionally, we compare the particle filter-based approach to our previous grid-based Markov localization approach. This work has been published at the 13th International Conference on Intelligent Autonomous Systems (Liu and Zell (2014)).

- We present a novel three-dimensional (3D) probabilistic sensor model of RFID antennas for mapping passive UHF RFID tags using mobile robots. The proposed 3D sensor model characterizes both detection likelihood and received signal strength. Compared to 2D-sensor model based approaches, the 3D sensor model gains a higher mapping accuracy for 2D position estimation. Especially, with this sensor model, we are able to localize tags in 3D by integrating the measurements from a pair of RFID antennas mounted at different heights on the robot. Furthermore, by integrating negative information (i.e. non-detections), the 3D mapping accuracy can be improved. Additionally, we utilize the KLD-sampling to reduce the number of particles for our specific application, so that our algorithm can be performed online. This work has been published at the 2013 IEEE/RSJ International Conference on Intelligent Robots and Systems (Liu *et al.* (2013)).

- We present a novel approach incorporating a combination of UHF RFID and odometry information into the motion control of a mobile robot for the purpose of path following in unknown environments. Our method utilizes RFID measurements as landmarks and enables the mobile robot to autonomously follow a path that was previously recorded in a manual training phase. In particular, we apply the teaching and playback scheme to perform this task, which has already been successfully used in different navigation systems with various sensors. Concretely, the robot is manually controlled to move along a desired path during the teaching stage. At the same time, RFID measurements and the associated motion information are recorded as reference data. In the second stage (i.e. playback stage), the robot follows this path autonomously. We compare the current RFID measurement to the previously recorded reference data to estimate the robot's relative position to the desired path. As a result, motion control commands are generated by fusing the position and the reference motion data to steer the robot. Our approach needs no prior information about the RFID sensor models, the distribution and the positions of the tags nor does it require a map of the environment. Particularly, it is adaptive to different reader power levels and various tag densities, which have a major impact on the RFID sensing performance. This work resulted in two conference publications: one was presented at the 19th International Conference on Software, Telecommunications and Computer Networks (Liu *et al.* (2011)), and

another one was presented at the 2012 IEEE/RSJ International Conference on Intelligent Robots and Systems (Liu *et al.* (2012)).

- We address the problem of tracking dynamic objects with a mobile agent using the signal strength from the tags attached to objects. Our solution estimates the position of an RFID tag under a Bayesian framework. More precisely, we combine a two stage dynamic motion model with a dual particle filter to capture the dynamic motion of the object and quickly recover from failures in tracking. This work resulted in a publication at the 2014 IEEE/RSJ International Conference on Intelligent Robots and Systems (Liu *et al.* (2014)).

Overall, we present probabilistic approaches for localizing RFID tags in 2D and 3D as well as an approach for path following of mobile robots in RFID-equipped environments. Moreover, we introduce an approach that utilizes the signal strength for perceiving and tracking dynamic objects equipped with RFID tags. All of our proposed approaches are validated with a service robot in different RFID-tagged environments.

1.3 Outline

The outline of this thesis is described as follows:

- In Chapter 2, we introduce some background knowledge about RFID technology and present the models of the robot and the approaches for state estimation as well as the way to learn the RFID sensor models.

- In Chapter 3, we present the Bayesian framework for mapping RFID tags . In order to recover from mapping failures and localize non-static RFID tags, we propose an adaptive particle filter. Furthermore, the usefulness of negative information is examined in this chapter.

- In Chapter 4, we present the applications of 3D sensor models for the RFID-based mapping, which consist of 3D mapping of RFID tags by our stereo antennas setup and the improvement of 2D mapping accuracy using 3D sensor models.

- Chapter 5 introduces a novel approach that combines RFID fingerprints and odometry information of a mobile robot for the purpose of path following in unknown environments. The proposed approach requires a teaching stage to record measurements along a desired path. These measurements, which serve as reference landmarks, are then used to guide the robot to follow a previously recorded path.

- For a service robot, the ability to track dynamic objects is essential to effectively provide assistance in its environment. In Chapter 6, we address the problem of tracking dynamic objects with a mobile agent using the signal strength from the RFID tags attached to objects.

- We finally summarize this thesis and show several possible extensions of this thesis in Chapter 7.

1.4 Experimental Platform

1.4.1 Experimental Environment

To conduct our experiments, we setup different indoor environments in our department (i.e. Department of Cognitive Systems) located at Sand 1, Tübingen. This department is part of the Wilhelm-Schickard-Institute for Computer Science of the University of Tübingen. For the localization of the robot, we built up 2D occupancy grid maps of the indoor environments (see Figure 1.1) through Vasco[1] which was already implemented in Carmen (Montemerlo *et al.* (2003)). The color of the cell in Figure 1.1 gives the probability that the cell is occupied by obstacles. For example, black means the cell is occupied, white means it is free, and blue means the occupancy of this cell is unknown. The artifacts of the maps have been cleaned by hand. More precisely, our experimental environments consist of the hallways (see Figure 1.1a) on the second floor of our institute as well as the library (see Figure 1.1b) on the first floor of our institute. These environments were also used for part of our AmbiSense project (Kooperation autonomer mobiler Systeme unter Berücksichtigung ambienter Sensoren), which was funded by the Baden-Württemberg Stiftung. We briefly describe our experimental environments as follows:

- **Hallway Environment:** The hallway environment mainly consists of a computer museum, several corridors, and a robot lab. A shelf with a size of $1 \times 2\,\mathrm{m}^2$ and made of metal is placed in the middle of the robot lab. On the shelf, we placed approximately 400 empty product packages labeled with RFID tags (Alien Technology Squiggle, ISO/IEC 18000-6C) at different heights. We also installed 71 permanent RFID tags on the furniture and the walls in the robot lab with different heights and 47 permanent tags in the corridor adjacent to the robot lab with the same height to the antenna (i.e. 0.8 m). This environment was also used by Schneegans *et al.* (2007), Vorst and Zell (2008), Schairer *et al.* (2008), Vorst *et al.* (2008b), Vorst *et al.* (2009), Rohweder *et al.* (2009), Vorst and Zell (2009), Vorst and Zell (2010b), Vorst *et al.* (2011), Vorst and Zell (2010a), Vorst *et al.* (2011), and Vorst (2011) for evaluating RFID-based applications using mobile robots.

- **Library Environment:** The library environment consists of wooden shelves, corridors, tables, and chairs. In the library, we labeled approx. 7000 books with both UHF and HF (High Frequency) RFID tags. These books are distributed at different

[1] http://carmen.sourceforge.net/doc/

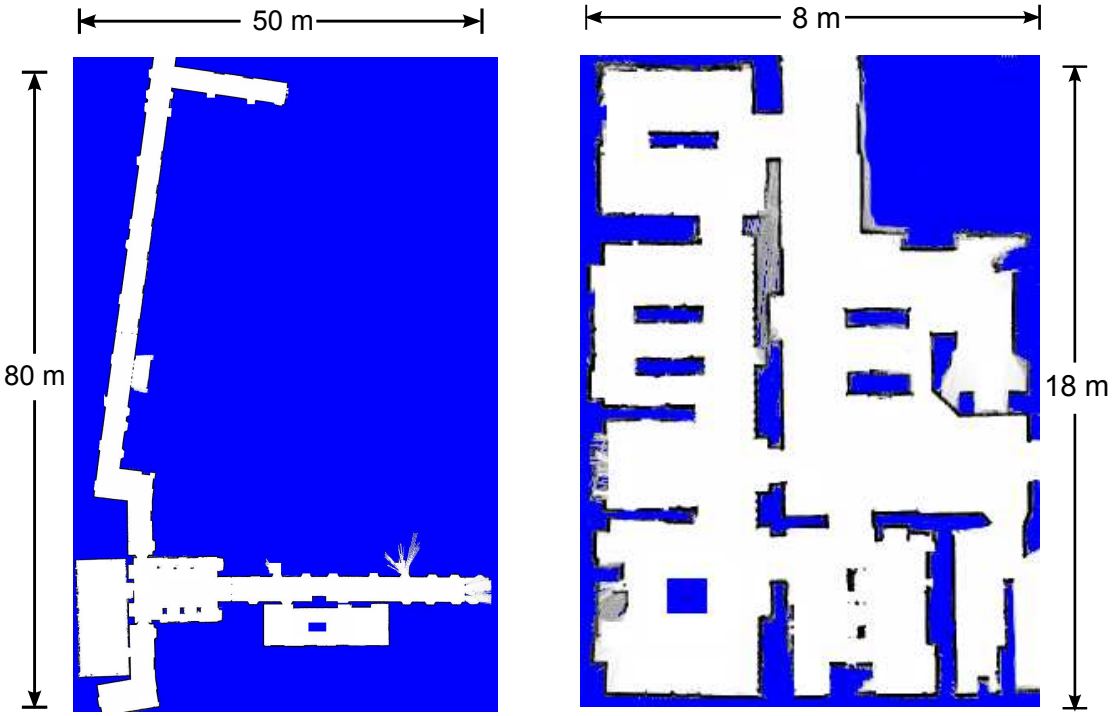

(a) The hallway environment (b) The library environment

Figure 1.1: The occupancy maps of the environments used for our experiments.

(a) The artificial supermarket (b) The real library

Figure 1.2: Snapshots of the environments used for our experiments.

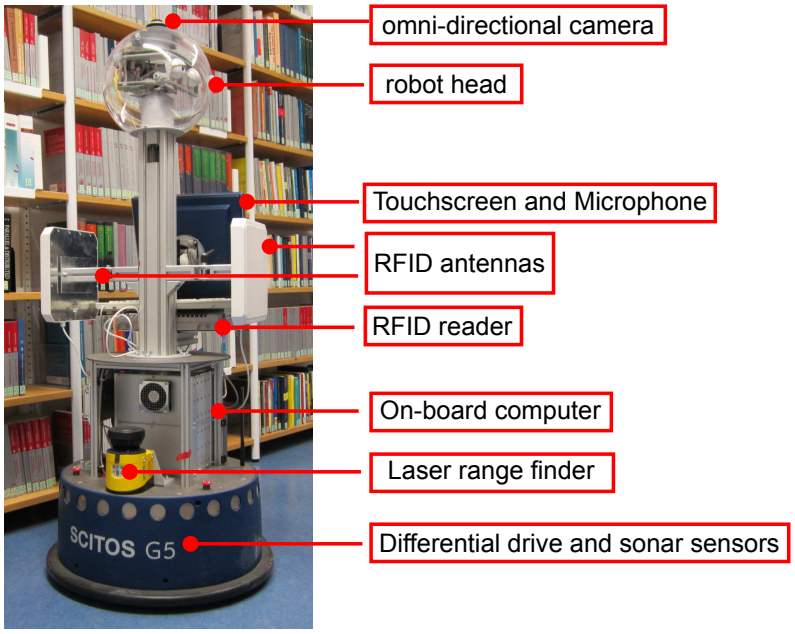

Figure 1.3: The experimental platform used in this thesis and the main sensors equipped on the robot.

heights (from 0.1 m to 2.3 m) on different shelves. This environment was originally set up for our third AmbiSense Workshop in November 2011[2]. The library is considered to be a densely tagged environment and a good scenario of testing RFID-related applications. For the experiments in Chapter 5 and Chapter 6, the robot has to travel through one narrow corridor with a width of only 1.1 m in the library.

In this thesis, some experiments are performed only in part of the environments listed above (e.g. mapping in Chapter 3 and Chapter 4) and some experiments are validated in both environments (e.g. path following in Chapter 5 and tracking in Chapter 6). Additionally, the setups of the antennas may differ from various applications. These variances are mentioned in the experimental parts of different chapters.

1.4.2 Robot Platform

We utilize a Scitos G5 service robot from MetraLabs (see Figure 1.3) as our experimental platform. The robot is powered by two lead-acid batteries, which can last for about 12 hours of normal usage at full charge. The main hardware of the robot is described as follows:

[2]http://www.wsi.uni-tuebingen.de/forschung/forschungsprojekt-ambisense/veranstaltungen/workshop-2011.html

- **Embedded Computer System:** The robot uses a Mini-ITX motherboard with an Intel Core^{TM} 2 Duo 2.16 GHz and 2 GB RAM. The computer is installed with Linux operating systems (Fedora with kernel 2.6.32.10-90 and Ubuntu 12.04). The robot is also equipped with a bluetooth dongle for the remote control.
- **Motion Module:** The motion of the robot is achieved by a differential drive. The robot is able to move at a maximum speed of 1.1 m/s and provide a payload of up to 50 kg. The position encoders embedded in the motors detect the movements of the robot and provide basic measurements to the odometry.
- **RFID System:** The robot is equipped with a Gen. 2 UHF RFID reader (Impinj Speedway R1000) as well as two circularly polarized RFID antennas (Laird Technologies SS8688P). The reader features a maximum reading range up to 10 meters. Additionally, the reader is able to measure the received signal strength of the detected tag. The RFID system works as a mono-static mode, which means the same antenna is used for transmitting and receiving the signals. We are able to specify the reader transmitting power level (from 20 dBm to 30 dBm) through the API (application programming interface) provided by the RFID driver.
- **Laser Range Finder:** The robot is equipped with a laser range finder (SICK S300 with an angular resolution of 0.5° in 270° field of view) for measuring the distance from the objects. The laser range finder is essential for some high level modules of the robot, e.g. localization and navigation as well as obstacle avoidance.

In addition, the robot is equipped with various sensors, which are not used in this thesis, such as sonar sensors for obstacle avoidance, a touchscreen for human robot interface, and a head with movable eyes for human robot interaction, a bumper for emergency stop, a wireless LAN (IEEE 802.11a/b/g) for communication, and an omni-directional camera for object detection.

The work conducted throughout this thesis is based on Carmen (Carnegie Mellon Robot Navigation Toolkit)[3], which provides the basic navigation, mapping, path planning, and obstacle avoidance functions for the robot. Recently we have been exporting our software into ROS (Robot Operating System)[4].

1.5 Notation

Table 1.1 summarizes the important terms and symbols used throughout this thesis. Boldface fonts are used for vectors in this thesis. Table 1.2 summarizes the abbreviations used throughout this thesis.

[3] http://carmen.sourceforge.net/
[4] http://www.ros.org/

Table 1.1: Some notations used in this thesis.

Symbol	Meaning
t	current time index
v, ω	the translational and the rotational velocity of the robot
W, R	the world coordinate frame and the robot coordinate frame
A, L	the number of antennas equipped on the robot and the number of RFID tags in the environment
A_i, L_j	the coordinate frame of antenna i and the coordinate frame of tag j
l_j	the position of tag j
$\mathbf{C}_a^r$	the transformation between antenna a and the robot
$\mathbf{x}$	the state vector. In the 2D localization of a mobile robot, $\mathbf{x} = (x, y, \theta)$
$\mathbf{z}$	the measurement perceived by the sensor on the robot
$\mathbf{u}$	control input of the robot
$p(\mathbf{x})$	probability density function
$p(\mathbf{z}\|\mathbf{x})$	the sensor model or the observation model
N	the number of particles in the particle set
b	baseline of our the stereo antennas setup
$\mathcal{N}(\mu, \sigma^2)$	Normal distribution with mean μ and standard deviation of σ
σ_s, σ_f	slow motion and fast motion parameters for tracking RFID tags
α, β	the number of particles drawn from the dual particle filter and the fast motion parameter respectively
$sim(\mathbf{g}_t, \mathbf{f}_j)$	the similarity between the current fingerprint $\mathbf{g}_t$ and the reference fingerprint $\mathbf{f}_t$
$e_{t,\theta}$	index difference between the left ($i_t^{(0)}$) and the right ($i_t^{(1)}$) antenna
$e_{t,d}$	the weighted average over the RSS differences between the current fingerprint and the K most similar reference fingerprints
$d_t(\mathbf{g}_t, \mathbf{f}_{j_k})$	difference of the received signal strength between the current fingerprint $\mathbf{g}_t$ and the reference fingerprint $\mathbf{f}_{j_k}$
$\mathbf{F}_t$	RFID fingerprint with the odometry information, i.e. $\mathbf{F}_t = (\mathbf{f}_t, \mathbf{m}_t)$
$\mathbf{f}_t$	RFID measurement at time t
$\mathbf{m}_t$	odometry measurement at time t, i.e. $\mathbf{m}_t = (v_t, \omega_t)$
$i_t^{(0)}$, $i_t^{(1)}$	the antenna index of the left and the right antenna in the reference fingerprints respectively
K_m, K_f	parameters used for controlling the path following approach
K_o, K_r	PID parameters for controlling the robot to follow the desired path
K	the parameter used for smoothing the signal strength for path following

Table 1.2: Some abbreviations used in this thesis.

Abbreviation	Meaning
AMCL	Adaptive Monte Carlo localization
COS	Cosine similarity
EKF	Extended Kalman filter
EM	Electromagnetic
ESS	Effective sample size
GPS	Global positioning system
GSM	Global system for mobile communications
HF	High frequency
KDE	Kernel density estimation
KLD	Kullback-Leibler distance
KNN	K-nearest neighbors
LF	Low frequency
MCL	Monte Carlo localization
PF	Particle filter
RF	Radio frequency
RFID	Radio-frequency identification
RSS	Received signal strength
RTLS	Real-time location system
SIR	Sequential importance resampling
SIS	Sequential importance sampling
SMC	Sequential Monte Carlo
UHF	Ultra high frequency
UKF	Unscented Kalman filter
VFH	Vector field histogram
WKNN	Weighted k-nearest neighbors

Chapter 2

Foundations

In this chapter, we introduce some foundations of RFID technology and probabilistic approaches for state estimation as well as modeling of the UHF RFID. The rest of this chapter is organized as follows. The background of the RFID technology and the models of the robot are described in Section 2.1 and Section 2.2, respectively. Afterwards, several state estimation approaches are introduced in Section 2.3. This is followed by the semi-autonomous approach used to generate the sensor model in Section 2.4. Finally, we summarize the chapter in Section 2.5.

2.1 Long Range Passive UHF RFID

2.1.1 Introduction

Radio-frequency identification (RFID) uses electromagnetic fields to automatically identify the tags affixed to objects without line of sight. There are two main components of an RFID system, namely interrogator or reader and transponder or tag. The reader communicates and exchanges information with the RFID tags via radio waves. The tag, which consists of an antenna and an integrated circuit, carries the identification information to be transmitted. The biggest advantage of RFID over bar code technology is that the tag does not need to be placed within line of sight of the interrogator. RFID technology now is used in many industrial applications, such as inventory management, asset tracking, and access control. For example, RFID tags can be placed on vehicles and provide access control services in parking lots without stopping the vehicles.

Particularly, long range passive ultra-high frequency (UHF) RFID system offers the identification of objects over a long reading range (e.g. 10 meters) without any additional power supply of the tag. Owing to their cheap price, these tags can be affixed to items or assets to automate the inventory process in retail stores, warehouses, and libraries. In this case, a person carrying the RFID device is able to identify items from a far distance, which avoids the traditional way of manual counting of assets and eliminates the error in inventory records. The labor cost of the inventory can be further reduced by using a mobile robot. The positions of the tags can be determined if the mobile robot is able to solve the self-localization problem, which is a well developed topic in robotics. More-

Table 2.1: The operating frequencies and the reading ranges of passive UHF RFID.

Frequency range	Typical frequency	Reading range	Tag Price
Low Frequency (LF)	125-134kHz	<0.5 m	1 $
High Frequency (HF)	13.56 MHz	<1.0 m	0.5 $
Ultra High Frequency (UHF)	865-928 MHz	1-10 m	0.15 $

over, each RFID tag carries a unique identifier. This makes RFID technology crucial in robotics, since it trivially solves the self-localization problem of the robot.

2.1.2 RFID Systems

Depending on their power sources, RFID tags can be categorized into passive and active tags. Active tags need a battery for the power supply and thus have a long reading range (up to 100 meters or more), while passive RFID tags do not need any battery and have to rely on electromagnetic waves transmitted from the reader to energize themselves and thus have a short reading range (up to 10 meters). Active tags are mainly used for tracking valuable items in real-time location systems (RTLS) and monitoring the environment, whereas passive tags are frequently used for inventorying assets using mobile readers or fixed readers in the environment. Due to their large size, short tag life, and high price, active tags are not suitable for tagging objects in everyday application. This is why we prefer passive RFID tags in this thesis.

There are many factors that have impact on the reading range of passive UHF RFID: the transmitting power of the reader, the frequency of reader, and the interference from the environment. With regard to the frequency of the reader, a comparison of passive RFID technologies is listed in Table 2.1. The LF or HF communication is based on magnetic induction or near field coupling. LF works at a low frequency band (e.g. 134 kHz) and thus has a short reading range. However, LF tags are not very sensitive to the interference from the environment and can be used in challenging environments including water or metal objects. Therefore, these tags can be implanted into animals for tracking or used in factories for data collection.

HF tags typically operate at 13.56 MHz and have a longer reading range than LH tags, whereas they are more sensitive to the environmental interference than LF tags. HF tags are usually used for payment, luggage tracking at the airport, ticketing, and asset tracking.

UHF RFID tags provide an even longer reading range (up to 10 meters) and are cheaper than LF or HF tags. UHF RFID tags obtain energy from the electromagnetic waves propagated by the antenna connected to the RFID reader. UHF RFID has a higher data transmission rate than LF and HF RFID. These features of UHF RFID make it suitable for many industrial applications, such as contactless payment, inventory management, access control or goods tracking. The performance of UHF RFID tags rapidly

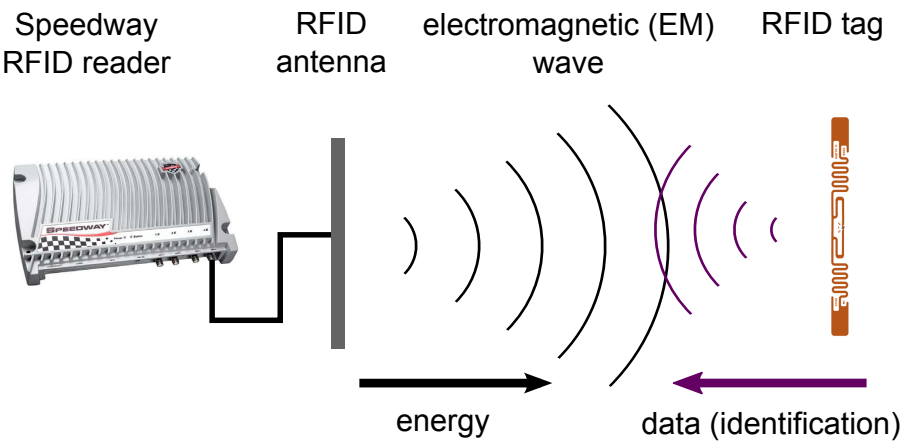

Figure 2.1: The communication mechanism of long range passive UHF RFID system.

deteriorates in proximity to metal, water or occlusions. The frequency of UHF RFID tags depends on the regulations and restrictions of the region. For example, Europe operates at 865-868 MHz and the USA typically operates at 902-928 MHz. In the UHF band, the most popular standard used currently is EPC C1G2, which is the abbreviation for EPCglobal UHF Class 1 Generation 2. EPCglobal (see EPCglobal (2013)), which was formed in 2003, mainly aims at establishing the standards as well as specifications for the worldwide adoption of passive RFID in the supply chain management. In this thesis, we focus on the long range passive UHF RFID, which is based on the EPC C1G2 standard. More details of the RFID system can be found at Weis (2007), Finkenzeller (2003), and Want (2006).

2.1.3 Long Range Passive RFID

The principle of UHF RFID operation is shown in Figure 2.1. In general, UHF RFID systems use radio waves for transmitting energy and communication. In contrast to the induction based near-field RFID, long range passive UHF RFID, which is also called far-field RFID, relies on backscatter modulation.

More precisely, the RFID antenna propagates an electromagnetic field generated from the reader, and only a small amount of energy reaches the tag's antenna, due to free space attenuation. The incident power absorbed by the tag from the electromagnetic wave is used for two purposes: one part of the energy is used to provide the power for the circuitry inside the tag; the rest of energy is reflected. The information (i.e. identity) of the tag is encoded inside the signal backscattered by the tag through a way of modulation, i.e. varying the amplitude or the phase of the signal by changing the impedance inside the tag. The reader is designed to capture this signal and decode it. Besides the identity of the tag, the new generation of RFID readers is able to provide the signal strength, which indicates the strength of a tag's reply. For example, some

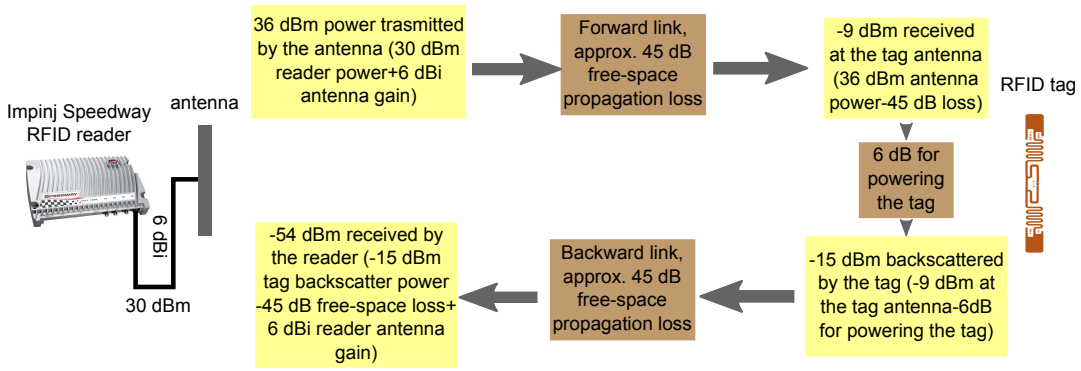

Figure 2.2: Forward and backward link of a passive UHF RFID system.

readers provide signal strength in dBm (Impinj Speedway) and some readers report the signal strength unitless (ThingMagic Mercury5e). Figure 2.2 shows a typical forward and backward link of an RFID system. In this example, the reader emits electromagnetic waves with a power of 30 dBm (1 W). The antenna additionally contributes a gain of 6 dBi. The propagation of electromagnetic wave is similar to Radar system. Therefore the Friis equation commonly used in the Radar system can be applied to trace the power of the RFID system. Theoretically, the relationship of the power at the transmitted antenna P_t and received antenna P_r can be simply described as follows (see Levis (2001)):

$$P_r = G_r G_t \left(\frac{\lambda}{4\pi R}\right)^2 P_t, \tag{2.1}$$

where λ is the wavelength of the radio signal and R is the distance between two antennas. G_r and G_t are the antenna gains of the receiver and transmitter respectively. It is important to note that this equation only holds under certain conditions (see Balanis (2005) for more detail). It assumes an ideal signal propagation in unobstructed environments, which is not suitable for real-world environments, where multi-path, distortion, reflection, and deflection exist. Moreover, this equation only holds in the far-field area (i.e. $R \gg \lambda$): it is not applicable if the receiver is too close to the transmitter (i.e. $R < \lambda$). Although in practice the situation will be much more complex, the Friis equation gives a first insight into the relationship between the receiver power and the transmitter power.

Quite different from active tags, passive tags do not send the signal to the reader actively, since they have to rely on the electromagnetic field propagated by the reader for power supply during reader interrogation periods. The incident power received by the tag is very small based on the inverse square law as shown by the Friis equation in Equation (2.1), i.e. the power received at the tag is inversely proportional to the square of distance from the reader to the tag. In order to successfully read a passive UHF RFID tag, two requirements must be satisfied: the tag must receive sufficient energy from the reader to power up the circuitry inside and the reader must be sensitive enough to hear the tag's

response. The detail about the backscatter modulation is described in Lehpamer (2007) and Karmakar (2011).

EPC Class 1 Generation 2 makes a major step towards the standardization in the field of UHF RFID and defines the protocols about the physical and logical requirements of the tag and reader in an RFID system. The new EPC Gen 2 standard brings many new features compared to the old protocols. For example, dense reader mode allows multiple readers to work together in one area without synchronization, which avoids the interference problem that was faced in the old protocols. During the scanning of the environment, the RFID reader has to differentiate between the tags when more than one tag are within its range. With the help of singulation, which is based on the Q algorithm (a variant of the Slotted Aloha algorithm), the reader is able to identify a specific tag among a number of tags without jamming each other (see Maguire and Pappu (2009)). Through this way, a typical reader is able to achieve a maximum reading rate of 1200 unique tags with 96 bits EPC numbers per second.

Moreover, EPC Gen 2 has a new feature called sessions, which allows multiple readers to simultaneously communicate with one tag without interference. Each tag has four sessions. The reader and the associated tag operate in only one of the four sessions during an inventory round. The concept of sessions allows a tag to keep tracking of its inventoried status based on the corresponding inventoried flag maintained by the tag and eliminates interference.

Another technique used to prevent RFID readers from interfering with each other is frequency hopping. During the operation, the frequency of the reader is chosen randomly (or in a predefined sequence) according to the frequency hopping table defined by the regulatory region. This strategy reduces the chance of possible interference (i.e. two readers attempt to interrogate the same tag at the same frequency). In non-frequency-hopping regions, this field is ignored. For example, the operating frequency of UHF RFID reader is between 902 and 928 MHz in the USA and thus the actual frequency of the RFID reader during the operation jumps randomly between these bands.

Passive UHF tags can be interrogated from a long reading range up to several meters. The reading range can be different, depending on the frequency of the reader, the power of the reader, the impact of the environment, and the antenna and tag characteristics, which are detailed as follows:

- **Reader Power:** According to the Friis equation, the incident power obtained by the receiver is proportional to the power emitted from the transmitter. The ideal reading range of the RFID is proportional to the square root of the reader power. A higher reader power gives a longer reading range. The maximum transmitted power of the reader is restricted by the hardware design as well as the regulation of the region. For example, for the Impinj RFID reader used in this thesis, the maximum reader transmitted power is 30 dBm (1 W). Additionally, we are able to adjust the reader power from 20 dBm (100 mW) to 30 dBm through the API provided by the driver.

Figure 2.3: Examples of passive UHF RFID tags. Top (from left to right): OMNI-ID large tag, OMNI-ID small tag, and Alien Technology Squiggle tag. Bottom (from left to right): Impinj Jumping Jack tag, Impinj propeller tag, and NXP pulse tag.

- **Reader Frequency:** The Friis equation also predicts that the incident power absorbed by the tag is proportional to the square of the wavelength (i.e. inverse of the frequency). As mentioned before, the frequency of the reader depends on the regulation of the region. As a result, for a given transmitted power, different regions may have different RFID reading ranges: for example, the readers used in Germany (865.6-867.6 MHz) have longer reading ranges than the ones used in the USA (902-928 MHz).

- **Impact from the Environment:** The radio signal from the RFID system may be distorted or interfered by the materials nearby. Particularly, water and metal objects can greatly affect the readability of a tag. Metal reflects the radio waves and water absorbs the radio waves and thus prevents the tag from receiving energy from the reader and results in a low reading rate of the tag. Moreover, multi-path problems frequently happen in indoor environments, due to reflections of the radio signal by walls, grounds, and ceilings. Signals received at the antenna come from a variety of paths due to the reflections of the environment. In this case, the overall signal received at the antenna is a sum of the signals over all paths. Sometimes these signals will interfere with each other and result in the signal fading.

- **Reader Antenna and Tag Characteristics:** Besides the 2D relative displacement of the tag to the antenna, the tag's orientation has a small influence on its readability. Moreover, depending on the manufacture of the RFID tags, tags may have slightly different characteristics.

2.1.4 Passive RFID Reader and Tag

For a specific application, it is important to purchase the right antenna. In general, there are two types of antennas: linearly polarized antenna (dipole antennas) and circularly polarized antenna, e.g. patch, helix, and crossed dipole antenna. The propagations of linear and circular antennas are different. Linear polarization (or plane polarization) propagates the electromagnetic wave along a given plane vertically or horizontally. Hence, the antenna and the tag must be placed with a fixed configuration in order to achieve a good performance of the reading rate. This kind of propagation gives the best performance when the tag orientation is known.

Circularly polarized antennas propagate electromagnetic waves along two planes in a circular spiral pattern. Due to the continuous emission of radio waves from the antenna, the electromagnetic waves are able to cover the tag with any orientation in the environment. Therefore, circular polarization is the best choice if the orientation of the tag is unknown or not fixed. With the same antenna gain, a linearly polarized antenna has longer reading range than circularly polarized antenna, since the energy (i.e. electromagnetic wave) is propagated in two separated planes for the circularly polarized antenna.

In practice, in order to achieve the best readability of the tag, one has to take into account the distribution of the tags in the environment. For example, if all tags are located on the same plane and the same orientation, a linearly polarized antenna is advantageous over a circular one. On the other hand, if one is not able to fix the tags' poses, most likely one needs to use a circularly polarized antenna. In our RFID-equipped scenario, tags are placed at different heights of the shelves and the robot has to detect a tag at different views to obtain a grain-fined position estimation of the tag. Therefore, we use a circularly polarized reader antenna throughout this thesis, e.g. the SS8688P from Laird Technologies. For the tag antenna, we choose the dipole antennas (Alien Technology Squiggle), which are commonly used in the related literature of robotics. Several examples of passive UHF RFID tags are shown in Figure 2.3.

An overview and a comparison of the performance between different passive UHF RFID tags are given in Chawla *et al.* (2013).

2.2 Modeling of the Robot

In this section, we introduce some basic knowledge about the coordinate frames of the robot system as well as its motion models. These concepts will be used for the mapping, path following, and tracking in the later chapters.

2.2.1 Introduction

There are many sensors on our service robot, for example a camera, an RFID reader, sonar sensors, a laser range finder and odometry. Among these sensors, three important

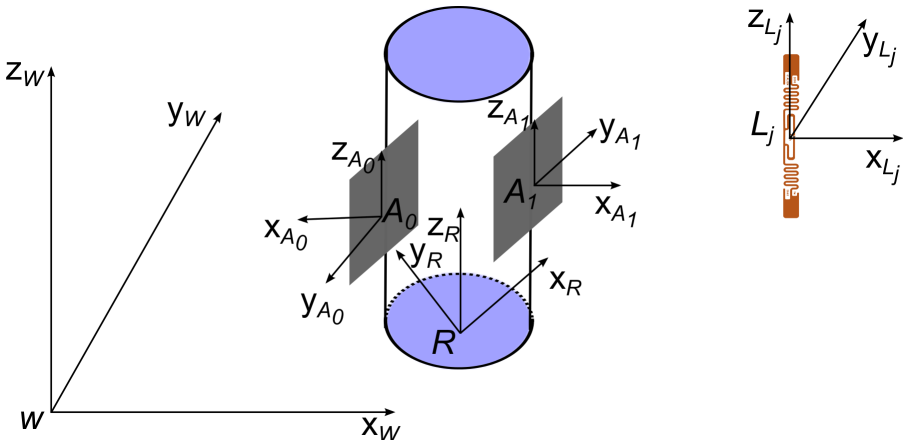

Figure 2.4: The coordinate frames used in this thesis.

sensors are involved in this thesis, i.e. the odometry, the RFID reader, and the laser range finder. Localization plays a vital role in building up a fully autonomous mobile robot. The odometry achieves the estimation of the robot's position relative to a starting location by means of dead reckoning, i.e. by integrating velocity measurements over time. It accumulates errors and therefore has to rely on other sensors (i.e. cameras or laser range finders) to eliminate the error. A widely used approach is to utilize visual features from lasers or cameras for the localization of the robot in the environment. In this case, the robot has to acquire a spatial representation of the environment (e.g. grid-based or topological map). Many techniques use probabilistic approaches to handle the uncertainty during the localization, for example particle filters and Kalman filters. In this thesis, we utilize GMapping (Grisetti *et al.* (2005)) to learn the occupancy grid maps of the environments from raw laser range data and odometry measurements. Afterwards, the robot applies adaptive Monte Carlo localization, which takes the map, laser scans, and odometry measurements as inputs for its localization. For an overview of the mapping for mobile robots, we refer the reader to Thrun (2003), Thrun *et al.* (2005), Roewekaemper *et al.* (2012), and Sprunk *et al.* (2014).

Before introducing the model of the robot and its sensors, it is important to describe the coordinate system used for our mobile robot (shown in Figure 2.4). The world coordinate frame (W) serves as the reference frame of the environment. R is the coordinate frame of the robot, whose origin is the center of the robot and locates in the ground plane of the world coordinate frame. The positive x-axis of the robot coordinate frame extends to the heading of the robot; the z-axis is parallel to the z-axis of the world frame; the y-axis obeys the right-hand rule. A_i is the coordinate frame of antenna i and L_j is the coordinate frame of tag j. The origins of A_i and L_j are the center of the antenna and the tag respectively. The x-axis of A_i is perpendicular to the antenna plane and points towards the direction of the maximum antenna gain; the y-axis locates in the antenna plane and is parallel to the ground plane; the direction of the z-axis is vertically upward.

Here we assume that the tag is rectangular. The z-axis of the tag lies inside the rectangle and is parallel to the longer side of the rectangle; x-axis points towards the direction of the maximum antenna gain; the y-axis again follows the right-hand rule.

To simplify the notation, we denote the position of the robot as $\mathbf{x}$, the pose of the antenna i as $\mathbf{a}_i$ and the location of tag j as l_j. Since reader antennas are fixed on the robot throughout this thesis, the transformation matrix between the antenna and the robot (i.e. $\mathbf{C}_a^R$) is known. For the mapping of RFID tags in Chapter 3 and Chapter 4, the robot is steered by manual control and the position of the robot is provided by a laser-based Monte Carlo localization approach. In contrast to the mapping, for the path following in Chapter 5 and the tracking in Chapter 6, the movement of mobile robot is controlled by the signal strength and the pose estimation of the tag.

2.2.2 Robot Motion

Since our robot only moves in two dimensions, the pose of the robot at time t is denoted as $\mathbf{x}_t = (x_t, y_t, \theta_t)$. x_t and y_t are the coordinates of the robot with respect to the world coordinate frame and θ_t is the global heading of the robot. The movement of the robot is considered to be a rigid-body transformation in 2D space. Given the true translation $\triangle d_t$ and rotation $\triangle\theta_t$ of the robot at time t, the kinematic model of the robot is described as (see Roy and Thrun (1999)):

$$x_{t+1} = x_t + \triangle d_t \sin(\theta + \triangle\theta_t/2) \tag{2.2}$$

$$y_{t+1} = y_t + \triangle d_t \cos(\theta + \triangle\theta_t/2) \tag{2.3}$$

$$\theta_{t+1} = \theta_t + \triangle\theta_t \tag{2.4}$$

The true movement of the robot is typically provided by the odometry. However, odometry accumulates errors mainly from two sources: systematic error (unequal design of two wheels, limited encoder sampling rate, and installing error) and non-systematic error (traveling on uneven terrain and wheel-slippage) (Borenstein *et al.* (1996)). To deal with the uncertainty of the odometry, the true movement of the robot is usually modeled by adding Gaussian noise with zero mean to the odometry measurement. It is important to note that the equation above only holds if the turning velocity during the given time is constant and the robot always moves along the direction it faces. The error can be ignored if the turning velocity is very small. Eliazar and Parr (2004) proposed a better model which takes into account various speed turns and does not depend on the starting and ending orientations of the robot.

For a differential drive robot used in this thesis, two independent wheels equipped with their own motors are placed on both sides of the robot body. An additional wheel is usually installed to balance the robot. Shaft encoders are able to provide information about the motion of the shafts, which can be converted into the speed of the wheels or the distance the wheels travel. The kinematic model of a differential drive robot is shown

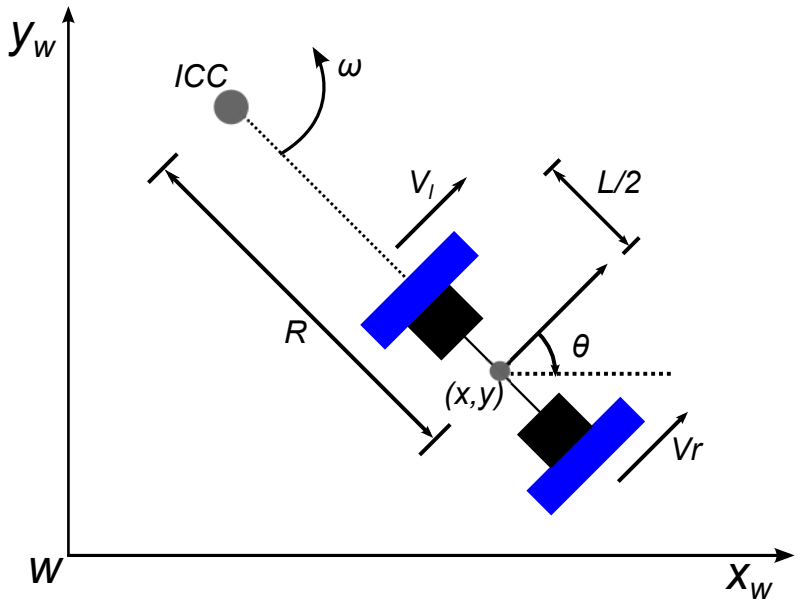

Figure 2.5: The kinematics of a differential drive robot.

in Figure 2.5. The point around which the robot rotates is known as the instantaneous center of curvature (ICC) (see Dudek and Jenkin (2000) for more information). This point has nearly zero velocity during a short period of time. The movement of the robot is achieved by varying the velocity of two motors. If both wheels rotate with the same speed and in the same direction, the robot moves straight. Otherwise, depending on the velocities of two wheels, the robot follows respective motion.

Since the rotational velocities ω of the left and right wheels around ICC are the same, we can write the following equation:

$$v_l = \omega(R - L/2) \tag{2.5}$$
$$v_r = \omega(R + L/2) \tag{2.6}$$

where L represents the distance between two wheels, which is a known parameter; v_l and v_r are the velocities of left and right wheel, respectively, and R is the distance from the ICC to the center of the robot. At any time interval $\triangle t$, the distance $\triangle d$ and orientation $\triangle\theta$ that the robot performs can be expressed as:

$$\triangle\theta = \omega\triangle t = \frac{v_r - v_l}{L}\triangle t \tag{2.7}$$
$$\triangle d = R\omega\triangle t = \frac{L}{2}\frac{v_r + v_l}{v_r - v_l}\frac{v_r - v_l}{L}\triangle t = \frac{v_r + v_l}{2}\triangle t \tag{2.8}$$

This means the movement of the robot can be fully determined by the velocities of two wheels. Sometimes, we prefer to transform the action space. Let $v = \frac{v_r + v_l}{2}$ and $\omega = \frac{v_r - v_l}{L}$.

Here v is regarded as an action of translation executed by the robot and ω means rotation. Therefore, the velocities of two wheels can be represented as functions of v and ω:

$$v_r = \frac{2v + \omega L}{2} \tag{2.9}$$

$$v_l = \frac{2v - \omega L}{2} \tag{2.10}$$

The low level velocities (i.e. v_r and v_l) are then used to control the motors inside two wheels with two independent PID controllers. Precisely, the control is achieved by a feedback from the motor encoder to the power of the motor.

2.3 State Estimation

State estimation from the noisy sensor measurements and motion data is a key step towards implementing a reliable and real-time control system in the field of mobile robots. However, the state of the system is usually not directly observable. In the context of mobile robots, state estimation addresses the problem of inferring the state of the world (i.e. position of the robot, or the positions of the objects in its environment) based on the actions performed by the robot and the measurements perceived by the sensors on the robot. In this thesis, we want to estimate the position of the tag and the pose of the robot along a predefined path.

The robot has to rely on its sensors and other sources to acquire the information about the state. Due to sensor limitations or the influence of the environment, the measurements from the sensors are usually corrupted by noise, which introduces a large amount of uncertainty to the state estimation. Probabilistic state estimation algorithms deal with the uncertainty in robot perception and action and compute the belief distribution over all possible states. In the rest of this section, we introduce the recursively probabilistic framework which is able to efficiently and incrementally estimate the state of the world by integrating the actions and the sensor measurements during the operation of the robot. We also describe three popular implementations of this framework, namely Kalman filters, histogram filters, and particle filters. Particularly, we describe the details of particle filters in Section 2.3.4, which are used in this thesis, due to their popularity, efficiency, and applicability in robotics.

2.3.1 Bayesian Framework

Recursive Bayesian estimation is a general probabilistic framework for recursively estimating the probability density function over a state, given the past measurements reported by the sensor and the actions performed by the robot. Formally, we want to estimate the state of a dynamic system $\mathbf{x}_{1:t}$ at discrete time steps $1:t$, given the actions $\mathbf{u}_{1:t}$ executed by the robot and the measurements $\mathbf{z}_{1:t}$ received by the sensor. We denote

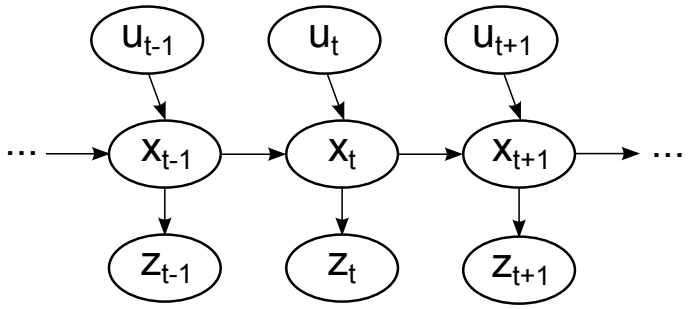

Figure 2.6: The dynamic Bayesian framework under the Markov assumption.

the posterior probability density function (belief) to be estimated as:

$$bef(\mathbf{x}_t) = p(\mathbf{x}_t|\mathbf{z}_{1:t}, \mathbf{u}_{1:t}) \tag{2.11}$$

For example, in the context of 2D robot localization, $\mathbf{x}_t$ is the position and the heading of the robot, $\mathbf{z}_t$ is the measurement from the laser range finder and $\mathbf{u}_t$ is the odometry information (i.e. velocity of the robot). The derivation of the Bayesian framework used in this thesis is based on the assumption that the system follows a Markov model, i.e. the state is complete. This means that the current state $\mathbf{x}_t$ only depends on the value on the previous state $\mathbf{x}_{t-1}$; the states before $t-1$ do not have any influence to the current state. Similarly, the observations at different time steps are independent, i.e. the observation at time t only depends on the state $\mathbf{x}_t$. Since the state is not directly observable, the system is considered to be a hidden Markov model, which is the simplest case of a dynamic Bayesian network (Friedman *et al.* (1998)). Figure 2.6 is the graphical representation of a Bayesian network under the Markov assumption. Applying the Bayes rule, Equation (2.11) can be factorized into:

$$p(\mathbf{x}_t|\mathbf{z}_{1:t}, \mathbf{u}_{1:t}) = \frac{p(\mathbf{z}_t|\mathbf{x}_t, \mathbf{u}_{1:t}, \mathbf{z}_{1:t-1})p(\mathbf{x}_t|\mathbf{u}_{1:t}, \mathbf{z}_{1:t-1})}{p(\mathbf{z}_t|\mathbf{u}_t, \mathbf{z}_{1:t-1})} \tag{2.12}$$

$$= \eta\, p(\mathbf{z}_t|\mathbf{x}_t, \mathbf{u}_{1:t}, \mathbf{z}_{1:t-1})p(\mathbf{x}_t|\mathbf{u}_{1:t}, \mathbf{z}_{1:t-1}), \tag{2.13}$$

where $\eta = 1/p(\mathbf{z}_t|\mathbf{u}_t, \mathbf{z}_{1:t-1})$ is constant given the state of $\mathbf{x}_t$. The Markov assumption assumes that the future measurements or actions are independent of the past measurements or actions given the current state, which implies that:

$$p(\mathbf{z}_t|\mathbf{x}_t, \mathbf{u}_{1:t}, \mathbf{z}_{1:t-1}) = p(\mathbf{z}_t|\mathbf{x}_t, \mathbf{u}_t) \tag{2.14}$$

Therefore, Equation (2.13) can be simplified as:

$$p(\mathbf{x}_t|\mathbf{z}_{1:t}, \mathbf{u}_{1:t}) = \eta\, p(\mathbf{z}_t|\mathbf{x}_t, \mathbf{u}_t)p(\mathbf{x}_t|\mathbf{u}_{1:t}, \mathbf{z}_{1:t-1}), \tag{2.15}$$

By applying the theorem of total probability to the rightmost part of the Equation (2.15), we obtain:

$$p(\mathbf{x}_t|\mathbf{z}_{1:t},\mathbf{u}_{1:t}) = \eta\, p(\mathbf{z}_t|\mathbf{x}_t,\mathbf{u}_t) \int p(\mathbf{x}_t|\mathbf{x}_{t-1},\mathbf{u}_{1:t},\mathbf{z}_{1:t-1}) p(\mathbf{x}_{t-1}|\mathbf{z}_{1:t-1},\mathbf{u}_{1:t}) \mathrm{d}\mathbf{x}_{t-1}. \quad (2.16)$$

Again we use the Markov assumption to simplify $p(\mathbf{x}_t|\mathbf{x}_{t-1},\mathbf{u}_{1:t},\mathbf{z}_{1:t-1})$ as:

$$p(\mathbf{x}_t|\mathbf{x}_{t-1},\mathbf{u}_{1:t},\mathbf{z}_{1:t-1}) = p(\mathbf{x}_t|\mathbf{x}_{t-1},\mathbf{u}_t) \quad (2.17)$$

Moreover, we notice that $\mathbf{u}_t$ can be safely removed from the conditional variables in $p(\mathbf{x}_{t-1}|\mathbf{z}_{1:t-1},\mathbf{u}_{1:t})$, since the future action $\mathbf{u}_t$ does not give any information to the current state estimation $\mathbf{x}_{t-1}$. Finally, we obtain the recursive version of Bayesian estimation:

$$p(\mathbf{x}_t|\mathbf{z}_{1:t},\mathbf{u}_{1:t}) = \eta\, p(\mathbf{z}_t|\mathbf{x}_t,\mathbf{u}_t) \int p(\mathbf{x}_t|\mathbf{x}_{t-1},\mathbf{u}_t) p(\mathbf{x}_{t-1}|\mathbf{z}_{1:t-1},\mathbf{u}_{1:t-1}) \mathrm{d}\mathbf{x}_{t-1}. \quad (2.18)$$

In general, the Bayesian framework computes the posterior probability density function of the state $\mathbf{x}_t$ given the measurements $\mathbf{z}_{1:t}$ and the actions $\mathbf{u}_{1:t}$ up to time t. Two conditional densities are essential to implement a Bayesian framework: the state transition probability $p(\mathbf{x}_t|\mathbf{x}_{t-1},\mathbf{u}_t)$, which is also called motion model, and the measurement probability $p(\mathbf{z}_t|\mathbf{x}_t,\mathbf{u}_t)$, which is also known as sensor model or perception model. The later sections in this chapter will give a detailed description about the modeling of these density functions in the field of RFID.

In practice, in order to achieve a robust approximation of the target distribution, the continuous state space has to be represented in an efficient way. We introduce some popular representations of the Bayesian filter in the following sections.

2.3.2 Kalman Filters

Kalman filtering, which is named after Rudolf E. Kalman (Kalman (1960)), addresses the problem of recursively estimating the state of a linear dynamical system with normal distributions. For a good tutorial of Kalman filters, the reader is advised to follow Welch and Bishop (1995). The Kalman filter is considered to be one of the simplest implementation of the Bayesian framework. It has been successfully used in a wide range of applications, particularly in control, localization, and navigation of autonomous vehicles. Kalman filters are built on the assumption that all error terms and measurements are normally distributed. More precisely, the normal distribution is represented as a multivariate Gaussian with a covariance. A drawback of Kalman filters is that the derivation of the equation is based on the linear difference equation, i.e. the state transition and the observation model must be linear. In practice, the system can be very complex and non-linear, which limits the application of basic Kalman filters.

To deal with the non-linear systems, several extensions of the basic Kalman filter have been developed, such as the extended Kalman filter (EKF) and the unscented Kalman

filter (UKF). The EKF linearizes the state transition and the observation model using the first-order Taylor series expansion. The performance of the EKF is especially poor if the state transition and the observation model are highly non-linear, since the linearization of the nonlinear system is achieved by propagating Gaussian random variables analytically. To solve this problem, the UKF uses a deterministic sampling technique (unscented transform) to choose a minimum set of sample points to represent the state distribution (i.e. mean and covariance) (Wan and Van der Merwe (2000) and Julier and Uhlmann (1997)). These points are then propagated through the true non-linear function. As compared to the EKF, the UKF captures the posterior state distribution to the third order Taylor series expansion, while the computational complexity is same as that of the EKF. Although these extensions are sufficient to deal with nonlinearities in the system, the nature of Gaussian representation confines these filters to the applications where the posterior probability can be approximated as a Gaussian. This drawback is addressed by the non-Gaussian filters, such as histogram filters introduced in Section 2.3.3 and particle filters described in Section 2.3.4.

2.3.3 Histogram Filters

Histogram filters, which are also called grid-based Markov approaches, decompose the state space into fine-grained and grid-based regions. The posterior probability in this case is represented by a histogram. This approach has been widely used in robot localization (see Russell and Norvig (2003) and Burgard *et al.* (1997)). Rather than representing the belief with the Gaussian as followed in the Kalman filter, histogram filters maintain a probability distribution over all possible states. This representation is able to represent complex, arbitrary, non-Gaussian, and multi-modal distributions. This approach is shown to have a good accuracy if the discretization of the states is reasonably high. The drawback is that we have to maintain a huge number of grid cells, which requires a high memory consumption. Moreover, updating the states of all grid cells is computationally expensive. Thus, this approach is not efficient in many real-time applications. To overcome this difficulty, some researchers proposed the selective updating, which only updates the likely cells (Fox *et al.* (1999)) and the tree-based representation, which is able to change the resolution of the grid dynamically (Burgard *et al.* (1998)). In our early research (Liu *et al.* (2013) and Rohweder *et al.* (2009)), we also used a grid-based representation for mapping RFID tags.

2.3.4 Particle Filters

Particle filters (Pitt and Shephard (1999) and Doucet *et al.* (2000)), which are also known as Sequential Monte Carlo (SMC) approaches, represent the probability density function with a finite number of random particles or samples (Arulampalam *et al.* (2002)). As a non-parametric implementation of Bayesian framework, the particle filter approximates

the distribution with a collection of samples and makes no assumption about the distribution of the density function, therefore it can represent a much wider range of distributions than the parametric approaches, such as Gaussian filters.

Particularly, we represent the belief by a weighted set of particles $\mathbf{S}_t = \{\mathbf{x}_t^i, w_t^i\}, i = 1,..,N$, where N is the number of particles. Each particle consists of the state hypothesis $\mathbf{x}_t^i$ and the associated weight w_t^i, which represents the importance of that particle. The sum of the weights has to satisfy that

$$\sum_{i=1}^{N} w_t^i = 1 \tag{2.19}$$

The target posterior distribution to be estimated can be approximated as:

$$p(\mathbf{x}_t|\mathbf{z}_{1:t}, \mathbf{u}_{1:t}) \approx \sum_{i=1}^{N} w_t^i \delta\left(\mathbf{x}_t - \mathbf{x}_t^i\right) \tag{2.20}$$

where $\delta(\mathbf{x}_t - \mathbf{x}_t^i)$ is the Dirac delta function centered at $\mathbf{x}_t^i$. The basic version of the particle filter is called sequential importance sampling (SIS). One important theory behind SIS is the importance sampling. Instead of generating particles according to the target distribution directly, the importance sampling generates particles from a different distribution, which is called proposal distribution. This is because in practice it is usually very hard to draw samples directly from the distribution we want to estimate, while it is much easier to sample according to the proposal distribution. To compensate for the mismatch between the target and proposal distributions, the particles have to be weighted by the perception model given the measurement received by the sensors on the robot. To summarize, the key idea of SIS is to draw particles according to the proposal distribution and weight them, so that they can correctly approximate the posterior probability at the next time step.

The algorithm is shown in Algorithm 1. SIS recursively executes the prediction and the update in the following ways:

1. As shown in Line 3 in Algorithm 1, the prediction step is used to integrate the action information into the Bayesian framework. In particular, a new state hypothesis $\mathbf{x}_t^i$ is generated based on the current state $\mathbf{x}_{t-1}^i$ and the control input $\mathbf{u}_t$. To implement this step, one has to construct the transitional probability $p(\mathbf{x}_t|\mathbf{x}_{t-1}, \mathbf{u}_t)$. It is obvious that the proposal distribution $q(t)$ is:

$$q(t) = p(\mathbf{x}_t|\mathbf{x}_{t-1}, \mathbf{u}_t) p(\mathbf{x}_{t-1}|\mathbf{z}_{1:t-1}, \mathbf{u}_{1:t-1}) \tag{2.21}$$

2. After an action performed by the robot, a new measurement $\mathbf{z}_t$ is perceived by the sensor on the robot. The correction step is executed to incorporate a new measurement into the Bayesian framework, as shown in Line 4 in Algorithm 1. More pre-

cisely, the importance weight w_t^i is updated according to the sensor model $p(\mathbf{z}_t|\mathbf{x}_t^i)$ given the measurement $\mathbf{z}_t$.

3. The weights of the particles are normalized to ensure that the sum of the weights over the entire sample space is one:

$$w_t^i = \frac{w_t^i}{\sum_{i=1}^{N} w_t^i} \tag{2.22}$$

Algorithm 1: Sequential Importance Sampling

Input: previous state: $\mathbf{S}_{t-1} = \{\mathbf{x}_{t-1}^i, w_{t-1}^i\}_{1 \leq i \leq N}$, control input: $\mathbf{u}_t$, measurement: $\mathbf{z}_t$

Output: new set of particles: $\mathbf{S}_t$

$\mathbf{S}_t \leftarrow \phi, \eta \leftarrow 0$
for *i=1 to N* **do**
  $\mathbf{x}_t^i \sim p(\mathbf{x}_t|\mathbf{x}_{t-1}^i, \mathbf{u}_t)$, //draw particle according to the motion model
  $w_t^i \leftarrow p(\mathbf{z}_t|\mathbf{x}_t^i)$, //update the weight according to the sensor model
  $\mathbf{S}_t = \mathbf{S}_t + \{\mathbf{x}_t^i, w_t^i\}$,
  $\eta \leftarrow \eta + w_t^i$
end
//normalize S_t,
for *i=0 to N* **do**
  $w_t^i = \frac{w_t^i}{\eta}$
end
return $\mathbf{S}_t$

The way to build up $p(\mathbf{x}_t|\mathbf{x}_{t-1}, \mathbf{u}_t)$ and $p(\mathbf{z}_t|\mathbf{x}_t)$ is application specific. In the context of robot localization, which cares about the position of the robot in an environment, $p(\mathbf{x}_t|\mathbf{x}_{t-1}, \mathbf{u}_t)$ is modeled as a combination of the odometry and the error models to deal with the uncertainty (i.e. zero-centered Gaussian distributions). The sensor model can be different depending on the way how the likelihood of the current measurement is computed. Fox *et al.* (1999) proposed a beam-based proximity model, which computes the density of a measurement from a laser scanner by integrating the densities of individual beams given the pose of the robot. In the case of RFID-based applications addressed in this thesis, both models (i.e. motion model and sensor model) are straightforward and will be described in the later chapters.

2.3.5 Resampling

The sequential importance sampling (SIS) introduces a phenomenon called particle degeneracy. Most of the particles have small weights close to zero, only a few particles

have high weights. Since the particles with small weights have no or little contribution in the estimation of the posterior, more particles are required to get a good posterior estimation, which needs more computational resources.

An approach to avoid this problem is resampling. In resampling, the particles with small weights are replaced by the ones with higher weights. The resampling is typically performed in a probabilistic way. Precisely, the particles are drawn with probabilities proportional to their weights. After this step, the weights of all particles are set to $1/N$. This finally leads to the sequential importance resampling (SIR), which is also referred to as the plain particle filter. The SIR is same as SIS, but with an additional resampling step. It forces the particles to be set to the areas with high posterior probability and thus focuses on the regions of high interest.

The resampling introduces a problem called particle impoverishment. The particles with high importance weights are selected many times, therefore the diversity of the particles is reduced. In the worst case, all particles might converge into a single particle which leads to the case that the entire distribution is represented by a single particle. Obviously, this violates the original idea of particle filters which aims at estimating the posterior probability density function with a set of distinct samples. In practice, the resampling should not be executed very frequently. It is necessary to find a criterion when resampling should be performed. On the one hand, if one resamples too often, the particle set may lose its diversity. On the other hand, if one resamples infrequently, we might have the degeneracy problem, since too many particles may be wasted in the low probability regions as mentioned before. A typical approach to decide if the resampling is necessary is to check the variance of the weights of the particles. A good measurement of this is the effective sample size (ESS), which is proposed by Liu (1996):

$$N_{ess} = \frac{1}{\sum_{i=1}^{N} \left(w_t^i\right)^2} \tag{2.23}$$

N_{ess} measures how well the particle set approximates the posterior. The worse the approximation is, the larger is the variance of the weights, hence a smaller N_{ess} and more degeneracy. The effective sample size is a useful indicator to determine whether resampling is required or not. As suggested in Doucet *et al.* (2000), the resampling should be executed, if N_{ess} drops below a threshold, e.g. $N/2$.

In the literature, three resampling algorithms have been widely used, which are systematic resampling, residual resampling (or remainder resampling), and multinomial resampling. We use residual resampling throughout this thesis. The choice of the resampling approaches is based on the comparison of different resampling approaches as given in Douc and Cappe (2005).

Another problem that the particle filter brings is particle deprivation. After resampling, there are no samples around the true state. This might be due to the reason that the sample size is too small to cover all possible regions of the state or the motion model is poor to place the particles in the right positions. Solutions to this problem include adding

random particles into the particle set, based on the latest measurements (Lenser and Veloso (2000)), the adaptive particle filter (Gutmann and Fox (2002)), and the mixture MCL (Thrun *et al.* (2000)).

2.4 Modeling of the Characteristics of the UHF RFID

The design of the probabilistic sensor model $p(\mathbf{z}|\mathbf{x})$ which features the likelihood of receiving a measurement $\mathbf{z}$ given the state $\mathbf{x}$ of the system plays an important role in Bayesian state estimation as described in Section 2.3.1. In this section, we survey the related work centered on the modeling of RFID and describe an approach to learn the sensor model. The RFID measurement gives two sources of information $\mathbf{z} = \{d, s\}$: a binary value d which indicates if the tag is detected or not; and the received signal strength s in case the tag is detected. The state $\mathbf{x}$ is the position of the tag we want to estimate, which can be either 2D or 3D. A proper design of the sensor model will give a better estimation and prevent it from diverging. For the path following in Chapter 5, an explicit sensor model is not required.

2.4.1 Related Work

Researchers have developed many techniques to model RFID from different perspectives. In this section, we briefly summarize these approaches based on various criteria. The related work presented here provides a survey of the related techniques used to model passive UHF RFID, but also covers some aspects of active ones.

The most important criterion to distinguish these models is the model variables. Depending on the RFID readers, the model can characterize the detection likelihood or received signal strength or both. Since the early RFID readers did not provide any signal strength information, only detection likelihood is considered into the sensor model (Hähnel *et al.* (2004), Alippi *et al.* (2006), Liu *et al.* (2006), Vorst and Zell (2008), and Vorst *et al.* (2008b)). The new generation of RFID readers does provide signal strength measurement of a detected tag, therefore some researchers integrate the signal strength into the sensor model to gain a more accurate representation of the sensor model (Hodges *et al.* (2007), Milella *et al.* (2008), Joho *et al.* (2009), Deyle *et al.* (2009), Liu *et al.* (2011), and Liu *et al.* (2013)).

Sensor-centric models (Hähnel *et al.* (2004), Vorst and Zell (2008), Joho *et al.* (2009), Deyle *et al.* (2009), and Liu *et al.* (2013)) only consider the characteristics of the tags in the antenna frame, i.e. the likelihood of a measurement given the displacement of the tag with respect to the antenna. However, due to the influence of the environment (see Section 2.1.4), the radio signal propagation highly depends on the location of the tag in a global environment. Therefore, many researchers focus on location-dependent representations (i.e. snapshots or fingerprints) of the sensor model (Schneegans *et al.* (2007), Vorst *et al.* (2008b), Liu *et al.* (2011), and Liu *et al.* (2012)). Both approaches

have their own advantages and disadvantages. The location-dependent approaches are able to capture the environmental factors that sensor-centric models are not able to cover, such as the materials the tags are attached to, the orientations of the tags relative to the antenna, or the obstacles that reflect or absorb electromagnetic waves. But location-dependent approaches require a time-consuming process of data recording and are also computationally expensive due to the comparison of these measurements. Therefore, for mapping or tracking of RFID tags, we prefer to use a sensor-centric model as detailed in Chapter 3, Chapter 4, and Chapter 6, while for the path following task in Chapter 5, we choose the location-dependent representation (i.e. fingerprints).

Another criterion to classify the approach of modeling RFID is the dimensionality. Some researchers used a 1D sensor model, which gives the likelihood of a measurement given the distance (Hightower *et al.* (2000), Ramadurai and Sichitiu (2003), Kloos *et al.* (2006), Whitehouse *et al.* (2006), and Schmid *et al.* (2011)) or the bearing to the tag (Kim *et al.* (2007), Zhang *et al.* (2007), Milella *et al.* (2009), Deyle *et al.* (2009), and Germa *et al.* (2010)). By integrating the measurements from multiple antennas, one is able to infer the 2D or 3D locations of the RFID tags. Other researchers have focused on a 2D sensor model which characterizes the x and y displacement of the tag with respect to the antenna (Kantor and Singh (2002), Hähnel *et al.* (2004), Ferris *et al.* (2006), Vorst and Zell (2008), Deyle *et al.* (2008b), Milella *et al.* (2008), and Joho *et al.* (2009)). 3D sensor models additionally consider the heights of RFID tags to better characterize the behavior of radio signal propagation and thus are able to improve the mapping accuracy of RFID tags as well as the localization accuracy of the robot (Mallinson *et al.* (2006), Hodges *et al.* (2007), Gerold (2007), and Liu *et al.* (2013)). Some researchers also consider the configurations of the reader as the parameters of the models, i.e. power level (Alippi *et al.* (2006), Deyle *et al.* (2008a), Chawla *et al.* (2010), and Lee *et al.* (2013)) or attenuation (Ota *et al.* (2008), Alghamdi and van Schyndel (2012), and Alghamdi *et al.* (2013)).

The sensor models can be notably different, depending on the way of deriving them. Some models in the literature are designed through the theoretical analysis of the signal propagation (Deyle *et al.* (2008b) and Mallinson *et al.* (2006)), while some researchers, including us, aim at empirically building up the model from the measurements collected through the environment (Hähnel *et al.* (2004), Joho *et al.* (2009), and Vorst and Zell (2008)). Typically, the derivation of the theoretical model is based on the theory of Friis equation, as described in Section 2.1.3. Some techniques that heuristically combine both approaches are also investigated in the literature (Milella *et al.* (2008) and Ota *et al.* (2008)). The advantage of the theoretical model is the mathematical representation of the sensor model, which can be easily transplanted into other systems without much revision. Moreover, only a small number of parameters are needed to represent the theoretical model, therefore less memory is required as compared to the empirical model. However, the propagation of the radio signal is highly influenced by many environmental factors and it is difficult to consider all aspects into a simple theoretical model. Thus, empirical models are much more efficient to capture these features in practice. Yet a large amount of prior training data is required to build up the empirical model.

Moreover, the model can be represented either deterministically or probabilistically. One example of a deterministic model is a proximity model, which represents the presence of an object in the close region to the antenna. This region is typically represented by a combination of arced regions (Mehmood *et al.* (2008), Raoui *et al.* (2009), and Germa *et al.* (2010)). Here we prefer a probabilistic sensor model (Hähnel *et al.* (2004), Milella *et al.* (2008), Vorst and Zell (2008), Joho *et al.* (2009), and Liu *et al.* (2013)) due to the noisy nature of RFID, as stated in Section 2.1.3.

2.4.2 Sensor Model

The sensor model is essential for the mapping or tracking of RFID tags. As concluded in Section 2.1.3, the most relevant parameter of the sensor model is the displacement of the tag in the antenna frame. Formally, we want to know the likelihood of receiving a measurement $\mathbf{z}$ at the relative position of the tag $\mathbf{x}$ in the antenna coordinate frame. Early RFID readers only provide a binary variable d which indicates if the tag is detected or not. This results in the so called tag detection sensor model.

$$p(\mathbf{z}|\mathbf{x}) = \underbrace{p(d|\mathbf{x})}_{\text{detection likelihood}} \tag{2.24}$$

The tag detection likelihood $p(d|\mathbf{x})$ is approximated as the ratio of positive detections (n^+) to total read attempts, i.e. a sum of positive detections and negative detections (n^-),

$$p(d|\mathbf{x}) = \frac{n^+}{n^+ + n^-} \tag{2.25}$$

Since the new generation of RFID readers also provides the signal strength information, it is straightforward to incorporate both sources of information (i.e. the detection and the signal strength) into the sensor model, which leads to the combined sensor model. The additional treatment of the signal strength gives a significant improvement of mapping and localization accuracy as shown by Joho *et al.* (2009). To be precise, in the combined sensor model, the likelihood of a measurement is formalized as:

$$p(\mathbf{z}|\mathbf{x}) = \underbrace{p(d|\mathbf{x})}_{\text{detection}} \underbrace{p(s|d,\mathbf{x})}_{\text{RSS}} \tag{2.26}$$

We further assume that the signal strength distribution is Gaussian, with a mean $\mu_{\mathbf{x}}$ and a standard deviation $\sigma_{\mathbf{x}}$:

$$s \sim \mathcal{N}(\mu_{\mathbf{x}}, \sigma_{\mathbf{x}}). \tag{2.27}$$

Therefore, the likelihood of receiving a signal strength s given the relative tag pose $\mathbf{x}$ in

the antenna coordinate frame is computed as:

$$p(s|d,\mathbf{x}) = \frac{1}{\sqrt{2\pi}\sigma_{\mathbf{x}}} \exp\left(-\frac{(s-\mu_{\mathbf{x}})^2}{2\sigma_{\mathbf{x}}^2}\right). \tag{2.28}$$

An alternative to the Gaussian-based approach is the histogram-based approach (Ladd *et al.* (2005)), which is also commonly used for modeling the signal strength in the related literature. Precisely, in the case of the histogram-based approach, the distribution of the signal strength is represented by normalizing the histogram intensity of the radio signal in the training data. The advantage of the histogram-based approach is the capability of modeling the non-Gaussian features of the radio signal due to various impacts from the environment. But the Gaussian models seem to provide the same accuracy as the histogram-based approach (see Ladd *et al.* (2005) and Haeberlen *et al.* (2004)). Moreover, the Gaussian-based models have the following advantages. First, the memory needed for storing a Gaussian-based model is much less in contrast to the histogram-based model. We only need two parameters to represent the Gaussian-based model, while the number of parameters required for storing a histogram is equal to the number of the entire signal strength values. Second, building up a histogram-based model requires a large amount of training data, while fitting a Gaussian only requires a small number of samples.

2.4.3 Semi-autonomously Learning of the Sensor Model

In order to generate the perception model (i.e. sensor model), some researchers used supervised approaches to record the measurements by varying the relative pose of the antenna and the tag. For example, Hähnel *et al.* (2004) rotated the robot in front of a tag affixed to a box. By repeatedly doing this at various distances to the tag and counting the reading rate at discrete grids, they obtained a grid-based representation of the sensor model.

The disadvantage of the supervised approach is that the recording phase takes a lot of time if only one tag is involved in the experiment. Moreover, this approach is based on the assumption that all tags have the same characteristic and the data is usually recorded under a rather controlled environment (i.e. without occlusions and other tags around) which is certainly not the case in practice, due to many influencing factors from the environment.

We utilized the semi-autonomous approach proposed by Vorst and Zell (2008) to learn the sensor model from empirical measurements. The idea behind this approach is to utilize the fact that the mobile robot can be localized by a rather accurate localization mechanism, for example laser-based Monte Carlo algorithm, and thus it can explore the environment and meanwhile collect the RFID measurements. This approach has been extended by Joho *et al.* (2009) in a fully unsupervised fashion. To build up the sensor model, a list of reference tags, whose positions are known, must be installed in the

environment beforehand. The sensor model, therefore, is learned by means of averaging the characteristics of tags across the entire database. Note that, in order to achieve a good position estimation in the mapping stage, the arrangement of the reference tags should be similar to the target scenario.

More precisely, the robot has to collect the measurements by traversing the environment either autonomously or manually in an exploration stage. During this stage, the RFID detections and the positions of the robot as well as the odometry data are stamped and recorded. Particularly, the position of the robot is estimated by a laser-based Monte Carlo localization algorithm. Based on the recorded measurements, an off-line stage is performed to generate the sensor model following the steps described below:

- **Data Preprocessing:** At each time step, the relative positions of the reference tags in the antenna coordinate frame are computed, given the global pose of the robot and the positions of the tags as well as the transformations between the antennas and robot. In this way, each tag produces a sample, which consists of the position $\mathbf{x}$ in the antenna coordinate frame and a measurement $\mathbf{z} = \{d, s\}$, which tells whether or not the tag is detected (i.e. $d = 1$ if the tag is detected, otherwise $d = 0$) along with its signal strength s. Let us denote the maximum reading range of the RFID reader to be D. We further constrain the dimensions of our sensor model to be [-2:D][-D/2:D/2] for x and y respectively. The samples whose positions are out of this range are ignored. The x-coordinates are allowed to be negative, since the antenna sometimes is able to detect the tags behind it. The choice of the y range is due to the symmetrical nature of the sensor model around the x-axis.

- **Model Generation:** We use these raw samples to compute the conditional probability density function $p(\mathbf{z}|\mathbf{x})$ of perceiving a measurement $\mathbf{z}$ given the relative position of the tag and antenna. This function is used as a representation of the sensor model and applied to the correction step of the particle filter for mapping and tracking of RFID tags. Throughout this thesis, we used a grid-based representation of the sensor model. The entire space of the model is discretized into two dimensional grids. For each grid (x, y), we count the positive detections $n^{+}_{(x,y)}$ and the negative detections $n^{-}_{(x,y)}$ and thus the detection likelihood is modeled as:

$$p(d|(x,y)) = \frac{n^{+}_{(x,y)}}{n^{+}_{(x,y)} + n^{-}_{(x,y)}} \tag{2.29}$$

  Similarly, we compute the statistics of the signal strength for each grid (x, y), which is represented by a Gaussian with mean $\mu_{(x,y)}$ and standard deviation $\sigma_{(x,y)}$.

- **Model Storage:** For each grid cell, we pre-compute the likelihood of receiving a positive detection with all possible signal strength values according to Equation (2.28) and store them as a look-up table. In this case, the memory required for

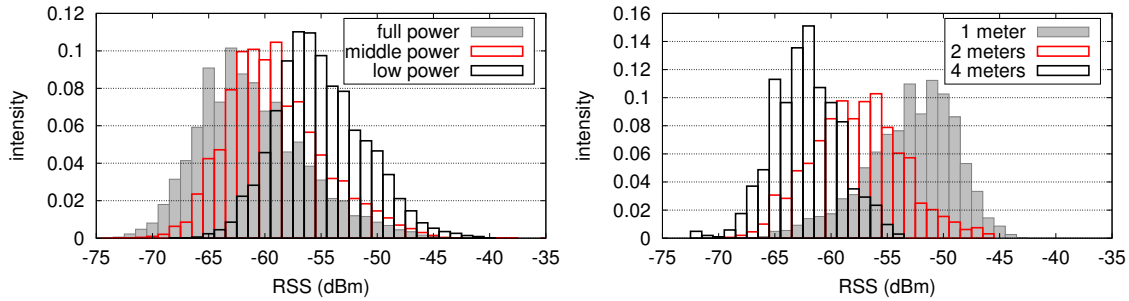

(a) RSS histogram with different power levels.

(b) RSS histogram at different distances.

Figure 2.7: (a) Histograms of the signal strength under different power levels; (b) Histograms of the signal strength at different distances. Note the histograms visualized here are normalized.

storing the model is proportional to the band of the signal strength and the grid size used for discretization. The grid size has to be chosen carefully: a large grid size may not be able to describe the details of the probability density function, while a too small grid size may lead to the overfitting problem, since small number of samples are not enough to give a good estimation of the probability density function in a given grid.

2.4.4 Experiments

We used the approach described in Section 2.4.3 to evaluate the reader characteristics under various configurations. The goal here is to obtain the sensor model for the purposes of mapping and tracking RFID tags based on the empirical measurements collected by the robot. The data was collected with our Scitos G5 service robot as shown in Section 1.4.2. We equipped the robot with two antennas at a height of 0.8 m and at angles of $\pm 45^{\circ}$ towards the forward moving direction of the robot.

To establish the sensor model, we placed 47 UHF RFID (Alien Technology Squiggle) tags at the height of the antennas with known positions on the walls of the corridor, which is adjacent to the robot lab (see Section 1.4.1) with a traversable area of approx. 90 m^2. In order to evaluate the influence of the environmental factors, we also placed tags on a bottle of water and on a metal box. The robot was manually steered at different trajectories with a maximum forward velocity of 0.3 m/s. The frequency of the reader was set to 2 Hz. The robot traveled approx. 2 km and 9 log files were recorded at the same time using the full reader power configuration (30 dBm). Each log file consists of at least 600 RFID measurements and the true positions of the robot. We also recorded three log files with the middle power level (i.e. 27 dBm) and three with the low power level (i.e. 22 dBm) to evaluate the model variances under the influence of different power levels.

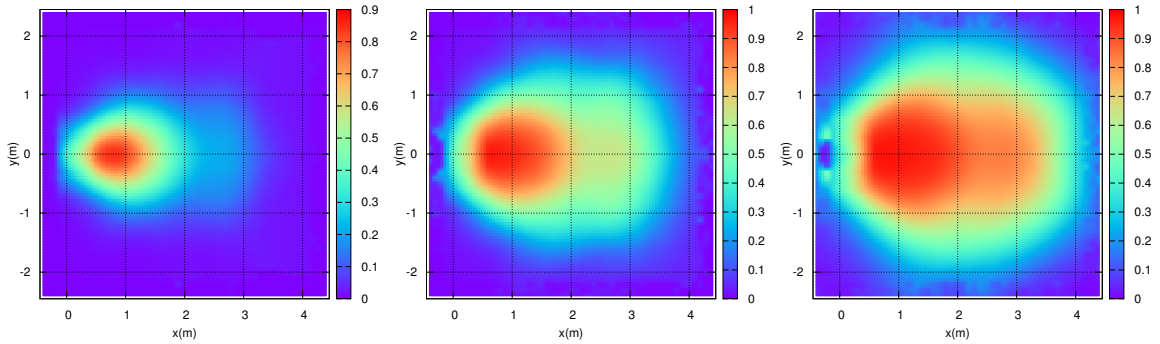

(a) Low power level (22 dBm) (b) Middle power level (27 dBm) (c) High power level (30 dBm)

Figure 2.8: Detection likelihood under different power levels.

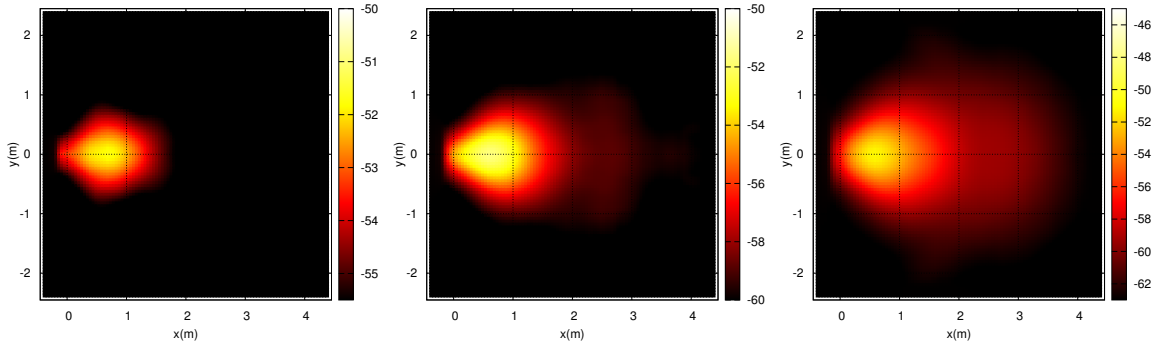

(a) Low power level (22 dBm) (b) Middle power level (27 dBm) (c) High power level (30 dBm)

Figure 2.9: Mean signal strength under different power levels.

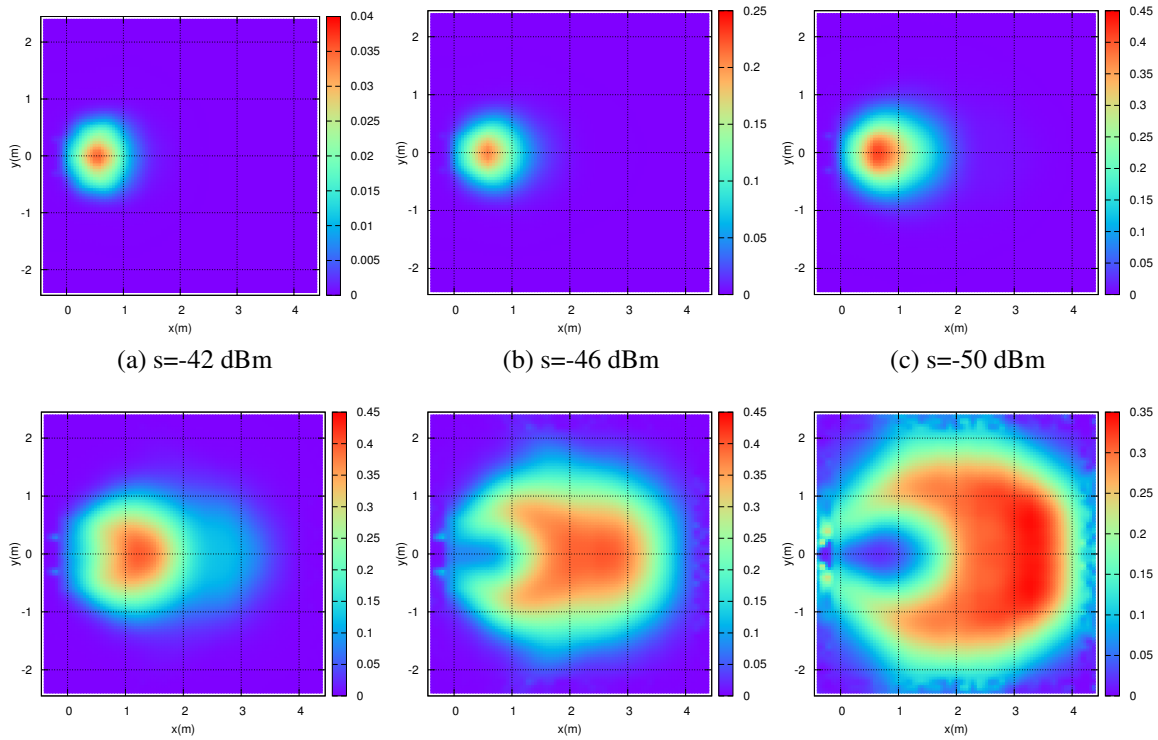

(a) s=-42 dBm (b) s=-46 dBm (c) s=-50 dBm

(d) s=-54 dBm (e) s=-58 dBm (f) s=-62 dBm

Figure 2.10: Likelihood of receiving a measurement with a specific signal strength.

Detection Characteristics with Different Power Levels

To understand the tag detection characteristics under the impact of different reader power levels, we first compared the tag detection model and the mean signal strength with respect to different reader power levels. Only Alien Technology Squiggle tags placed on the walls were used to generate the sensor model in this series of experiments. The grid size of the sensor model was set to 0.1 m. The distributions of the signal strength over various power scales are visualized in Figure 2.7a. As one can see in Figure 2.7a, with a higher reader power level, the reader is able to provide a wider range of the signal strength (see [-72 dBm:-38 dBm] for the high power level and [-68 dBm:-38 dBm] for the low power level), since the tag requires a minimum power to energize its circuitry (see Section 2.1.3), which leads to a change of the signal strength distribution in accordance with the changes of the reader power. The distributions of the signal strength at different distances are visualized in Figure 2.7b. One can infer that the distribution of the signal strength can be fitted with a Gaussian very well. Moreover, the signal strength with a large distance is smaller than the one with a small distance. For example, the mean signal strength at 4 meters is about -62 dBm, as compared to -57 dBm at 2 meters.

The detection likelihood and the mean signal strength with reference to different reader

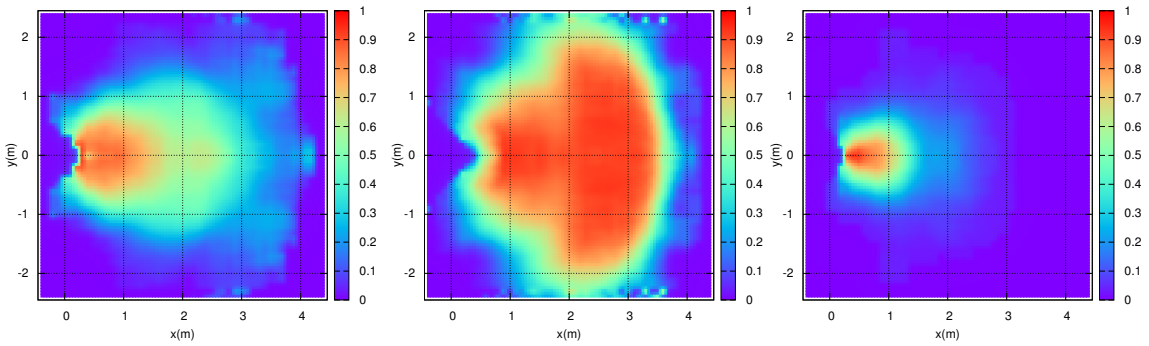

(a) Impinj jump jack (b) OMNI-ID large (c) OMNI-ID small

Figure 2.11: Detection likelihood of different types of RFID tags.

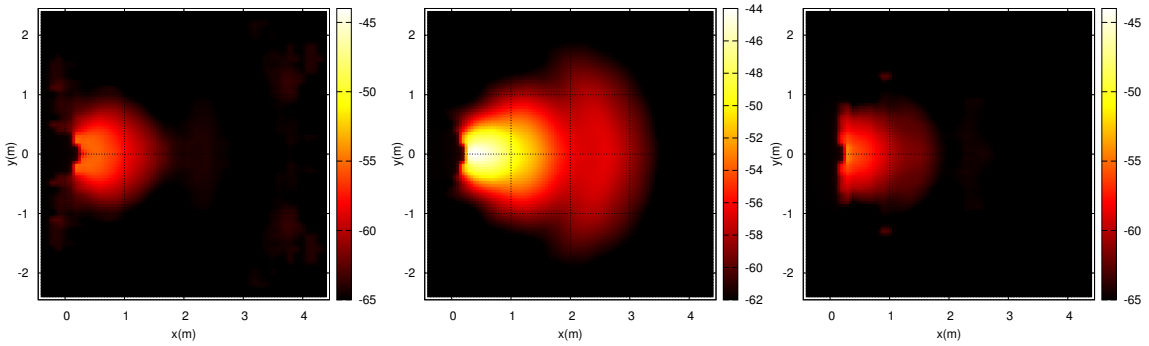

(a) Impinj jump jack (b) OMNI-ID large (c) OMNI-ID small

Figure 2.12: Mean signal strength of different types of RFID tags.

power levels are visualized in Figure 2.8 and Figure 2.9, respectively. As shown in Figure 2.8, the detection range with a high power level is larger than the one with a low power level. Additionally, one can notice that the propagation of the radio wave is highly directional, since the detection mainly happens in the positive x-axis. The reader sometimes is able to detect the tag beyond 6 meters at the full reader power level. Detections in the negative x-axis, i.e. behind the antenna, happen rarely. Moreover, the detection region does not follow a strict confined shape: there is a transitional region from high detection probability to low detection probability. Combining the signal strength model (i.e. mean signal strength as shown in Figure 2.9 and the standard deviation which is not shown here) and the tag detection model (see Figure 2.8), we are able to compute the combined sensor model, as shown in Figure 2.10, which visualizes the likelihood of detecting a tag with a given signal strength. As can be seen in Figure 2.10, a higher signal strength provides a strong belief about the position of the tag, while a lower signal strength introduces uncertainty about the position of the tag.

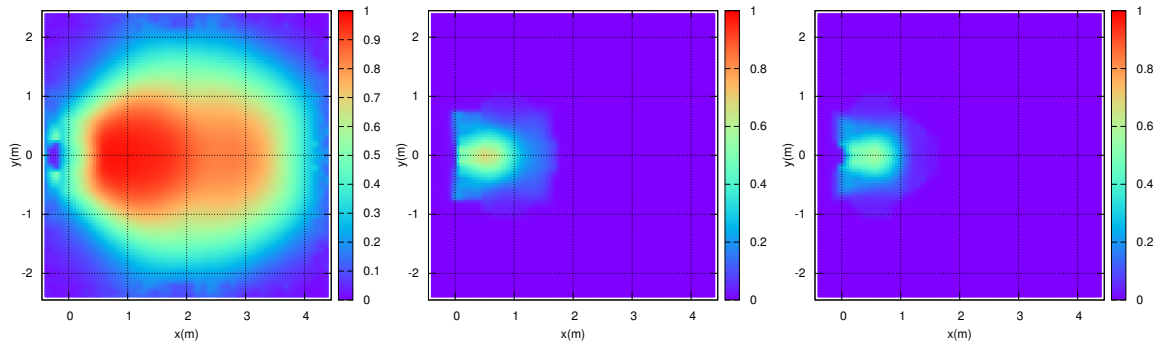

(a) The standard case (tags attached on the walls)

(b) Tag attached to a water bottle

(c) Tag attached to a metal box

Figure 2.13: Detection likelihood under the influence of different materials.

Detection Characteristics of Different Types of Tags

Different types of tags may have various characteristics. In order to show this, we generated sensor models of another three types of RFID tags, namely OMNI-ID large tag, OMNI-ID small tag, and Impinj Jumping Jack tag. These models are generated with the full reader power level, as shown in Figure 2.11 (detection likelihood) and Figure 2.12 (mean signal strength). As shown in Figure 2.11 and Figure 2.12, the characteristics of different types of tags can be drastically different. OMNI-ID small tags have the shortest reading range, and OMNI-ID large tags have the largest reading range. Impinj Jumping Jack tags have a smaller reading range as compared to Alien Technology Squiggle tags (see Figure 2.8c) and the OMNI-ID large tags, while they provide a larger reading range than OMNI-ID small tags. The statistics of the signal strength are also different as can be seen in Figure 2.12. The OMNI-ID large tags seem to be able to provide a higher signal strength value than other types of RFID tags, while the OMNI-ID small tags give a relatively lower signal strength value. Evaluating the behavior of different RFID tags is helpful in achieving good mapping results, as shown in Chawla *et al.* (2013). We usually choose the tags that have larger reading range, since this tends to give more tag detections, which will lead to better inventory performance and mapping results.

Detection Characteristics of Tags Affixed to Different Objects

Up to now, all of the RFID sensor models are generated in a relatively ideal or controlled environment (i.e. the tags are affixed to walls without any interference of the material nearby). It is reasonable to apply this sensor model in controlled infrastructures. However, in practice, the mobile robot has to deal with the tags affixed to any kind of objects. For example, metal shelves, which are commonly used for many industrial environments due to the low price and mobility, may have a high influence on the readability and the signal strength of RFID tags. Many products, which contain water also challenge the

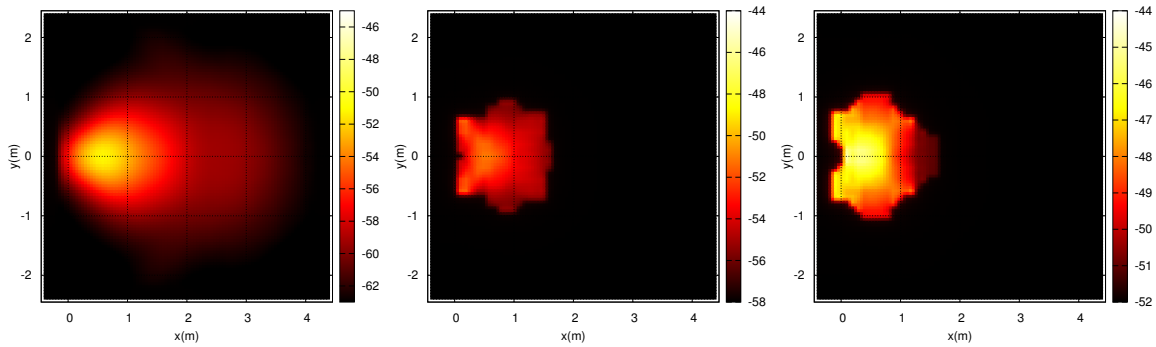

(a) The standard case (tags attached on the walls)

(b) Tag attached to a water bottle

(c) Tag attached to a metal box

Figure 2.14: Mean signal strength under the influence of different materials.

readability of the tags. To show the variance of the sensor models, we fixed the tags to two different objects, namely a bottle of water and a metal box. The resulting tag detection model and the mean signal strength are shown in Figure 2.13 and Figure 2.14, respectively. One can see the deviation of these sensor models is quite significant. The reading ranges in both cases become smaller, while the signal strength is quite different: the average signal strength of the tag affixed to a water bottle gets lower due to the absorptions of the water, while the signal strength in the case of metal box becomes higher due to the reflections of the metal.

Unfortunately, the literature related to the mapping of UHF RFID tags paid very little attention to the problems of the model variances. Most of the experiments in the related work were conducted in controlled environments. This is one reason why the traditional particle filters have the problem of mapping failures under uncontrolled environments, which is addressed in the next chapter. Obviously, one could think of designing a sensor model for individual RFID tags, since each tag provides a unique identifier; however, the huge effort involved in this process prevents its usage in extensive applications.

Memory Storage and Time Consumption

The time used to generate the sensor model and the memory required to store the sensor model under different grid sizes are compared in Table 2.2. The experiments were conducted based on processing nine log files recorded at full power level using an Intel Core i5-2410M@2.3 GHz CPU, with 4 GB RAM. As seen in Table 2.2, storing a model with a smaller grid size requires more memory than a larger grid size. Moreover, computing the sensor model with a smaller grid size obviously takes more time than a larger grid size. Since the sensor model is generated in an off-line fashion, the computational time is not an issue in our case.

Table 2.2: Analysis of the time used for computing the sensor model and the memory required for storing the sensor model under different grid sizes.

Grid size [m]	0.01	0.05	0.1	0.2	0.5
Time consumption [s]	874.47	36.67	8.75	1.43	0.22
Memory consumption [MB]	98.65	8.28	2.82	0.85	0.15

2.5 Conclusions

In this chapter, various RFID sensing technologies were introduced for the identification of tags through radio waves. The techniques can be different based on the radio frequencies and the sources of power supply. Particularly, the passive UHF RFID, which is used in many industrial environments nowadays, provides a way of identification without line of sight. We discussed the opportunities and challenges of using UHF RFID as a sensing technology for mobile robots. On the one hand, RFID tags can be affixed to items and automate the traditional inventory process. From the perspective of mobile robots, these tags can be additionally used as landmarks for the localization or navigation. On the other hand, the long range passive UHF RFID faces some challenges: the radio signal is hard to model, since it is extremely sensitive to reflections, diffractions, or absorptions of the environment.

In Section 2.2, the key coordinate frames used in this thesis are clarified and the motion model of the robot is described. We presented three popular probabilistic estimation approaches, namely histogram filters, Kalman filters, and particle filters, for the state estimation. Different approaches have their own advantages and disadvantages, but all of them are designed to deal with the uncertainty and derived under the Bayesian probabilistic framework. Especially, we described the particle filter in detail, which is chosen and mainly used in this thesis.

In Section 2.4.3, we described the semi-autonomous approach to learn the sensor model. The sensor model is generated by the empirical measurements collected by the mobile robot during an exploration phase. We conducted extensive experiments to study the behavior of RFID under different reader power levels, various tag types, and different materials that the tags are attached to.

Based on the measurements collected by the robot, the semi-autonomous approach is able to reduce the human intervention for the model generation. Yet, the positions of the reference tags have to be measured in advance. Joho *et al.* (2009) proposed a fully unsupervised approach to learn the sensor model based on a coarse detection sensor model without having any information about the true tag positions. They also showed that their sensor model is comparable to the one produced by the semi-autonomous approach.

In some applications, it is necessary to generate the sensor models with respect to different reader configurations (i.e. reader power levels). For example, integrating the measurements from different reader power levels helps to quickly localize RFID tags

(Lee *et al.* (2013) and Deyle *et al.* (2008a)). However, learning the models with different reader parameters is significantly hard and time-consuming, since each configuration requires a large number of measurements to be recorded by the robot. A simple idea for saving human effort is to downscale the sensor model at full read power level or interpolate the sensor models for different power levels.

In the subsequent chapters, we are going to use the techniques described in this chapter for the purpose of mapping RFID tags, path following for the mobile robot, and tracking dynamic RFID tags.

Chapter 3

Mapping of RFID Tags

In this chapter, we address the problem of mapping RFID tags, particularly in 2D using a probabilistic framework with a mobile robot. The rest of this chapter is organized as follows. After an introduction in Section 3.1, we review the related work in Section 3.2. Then, we describe the Bayesian framework for localizing RFID tags in Section 3.3. The implementation of a particle filter is presented in Section 3.4 and Section 3.5. We introduce a sensor resetting technique in Section 3.6 and present how to integrate negative information in Section 3.7. Finally, we show the experimental results in Section 3.8 and summarize this chapter in Section 3.9.

3.1 Introduction

Robot-assisted applications in commercial surroundings such as supermarkets, warehouses, and logistics centers have drawn more and more attention. For these environments, there is an increasing use of UHF RFID tags for labeling products, assets, or equipments. If a robot is equipped with an RFID reader in such environments, an automated inventory becomes possible. Compared to the traditional inventory process, the products can not only be itemized but also be localized by a sequence of RFID readings (Hähnel *et al.* (2004), Joho *et al.* (2009), and Vorst (2011)) from a mobile RFID reader. Although RFID technology solves the object identification problem trivially due to the unique identifier of the tag, it does not provide any location information about the object. The RFID-based mapping aims at acquiring a spatial arrangement of the RFID tags in the environment. The resulting map gives the location information about the tags, which can help the user to find the missing objects or reason about which object is relocated. Moreover, it can also serve as a reference for the robot localization (Hähnel *et al.* (2004) and Vorst *et al.* (2011)) or navigation (Kulyukin *et al.* (2004)).

However, mapping of RFID tags is quite challenging. On the one hand, the measurements (e.g. tag detection or signal strength) of the UHF RFID highly depend on the relative position of the tag to the antenna. On the other hand, the propagation of radio waves is hard to model due to the influence of many environmental effects (e.g. reflection, diffraction, or absorption). The RFID reader may report rather different received signal strength values, even if the relative pose between the tag and the antenna is

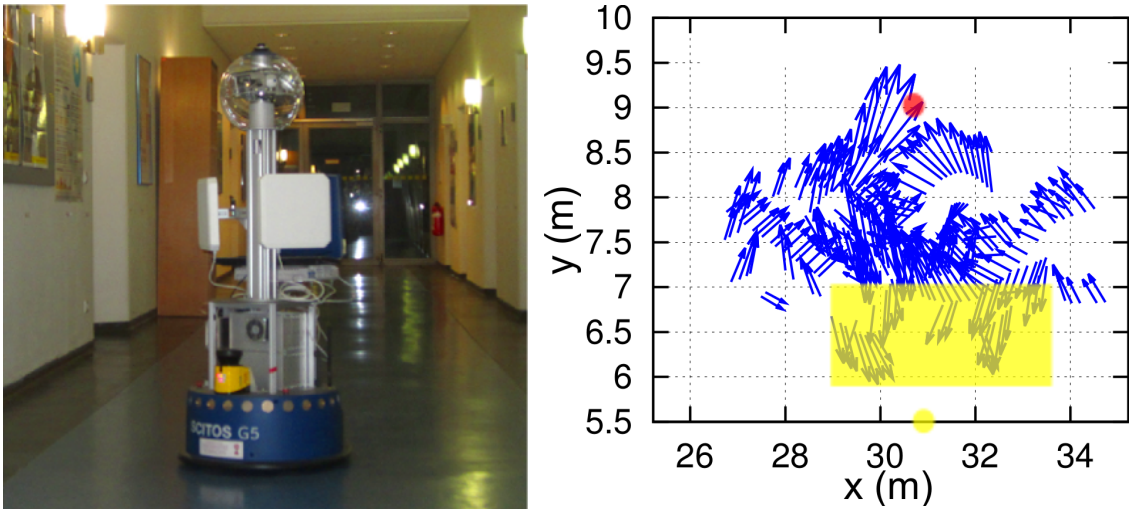

(a) Robot in a corridor environment

(b) Detection events of a tag

Figure 3.1: The scenario where the robot was collecting RFID measurements in an RFID-tagged corridor environment. (a) A snapshot of the environment and the robot. Several post boards, made of metal, are placed on the walls of the corridor. (b) The detection events (blue vectors) of one tag. The lengths of the vectors are scaled according to the values of the signal strength. The true tag position is marked with a red circle.

constant.

As can be seen in Figure 3.1b, which depicts the detection events obtained by our robot (see Figure 3.1a) of one tag in a corridor environment. Since the tag locates very close to the metal board, we observed many ghost detections (marked with yellow box). If these ghost detections are integrated into the particle filter at first, after performing resampling, there will be no particles around the true position of the tag. Therefore, the particle filter converges to the wrong positions (the yellow circle) and the normal particle filter is not able to recover from these failures. Another reason that may lead to mapping failures is that the robot stays at one local area and continuously makes measurements inside that area (see Deyle *et al.* (2008b) for more information).

Therefore, in this chapter, we use the adaptive particle filter (also called adaptive Monte Carlo localization (AMCL)) to recover from mapping failures of static RFID tags and localize non-static RFID tags. We distinguish non-static tags from dynamic ones in this chapter, since dynamic tags are always moving, whereas this chapter focuses on non-static ones, whose positions do not change frequently. Our work is motivated by the fact that in the future the robot is able to continuously perform inventory in RFID-equipped infrastructures (e.g. libraries or supermarkets): the robot has to map the positions of all tags attached to the items on-line; meanwhile the items may be moved (re-located) by the customers. For human-robot interaction, the robot is asked to find specific items or missing items during its operation. We also incorporate the negative information into

AMCL to improve the mapping accuracy and accelerate the speed of recovery from mapping failures and relocalizations of non-static RFID tags. Additionally, we compare the particle filter-based approach to our previous grid-based Markov localization approach. This chapter is based on our IAS publication (Liu and Zell (2014)).

3.2 Related Work

Mapping RFID tags with a mobile robot, which is addressed in this thesis, is a special way of localizing RFID tags by means of a number of measurements perceived by a mobile reader with known positions in an environment. For many industrial environments, a common and cheap way for localizing RFID tags is to install multiple RFID readers at different positions in the environment (Chawla *et al.* (2010), Azzouzi *et al.* (2011b), Azzouzi *et al.* (2011a), and Shirehjini *et al.* (2012)). The smart shelf is an example of this case (Lau *et al.* (2008), Medeiros *et al.* (2008), and Choi *et al.* (2012)).

3.2.1 Mapping with Fixed Antenna Configurations

The coarse position of the RFID tag can be determined through a way called proximity: the detection of a tag from an antenna with a known position tells that the tag is nearby without any tag ambiguity. By using the measurements from several RFID antennas, whose detection regions intersect, the positions of the tags can be further refined. Alippi *et al.* (2006) proposed a method for localizing passive RFID tags based on Bayesian approach by installing several RFID readers in the environment. Particularly, the tags are localized by scanning each angular sector at different power levels with an RFID reader. The mean mapping error of this approach is approx. 0.65 m with four readers transmitting at 0.1-3 W in an environment with a size of 5 m$\times$4 m.

Bahl and Padmanabhan (2000) proposed a system called RADAR, based on radio-frequency (RF) to locate and track users inside buildings. RADAR achieves the localization of an object by triangulating the signal strength from multiple base stations based on the empirical measurements and the signal propagation models. Their system is able to localize the target with an accuracy of 2 to 3 meters. LANDMARC presented in Ni *et al.* (2003) is a location sensing system which aims at locating RFID tags affixed to objects in indoor environments. In order to improve the overall localization accuracy, a large number of reference tags are utilized with a configuration of a grid array. The position of the tag is determined by fusing the positions of its four nearest neighbored tags. This system has to rely the signal strength to approximate the distance from the tag to the reader. However, the RFID reader in their experiments is not able to provide any measure about the signal strength; therefore, in order to estimate the signal strength of a tag, they have to perform a scan with various reader power levels, which requires approximately one minute each time. The unnecessary scanning time can be eliminated using the new generation of RFID readers which reports the signal strength directly. As

reported by the author, with four readers installed in a lab with a size of 4 m$\times$7 m and one reference tag per square meter, they are able to localize the objects with a mean error of 1 meter and the worst error of 2 meters.

Chawla *et al.* (2010) proposed a multi-antennas framework that allows to quickly and precisely localize static as well as mobile tags. By varying the power levels of the antennas, the positions of tags are determined via the empirical power-distance relationships, which are calibrated using reference tags with known positions. They also used multi-tags to reduce the uncertainty of the estimation. They are able to localize the tags with an accuracy of 15 cm in a few seconds. Their experiments were only conducted in a limited environment (a rectangular region with an area of 6 m^2) and the application of their approach in cluttered environments needs to be investigated.

Choi *et al.* (2012) proposed an approach to localize the objects tagged with passive UHF RFID tags on a smart shelf using a single RFID reader antenna. Their approach also needs to rely on the reference tags for the position estimation. But in contrast to the previous *k*-nearest neighbors (KNN) algorithm, they infer the presence of a neighboring tag using the changes of a tag's readability. According to their experiments with nine box-level objects on two wooden shelves with a total size of 91 cm$\times$152 cm, they achieved a mean accuracy of 18.48 cm, which gives an approx. 70% improvement as compared to the previous KNN algorithm.

3.2.2 Mapping with Mobile Antenna Setups

Rather than placing multiple RFID antennas at fixed positions to infer the positions of RFID tags, many researchers, including us, prefer to map RFID tags by moving a mobile robot carrying an on-board RFID reader to various positions in an environment. The position of the robot is usually determined by another positioning system, such as laser-based Monte Carlo localization. In this case, the locations of the tags are inferred by integrating several observations at different positions.

A number of approaches have been proposed to locate (i.e. map) the RFID tags using mobile RFID readers. These approaches mainly differ based on how the sensors are modeled (see Section 2.4) or which approach is used to infer the positions of the tags (i.e. histogram filters, Kalman filters, or particle filters). However, the problems of mapping tags under uncontrolled environment are rarely addressed.

Hori *et al.* (2008) proposed a multi-sensing-scheme to locate an RFID tag using a mobile RFID reader. In particular, they used a probabilistic framework to integrate the measurements from a reader by varying its sensing range. Combining with different movements of the robot, the estimation error of the tag can be reduced. However, the experiments were only conducted in computer simulations.

Some researchers (Kleiner *et al.* (2006) and Kleiner *et al.* (2007)) utilized RFID technology for search and rescue tasks in disaster areas. They proposed an approach which enables the robot to solve the problem of simultaneous localization and mapping (SLAM) based on RFID tags distributed in the environment. Additionally, they showed that RFID

tags can be used to coordinate the exploration of a team of robots. In their work, they assume the tag detections are within a range of 1 m in order to provide a good positioning accuracy. Therefore, only HF RFID tags (Ario RFID chips from Tagsys and a Medio S002 reader that provides a maximum reading range of 30 cm) were used in their experiments. For an extension of this approach to UHF RFID tags, one can refer to Vorst and Zell (2010b) and Forster *et al.* (2013).

Ferret and Sherlock are two systems that are proposed in Liu *et al.* (2006) and Nemmaluri *et al.* (2008) for the localization of static as well as nomadic tags (tags that do not change locations frequently) in a room or an office environment. The first system utilized the mobility of a user who carries a hand-held RFID reader to produce several readings from multiple perspectives. The location of the object can be inferred by refining the coverage regions at these views. The second system aimed at localizing the objects by scanning the environment with steerable RFID reader antennas at fixed positions. However, the localization time took so long that it limits the further applications of these approaches. For example, Ferret needs approx. 2 minutes to localize an object, while Sherlock requires about 1 minute to perform a fast scan.

Hähnel *et al.* (2004) utilized a probabilistic sensor model to estimate the positions of RFID tags with a mobile robot, whose poses were determined by a laser-based FastSLAM approach in a known environment. Joho *et al.* (2009) improved the mapping accuracy by modeling the characteristics of both signal strength and tag detection events. Milella *et al.* (2008) estimated the positions of RFID tags by a fuzzy logic using a fuzzy RFID antenna model. Rather than designing the models from empirical data, Deyle *et al.* (2008b) derived the model based on radio signal propagation using the Friis equation for the localization of RFID tags. The signal strength there was approximated by switching the reader power between nine different values. Moreover, some researchers also fused the measurements from other sensors to improve the mapping accuracy, which will be detailed in Chapter 6.

Ehrenberg *et al.* (2007) designed a system called LibBot, which utilized a mobile robot equipped with an RFID reader for the purpose of inventory in a library, where all books were equipped with HF RFID tags. The proposed system can be used to localize the books and detect the misplaced books. Since HF sensors have a short reading range (i.e. approx. 15 cm for the reader used by the authors), the misplaced tags can be detected reliably. As reported by the authors, they are able to localize the books with a mean error of 0.9 cm on a wood shelf and 1.3 cm on a metal shelf.

Although the sensor model of RFID is shown to be highly non-Gaussian, Miller *et al.* (2010) used Kalman filters to track assets with RFID tags for inventory management. According to their experiments in an indoor environment with a size of 48 m$\times$14 m, the assets can be localized with a mean error less than 80 cm.

Patil *et al.* (2005) presented an automatic location sensing system for tracking RFID tags affixed to assets in indoor environment. The robot periodically moves in the working space and perceives the measurements of the tags installed on the ceiling of the indoor building. The position of the robot is estimated by a Wifi positioning system with a

mean accuracy of about 1 m. Their experiments showed that the tagged objects can be estimated with an accuracy of 1.5 m.

3.3 Bayesian Framework for Mapping RFID Tags

In this thesis, the positions of the tags are estimated by a Bayesian inference similar to Hähnel *et al.* (2004), Joho *et al.* (2009), and Vorst and Zell (2008). Formally, we denote the number of RFID tags around the environment by L. The measurements gathered by the mobile robot at positions $\mathbf{x}_{1:t} = \{\mathbf{x}_1, \cdots, \mathbf{x}_t\}$ until time t are represented as $\mathbf{f}_{1:t} = \{\mathbf{f}_1, \cdots, \mathbf{f}_t\}$. Here $\mathbf{f}_t$ consists of the measurement queried by the RFID antennas at time t: $\mathbf{f}_t = \{\mathbf{f}_t^{(1)}, \cdots, \mathbf{f}_t^{(A)}\}$, where A is the number of antennas attached to the RFID reader. The measurement $\mathbf{f}_t^{(a)}$ is expressed as a sequence $\mathbf{f}_t^{(a)} = \{f_{t,1}^{(a)}, \cdots, f_{t,L}^{(a)}\}$, where $f_{t,j}^{(a)}$ represents the measurement (i.e. received signal strength) of tag j observed from antenna a at time step t. In addition, let $\delta_t^{(a)}$ denote the position of the tag with reference to antenna a's coordinate system at time t. In this chapter, we only consider the 2D position of the RFID tag and thus $\delta_t^{(a)} = (x, y)$. We can compute $\delta_t^{(a)}$ by simply transforming the robot coordinates with a fixed transformation matrix $\mathbf{C}_a^r$, since the antennas are fixed on the robot, as shown in Figure 3.1a.

To estimate the location l_j of tag j at time t, we need to know the posterior probability $p(\mathrm{l}_j | \mathbf{f}_{1:t}, \mathbf{x}_{1:t})$. In our case, we consider the position of the tag in two dimensions and thus $\mathrm{l}_j = (x_j, y_j)$. According to the Bayesian theory and the Markov assumption (see Section 2.3), $p(\mathrm{l}_j | \mathbf{f}_{1:t}, \mathbf{x}_{1:t})$ can be rewritten as:

$$p(\mathrm{l}_j | \mathbf{f}_{1:t}, \mathbf{x}_{1:t}) = \eta_{1\ldots t} \prod_{i=1}^{t} p(\mathbf{f}_i | \mathrm{l}_j, \mathbf{x}_i) p(\mathrm{l}_j) \tag{3.1}$$

$$= \eta_{1\ldots t} \prod_{i=1}^{t} \prod_{a=1}^{A} p(f_{i,j}^{(a)} | \mathrm{l}_j, \mathbf{x}_i) p(\mathrm{l}_j) \tag{3.2}$$

$$= \eta_{1\ldots t} \prod_{i=1}^{t} \prod_{a=1}^{A} p(f_{i,j}^{(a)} | \delta_t^{(a)}) p(\mathrm{l}_j) \tag{3.3}$$

The formulas above allow us to iteratively estimate the position of a tag by applying the sensor model based on the measurements observed by the robot. η_t is a normalizer. The most important part in Equation (3.3) is $p(f_{i,j}^{(a)} | \delta_t^{(a)})$, which is called sensor model. It characterizes the likelihood of receiving a measurement $\mathbf{f}_i$ given the current state estimation. The formulas above are derived under the following assumptions (cf. Hähnel *et al.* (2004) and Vorst (2011)): the current observation $\mathbf{f}_t$ is independent of previous observations $\mathbf{f}_{1:t-1}$; the observation of one tag is independent of other tags in the environment; only the relative displacement between the tag and the antenna is relevant to our sensor model.

Certainly, these assumptions are too strict in practice. First, the readability and signal strength of a tag are influenced by the neighboring tags (Choi *et al.* (2012)). Furthermore, location-specific factors, such as the materials the tags are attached to, obstacles in the environment, orientation between the tag and the antenna or other radio devices in the environment, have high influence on the signal propagation. Thus, many authors applied location-fingerprinting techniques to improve the localization accuracy of a mobile agent (Vorst *et al.* (2011) and Ni *et al.* (2003)). These approaches estimate the position of a mobile agent from a set of pre-collected observations. They showed a slight improvement to the model-based approaches (Vorst *et al.* (2011)). However, the concern of this chapter is mapping of RFID tags, which requires an explicit sensor model and it is almost impossible to take all environmental factors into account.

3.4 Particle Filters-based Mapping

Many implementations of recursive Bayesian filters have been proposed in the literature, as described in Section 2.3. Among them, Kalman filters, which are built on the assumption that the system is linear and all error terms obey Gaussian distributions, have numerous applications in a variety of areas. However, the Gaussian assumption does not hold for our sensor model, as visualized in Figure 2.8 and Figure 2.9.

In this chapter, the position of each RFID tag is estimated by an individual particle filter. Each particle filter consists of N samples of position hypotheses with reference to the world coordinate frame and associated weights w^i. In this chapter, we only consider the 2D pose estimations of RFID tags, therefore $\mathbf{x}^i = (x^i, y^i)$. The position of the tag is computed by a weighted mean among all particles:

$$\bar{l}_j = \sum_{i=1}^{N} w^i \mathbf{x}^i \tag{3.4}$$

The particles are initialized uniformly around the area of the antenna position, at which the tag is first detected. Specifically, x and y coordinates are restricted by the maximum reading range of the RFID reader.

The previous RFID-based mapping strategy utilized a static configuration of the particle filter (see Hähnel *et al.* (2004) and Vorst (2011)): we neither use motion information to predict the particles nor apply resampling, since we assume the tags to be static. Therefore, this approach is considered to be identical to a histogram filter or a grid-based Markov localization approach. Obviously, in this case, a good and robust position estimation is usually supported by a large number of particles, which requires expensive computational cost and high memory storage. Also additional resources need to be allocated for other modules (e.g. localization, path planning, and obstacle avoidance) that provide autonomous behavior of a mobile robot.

This chapter, in contrast, utilizes a standard particle filter, which additionally incor-

porates an injection strategy and negative information. In general, the particle filter is executed recursively with the following three steps:

1. *Prediction*: we draw a particle for each particle according to the motion model of the tag. Since we do not have any information about the movement of the tag, we represent the motion model by a random walk: $\mathbf{x}_t^i = \mathbf{x}_{t-1}^i + \mathcal{N}(0, \sigma^2)$.

2. *Correction*: we assign each particle $\mathbf{x}_t^i$ with a new weight w_t^i according to the sensor model when a new measurement $\mathbf{f}_t$ arrives.

3. *Resampling*: we generate a set of new samples as a replacement of the old sample set. In general, the probability that a particle appears in the new particle set depends on its weight.

3.5 Perturbation of the Particles

Following Liu and West (2001), we realize the perturbation after resampling, which is also used by Joho *et al.* (2009) and Vorst (2011) for RFID-based mapping. This strategy is used to prevent the loss of information and solve the sample attrition problem. Particularly, let $\overline{\mathbf{x}}_{t-1}$ and $\mathbf{V}_{t-1}$ be the mean and covariance of all particles. The new position of particle i is determined by perturbing the position of this particle according to a Gaussian distribution with a mean $\alpha \mathbf{x}_{t-1}^i + (1-\alpha)\overline{\mathbf{x}}_{t-1}$ and a standard deviation $h^2\mathbf{V}_{t-1}$:

$$\mathbf{x}_t^i \sim \mathcal{N}(\alpha \mathbf{x}_{t-1}^i + (1-\alpha)\overline{\mathbf{x}}_{t-1}, h^2\mathbf{V}_{t-1}), \tag{3.5}$$

where h and α are two parameters that determine the scale of perturbation, which only rely on $\rho \in (0,1]$:

$$h = \sqrt{1 - \left(\frac{3\rho - 1}{2\rho}\right)^2} \text{ and } \alpha = \sqrt{1-h^2}, \tag{3.6}$$

here ρ is used control the degree of perturbation. A large ρ gives a low degree of perturbation, while a small ρ provides a high degree of perturbation. As suggested by Liu and West (2001), a good ρ is usually between 0.95 and 0.98. We fix ρ to 0.95 for the rest of this chapter.

3.6 Dealing with Mapping Failures

Normal MCL algorithms have the problem that they are not able to recover from the kidnapped robot problem (mapping failures or tag relocations in our case). Lenser and Veloso (2000) showed that this problem could be solved by a sensor-resetting strategy (i.e. adding random particles at each sensor update). In this chapter, we choose an adaptive MCL (A-MCL), since it provides an elaborate way to determine the number

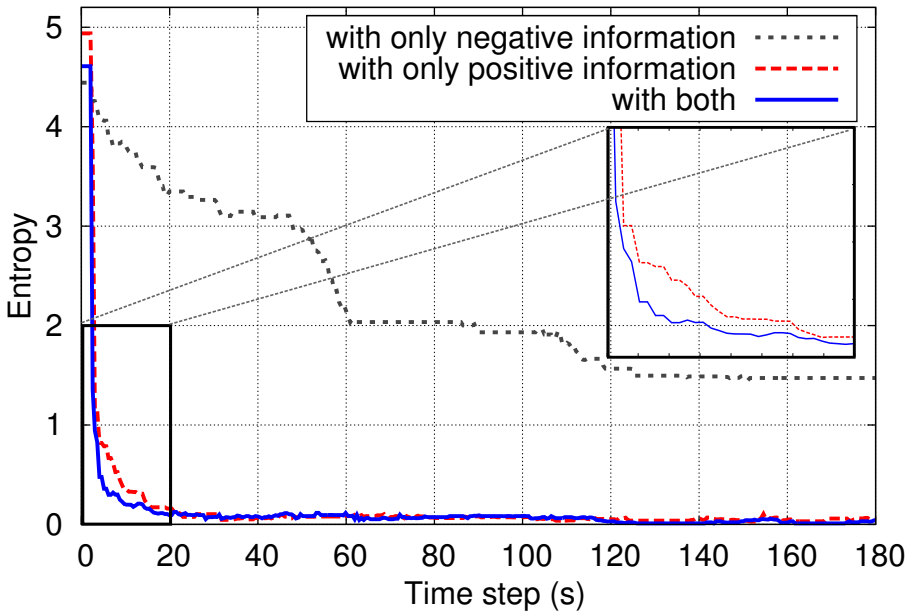

Figure 3.2: Entropy of the particle set with and without the negative information.

of particles required to be injected. For a comparison of different sensor-resetting approaches, one can refer to Gutmann and Fox (2002). The main idea of AMCL is to keep tracking the long- and short-term average of particle weights (w_l and w_s) over time and determine the number of particles to be added at each sensor update.

$$\begin{aligned} w_l &= w_l + \alpha_l(w_a - w_l) \\ w_s &= w_s + \alpha_s(w_a - w_s), \end{aligned} \tag{3.7}$$

where w_a is the average weight of the current particle set after evaluating a sensor measurement:

$$w_a = \frac{1}{N}\sum_{i=1}^{N} w^i \tag{3.8}$$

The ratios α_s and α_l ($0 \leq \alpha_l \ll \alpha_s \leq 1$) are two parameters that control the smoothness of the average likelihood. At each sensor update, AMCL randomly adds particles with a probability of:

$$\max\left(0, 1 - \frac{w_s}{\nu w_l}\right) \tag{3.9}$$

The newly added particles are sampled using the sensor model according to the current measurement. The value ν is used to control the level of injection. Concretely, $w_s < \nu w_l$ indicates there is a sudden decrease of the estimation quality and a set of additional samples is required to be injected.

3.7 Integrating Negative Information

In this chapter, negative information (e.g. non-detection) means the absence of a detection when a tag is expected to be detected. Generally, negative information is usually considered to be less useful than positive information (see Hoffmann *et al.* (2005)). For example, detecting a tag provides much more information than not observing a tag, since there are many possible positions where the robot is not able to detect the tag. Only using negative information, the particle filter is not able to converge in our case, as shown in Figure 3.2. There, we plotted the entropy of the particle distribution (see Stachniss *et al.* (2005) for details) using negative information and without using negative information during the mapping of one tag. As can be seen, only with negative information, the entropy is not able to drop below 1.0. Whereas it is clear that negative information accelerates the convergence process, which can be seen at $t = 10\,\mathrm{s}$ in Figure 3.2. Moreover, negative information provides a measure about the quality of the estimation and thus it can be incorporated into AMCL and the system is able to recover from mapping failures quickly.

The detection and the non-detection are regarded as mutually exclusive events in this chapter, therefore the non-detection model $p(\overline{d}|(x,y))$ is computed as:

$$p(\overline{d}|(x,y)) = 1 - p(d|(x,y)) \tag{3.10}$$

To save computational time, we propose the following two techniques to integrate negative information: First, we check the distance between the non-detection pose and the estimated pose. If it is above a distance threshold, which is set to five meters in this chapter, this measurement is ignored. This is because a non-detection, which is far away from an estimated pose, does not have any impact on the current particle set. Second, we measure the utility of the negative information by:

$$U = \frac{1}{N}\sum_{i=1}^{N} p(\mathbf{f}_t|\mathbf{x}_{t-1}^i). \tag{3.11}$$

If U is larger than a threshold ϑ_U, we reject this measurement. The idea of this is straightforward: a larger U means that this measurement is less informative to the current particle set than a smaller U, since the weights of all particles stay the same if this measurement is integrated. This allows us to filter out most negative information. However, computing Equation (3.11) requires as much time as the prediction step. To further reduce the computational burden, we only measure the utility of the mean $\overline{\mathbf{x}}_{t-1}$, which is already computed at the perturbation step (see Section 3.5).

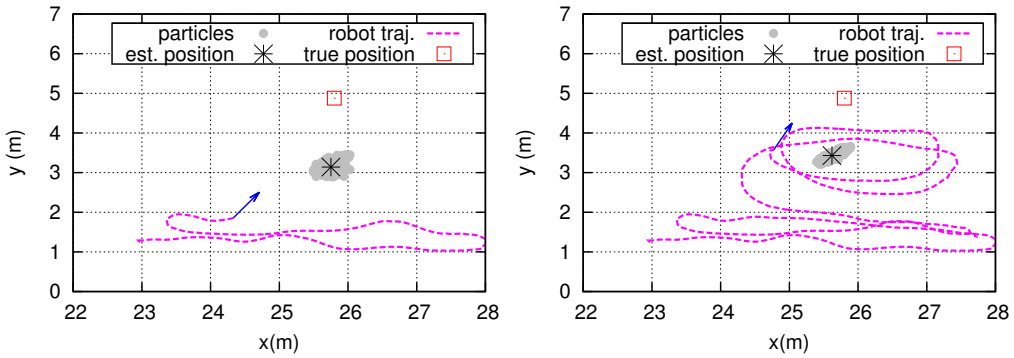

(a) After updating 132 measurements

(b) Mapping failure

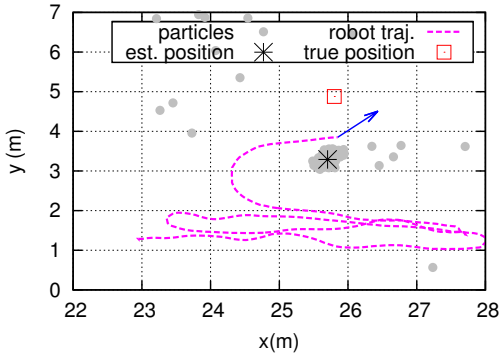

(c) Injection without negative information

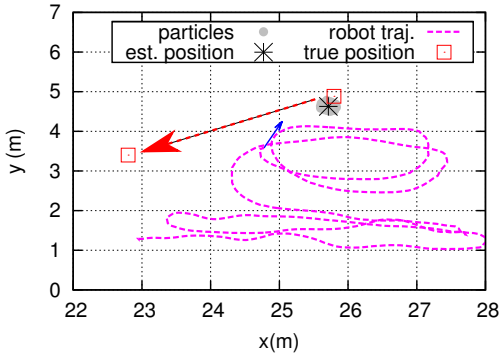

(d) Successfully localize the tag

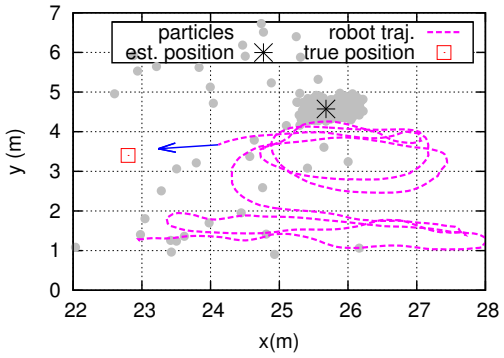

(e) Injection without negative information

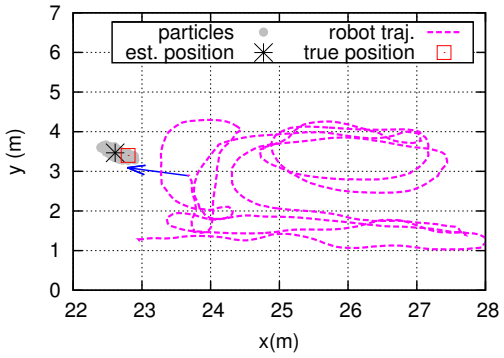

(f) Final state of a particle filter

Figure 3.3: Visualization of mapping failure, tag relocation and recovery from failure without negative information. The blue arrows represent the poses of the antennas with maximum signal strengths of the latest observations. (a) After processing 132 RFID measurements, the particle filter converges to a wrong position, which is approx. 1.7 meters away from the true position and no particles are close enough to the tag's true position. (b) Normal MCL is not able to recover from this mapping failure. After processing all measurements, the final localization error is 1.64 m without AMCL. (c) AMCL decides to inject particles after processing 243 measurements. (d) The tag is successfully localized using AMCL. At the same time, the tag is relocated to another position by hand, as indicated by the red arrow. (e) After processing 450 measurements, AMCL decides to inject particles. (f) The tag is relocalized successfully.

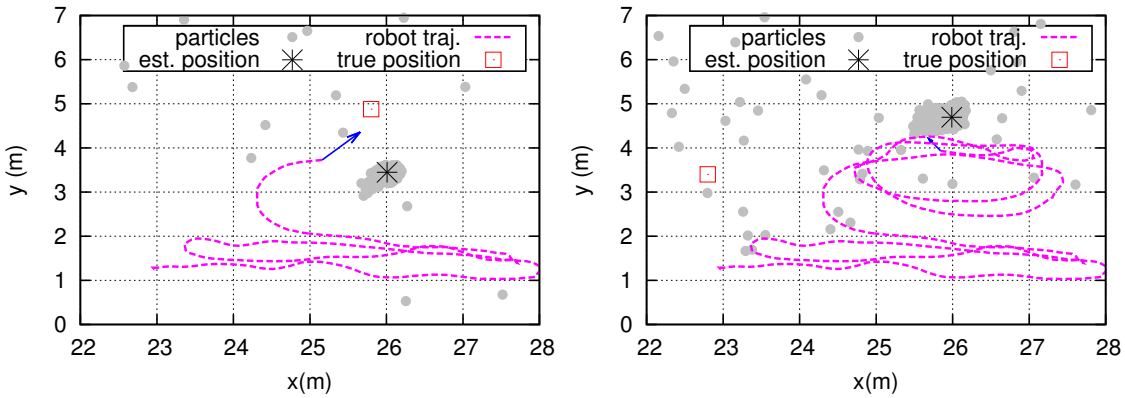

(a) Particle injection with negative information

(b) Particle injection with negative information

Figure 3.4: Recovery from mapping failure and tag relocalization with negative information. (a) With negative information, after processing 236 measurements, AMCL decides to inject particles. (b) With negative information, after processing 431 measurements, AMCL decides to inject particles.

3.8 Experimental Results

3.8.1 Setup

We used a Scitos G5 mobile robot from Metralabs (see in Section 1.4.2) as our experimental platform. We used the log files recorded at Section 2.4.4 at full reading power level. For the evaluation of the mapping performance, our experiments were performed by validating one tag in one log file using the sensor model learned from the rest of tags in all log files. This process was repeated 40 times to capture the random features of the particle filter. The values of α_l and α_s were set to 0.005 and 0.1, respectively.

3.8.2 Performance Evaluation without Negative Information

A preliminary experiment was conducted to show the ability of our system to recover from mapping failures and localize non-static RFID tags. We set $N = 200$ for this series of experiments. In the case of AMCL, we used $\nu = 0.7$. Figure 3.3 shows an example of mapping failure (see Figure 3.3a and Figure 3.3b) using normal particle filters and recovery from this failure (see Figure 3.3c and Figure 3.3d) using AMCL. It is clear that the normal MCL, with a final localization error of 1.64 m, failed to localize the tag, as can be seen in Figure 3.3b. Our explanation for this, which is based on the examination of the related literature, is the problem of particle depletion: the particle filter, which works as a way of stochastic approximation, converges so fast to the region with highest belief that there are no samples surviving nearby the true position.

It is worth to mention that Figure 3.3 is only one case of mapping failures, in practice,

this may happen quite often due to the harsh characteristics of radio signals in dynamic environments or robot trajectories. Using AMCL, as can be seen in Figure 3.3c, the robot detected an inconsistency between the measurement and the current sample set and thus started to add random particles. After injection, the particles converged to the true position gradually (see Figure 3.3d), with a final error of 0.35 m. Moreover, to demonstrate the capability of our system to localize non-static RFID tags, the tag was moved to a different place by hand, as shown by the red arrow in Figure 3.3d. As can be seen in Figure 3.3e and Figure 3.3f, our system is also capable of localizing non-static RFID tags.

In the following experiments, we evaluated the impact of the parameter ν on the overall mapping accuracy of static RFID tags without using negative information. Different noise levels (i.e. σ) were tested, but we only present the results of $\sigma = 0.01$ in this chapter due to the limited space. We fixed $N = 200$ for all experiments. Figure 3.5a plots the mean and standard deviation of mapping error under different values of ν without using negative information. In general, the choice of $\nu = 0.7$ achieved best results for our experiments. A too large or too small ν obviously resulted in worse results. For example, as compared with $\nu = 0.0$ (i.e. without AMCL) and $\nu = 0.7$, the mapping error was reduced from 0.365 m to 0.342 m, which is an improvement of 6.3 %. This is because a small ν (e.g. $\nu \leq 0.1$) is not able to sense a mapping failure correctly; while a large scale of injection (i.e. higher ν values) sometimes decides to inject particles even when the tag is well localized, which results in an overall decrease of the mapping accuracy.

3.8.3 Influence of Negative Information

In the next series of experiments, we evaluated the ability of our system to recover from mapping failures and tag relocations by integrating negative information. Again, we ran our algorithm on the same log files taken at Section 3.8.2 by incorporating negative information ($\vartheta_U = 0.2$). As shown in Figure 3.4a and Figure 3.4b, evaluating negative information helps to accelerate the recovery process. For example, for recovery from mapping failure using negative information, the injection happened after receiving 236 measurements (see Figure 3.4a), which is earlier than the case without utilizing negative information (243 measurements, see Figure 3.3c). For the case of localizing non-static RFID tags, the injection took place at the 431th update (see Figure 3.4b) with negative information, as opposed to the 450th without negative information (see Figure 3.3e).

We analyzed the influence of negative information on the mapping accuracy for static RFID tags in the following experiments, as illustrated in Figure 3.5b. We compared the mapping results between a grid-based approach ($N = 2000$) and AMCL ($\nu = 0.0$, $\nu = 0.3$, $\nu = 0.5$, $\nu = 0.7$ and $\nu = 0.9$) by adding different levels of negative information. We set $N = 200$ for AMCL. As can be seen in Figure 3.5b, for the grid-based approach, the mapping accuracy got worse by incorporating negative information. The reason for this can be found in Vorst's dissertation (Vorst (2011)). On the contrary, for AMCL the mapping error is not an increasing function with reference to the levels of negative

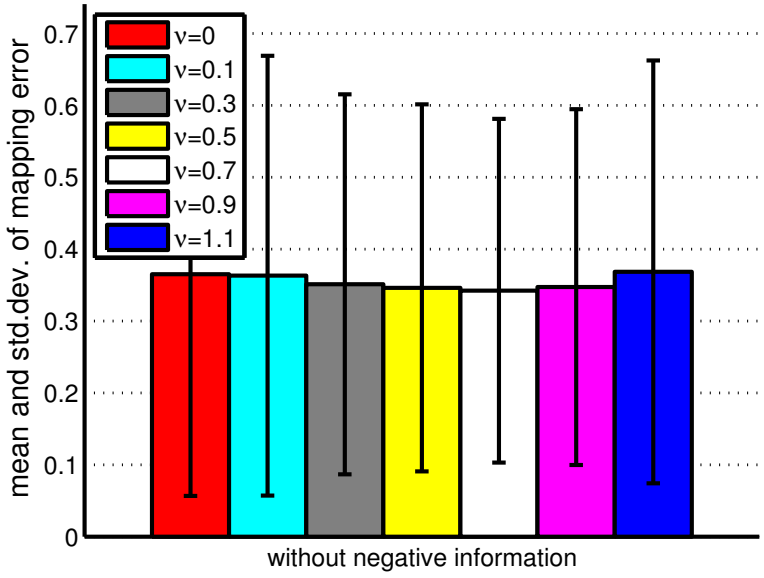

(a)

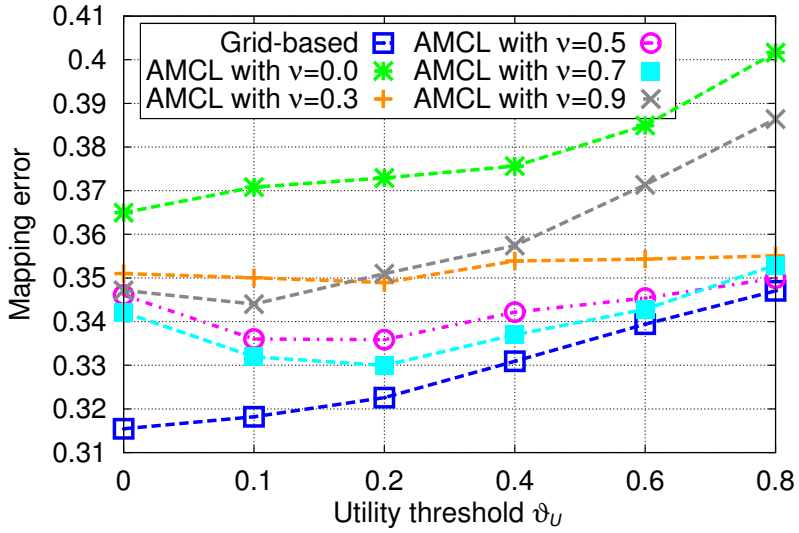

(b)

Figure 3.5: Evaluation of the mapping accuracy under the impact of different parameters. (a) Mapping accuracy under the impact of the parameter ν without the integration of negative information (i.e. $\vartheta_U = 0$). (b) Mean mapping error under the influence of parameter ν with the integration of different scales of negative information. For a better visualization, we do not show the standard deviation of the mapping error here.

information integrated. As can be seen in Figure 3.5b, the choice of $\vartheta_U = 0.2$ performed best for AMCL, with an improvement of approx. 3.5 %, as compared to $\vartheta_U = 0.0$ (from 0.342 m to 0.329 m). That is to say, negative information is not able to improve the mapping accuracy of a well mapped tag (e.g. no improvement for grid-based approach), whereas it can be used to measure the decrease of the quality of the estimation for a badly localized tag, therefore improves the average mapping accuracy (e.g. the improvement by integrating proper amount of negative information using AMCL). Moreover, as can be seen in Figure 3.5b, with too much negative information (e.g. $\vartheta_U > 0.4$), the mapping error was increased. The reason for this is that negative information with large utility introduces more uncertainty than the information it yields, since we use a Gaussian noise model with fixed standard deviation in our prediction step. Thus, in the future research, it is interesting to see if the mapping accuracy can be improved by using more precise motion models.

3.8.4 Comparison to a Grid-based Markov Approach

In the next experiments, we compared the particle filter-based approach to the previous grid-based Markov localization approaches (Hähnel *et al.* (2004), Liu *et al.* (2013), and Vorst (2011)), which utilized a static configuration of the particle filter: we neither use motion information to predict the particles nor apply resampling, since we assume the tags to be static. For the particle filter-based approach, we used $\nu = 0.7$ and integrated negative information ($\vartheta_U = 0.2$). As can be seen in Figure 3.6, with $N = 200$ for the particle-based approach, we got a mean mapping error of 0.329 m, which can only be achieved by $N \geqslant 2000$ for the grid-based approach. Moreover, we obtained nearly the same mapping results with $N \geqslant 500$ for the particle filter-based approach. For the grid-based approach, we achieved a mean mapping error of 0.302 m with $N \geqslant 4000$, which is approx. two centimeters smaller than the best accuracy we achieved from AMCL (e.g. 0.318 m with $N = 4000$). Our explanation for this is that the grid-based approach represents the belief with discretized grids (histograms), while particle filters only use a set of samples to represent the most relevant region of the belief, which more or less lose some information during the execution. However, the disadvantage of the grid-based approach is that the number of particles required has to be scaled with the size of the estimation space: for example, if the range of the RFID reader becomes larger in the future, we need more particles to get a good position approximation. Another drawback of the grid-based approach is that it is not able to deal with non-static RFID tags, since the poses of the particles are fixed.

3.8.5 Time Complexity

As listed in Table 3.1, we evaluated the running time of different approaches based on processing nine log files, which consist of 85235 RFID detections and 360591 non-detections with distance filtering. All algorithms were run on an Intel Core i5-2410M

Table 3.1: Total time consumption (in seconds) of different approaches.

Method	Number of particles (N)					
	100	200	500	1000	2000	4000
Grid-based	8.2	14.8	32.8	66.2	121.7	241.1
AMCL, $\vartheta_U = 0.0$	21.4	34.7	92.3	162.7	327.5	661.5
AMCL, $\vartheta_U = 0.2$	22.6	38.4	98.9	192.3	375.23	733.2
AMCL, $\vartheta_U = 0.8$	30.4	50.8	124.6	238.0	467.3	937.7

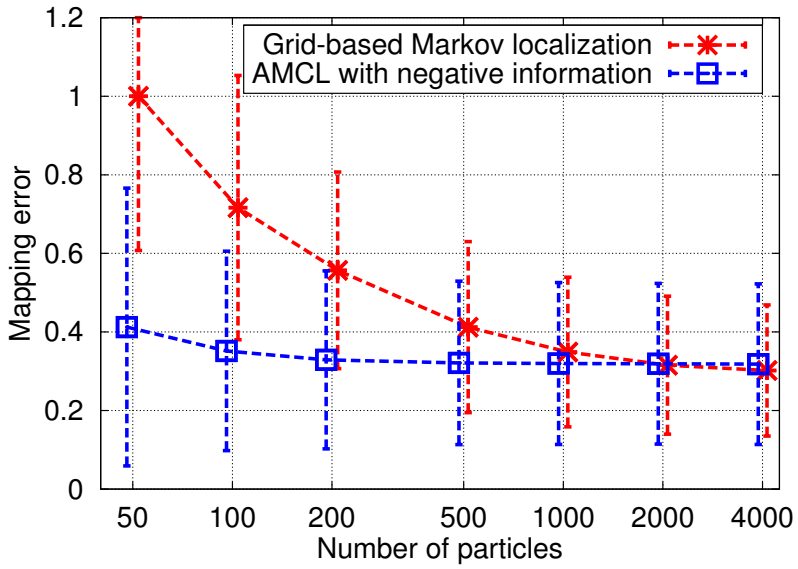

Figure 3.6: The comparison of a grid-based approach and a particle filter-based approach.

@2.3 GHz CPU, with 4 GB RAM. As can be seen in Table 3.1, with the same number of particles, AMCL consumes more time due to the additional resampling and perturbation steps, but achieves better mapping accuracy, as compared to the grid-based approach. For example, with $N = 200$ and $\vartheta_U = 0.2$, AMCL took nearly three times as long as the grid-based approach (38.4 s for AMCL *versus* 14.8 s for grid-based approach). But at the same time, AMCL gave a better mapping accuracy (0.329 ± 0.22 for AMCL and 0.557 ± 0.25 for grid-based approach respectively), as can be seen in Figure 3.6. In practice, it is fast enough to use AMCL with 200 particles, which only needs approx. 0.45 ms for one filter update, to deal with hundreds of RFID detections per second in densely tagged environments. Moreover, as can be seen in Table 3.1, evaluating negative information slightly requires more computational time. With the best parameter choices for $N = 200$ (i.e. $\vartheta_U = 0.2$ and $\nu = 0.7$), the computational time is only increased by 5 % (from 21.4 s to 22.6 s), as compared to the test without negative information ($\vartheta_U = 0.0$). At the same time, we got an improvement of 3.5 % for the mapping accuracy (from 0.342 m to 0.365 m, see Section 3.8.3).

3.9 Conclusions and Future Work

In this chapter, we showed how to use the probabilistic framework for the localization of RFID tags. Since the propagation of radio signals is hard to predict, the traditional particle filters face the problem of mapping failures. We addressed this problem by measuring the quality of the estimation and adding random particles if it is necessary. We summarize the contributions of this chapter as follows:

- We investigated AMCL, which is able to solve the problem of mapping failures and relocalizations of RFID tags.
- We examined the usefulness of negative information in the context of RFID-based mapping and showed that negative information helps to improve the mapping accuracy and quickly recover from mapping failures.
- We compared a particle filter-based mapping approach to our previous grid-based Markov localization approach and pointed out their advantages and disadvantages.

Extensive experiments with a Scitos G5 service robot were conducted to verify the effectiveness of our approach. Compared to normal MCL, with 200 number of particles, AMCL improves the mapping accuracy by 6.3 % (from 0.365 m to 0.342 m) without further examination of negative information. By integrating negative information, the mapping accuracy is improved by 3.5 % (from 0.342 m to 0.329 m). As compared to our previous grid-based Markov approach, we are able to save approx. 70 % of the computational cost (from 121.7 s using the grid-based approach with $N = 2000$, to 38.4 s using AMCL with $N = 200$ and $\vartheta_U = 0.2$) and approx. 90 % of memory storage (from 2000 particles to 200 particles), while the mean mapping accuracy only decreases by two centimeters.

There are several possible extensions of this work: One direction could be the integration of an outliers-removal approach, which deals with the ghost detections of RFID tags due to environmental effects on radio signal propagation, to improve the mapping accuracy. Furthermore, it would be interesting to fuse visual information (e.g. features, shapes, and textures) from cameras for object recognition or object detection.

Chapter 4

Mapping of RFID Tags with a 3D Sensor Model

In this chapter, we address the problem of mapping RFID tags using a 3D sensor model based on the work presented in the previous chapter. Compared to the 2D sensor model based approaches, the 3D sensor model achieves a higher mapping accuracy for the 2D position estimation. In particular, with this sensor model, we are able to localize the tags in 3D by equipping the robot with two antennas at different heights. Furthermore, by integrating negative information (i.e. non-detections), the 3D mapping accuracy can be improved. Additionally, we utilize KLD-sampling (KLD is short for Kullback-Leibler distance, see Cover and Thomas (1991)) to reduce the number of particles for our specific application, so that our algorithm can be performed online.

The rest of this chapter is organized as follows. After a short introduction in Section 4.1, we review the related work in Section 4.2. Then, we describe how to localize a tag in 3D with our stereo antennas setup in Section 4.3. Section 4.4 explains how to use KLD-sampling to adapt the particle set. In Section 4.5, we describe how to apply non-detections to improve the mapping accuracy. Finally, we present our experimental results in Section 4.6 and conclude this chapter in Section 4.7.

4.1 Introduction

In Chapter 3, we presented a Bayesian approach to localize RFID tags in 2D based on 2D sensor models. There we assume that the detection characteristics of RFID tags highly depend on the 2D relative position between the antenna and the tag. However, the behavior of RFID tags (detection likelihood and received signal strength) does not only depend on the 2D displacement of the tag with reference to the antenna coordinate frame, but also highly relies on the heights of the tags. We observe in Figure 4.1 that the measurements (detection counts and mean received signal strength) from RFID readers vary with regard to the heights of the tags. Therefore, the extension of the sensor model into 3D is useful and straightforward, particularly in the environments in which the tags are distributed at different heights. To our knowledge, no study about mapping RFID tags using a 3D sensor model has been published before.

Therefore, we propose a 3D RFID sensor model for mapping RFID tags in this chapter. Unlike the existing 2D sensor models, our 3D sensor model characterizes the detection behavior of the RFID antenna with respect to the 3D position of an RFID tag. The contribution of this chapter is threefold. First, by applying our 3D sensor model, the 2D position estimation of RFID tags can be improved in comparison to our previous 2D sensor model. Since the positions of the antennas are fixed on the robot for our application, by using only one antenna or multiple antennas mounted at the same height on the robot, we are not able to determine the height of an RFID tag unambiguously due to the symmetrical radiation property of RFID antennas. Therefore, as a second contribution, we show how the ambiguity can be resolved and the mapping error can be reduced by a pair of RFID antennas installed at different heights on the robot. Third, we show that the 3D position estimation can be further improved by incorporating non-detections for our specific stereo antennas configuration. Finally, we employ KLD-sampling to reduce the number of particles. This enables our algorithm to perform the mapping task in real-time. This chapter is based on our publication (Liu *et al.* (2013)), which was presented at IROS 2013.

4.2 Related Work

A variety of approaches concerning mapping RFID tags using mobile robots have been proposed in the literature. A comprehensive review of the related work about RFID mapping is presented in Section 3.2. Many researchers focus on mapping UHF RFID tags using 2D sensor models (Hähnel *et al.* (2004), Vorst and Zell (2008), Joho *et al.* (2009), Deyle *et al.* (2008b), Rohweder *et al.* (2009), and Germa *et al.* (2010)), yet few address the issue of localizing RFID tags with 3D sensor models.

Several researchers have proposed to fuse the measurements from other sensors, like laser range finders, or visual sensors with RFID measurements, to determine the 3D positions of RFID tags. Germa *et al.* (2010) combined RFID measurements with visual information to track people with a mobile robot in a crowded environment by fusing the data from the camera and the RFID reader using a particle filter. They also proposed several mechanisms to make the tracker more robust against occlusions and target losses than vision-based systems. Moreover, they designed a control policy based on multi-sensor data to follow a person. Although the experiments were only performed with a color camera, the extension to a depth camera (RGB-D camera) is straightforward. Deyle *et al.* (2009) generated an image representation, which characterizes the spatial distribution of signal strength for an RFID-tagged object. In particular, the RSS image is constructed by measuring the RSS value at each bearing while panning and tilting an RFID antenna. By aligning the RSS image with the measurement from a color camera and a 3D laser scanner, they are able to localize the RFID tags in 3D. Particularly, this approach is developed for the manipulation of a mobile robot in home environments. Their approach enables the robot to discover the objects of interest, estimate their positions,

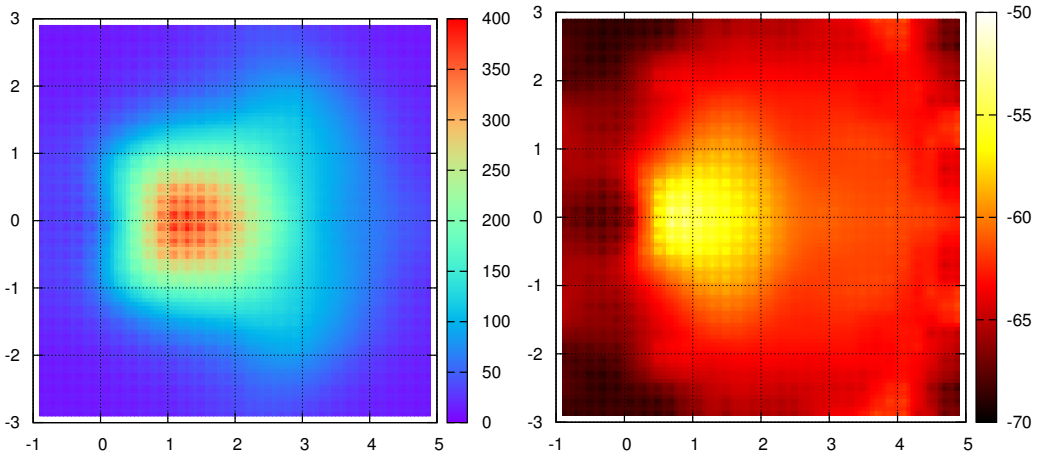

(a) Detection counts at 0 m (b) Mean RSS at 0 m

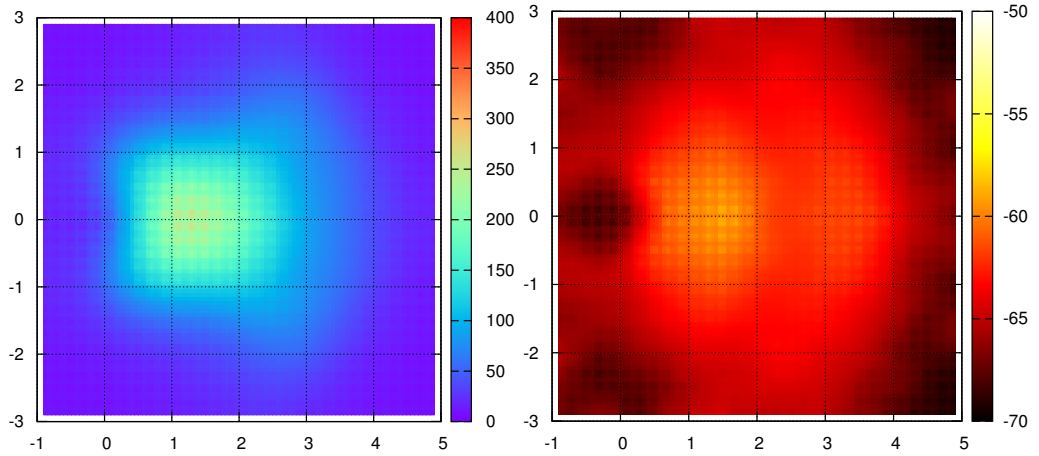

(c) Detection counts at 0.8 m (d) Mean RSS at 0.8 m

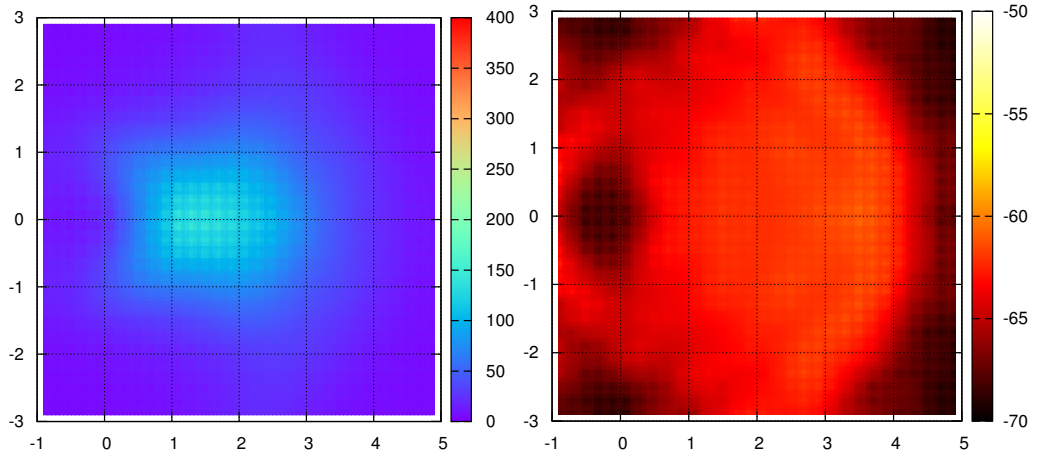

(e) Detection counts at 1.6 m (f) Mean RSS at 1.6 m

Figure 4.1: Visualization of the detection counts (left) and mean RSS values (right) of an RFID antenna with reference to different heights of RFID tags at full reader power level.

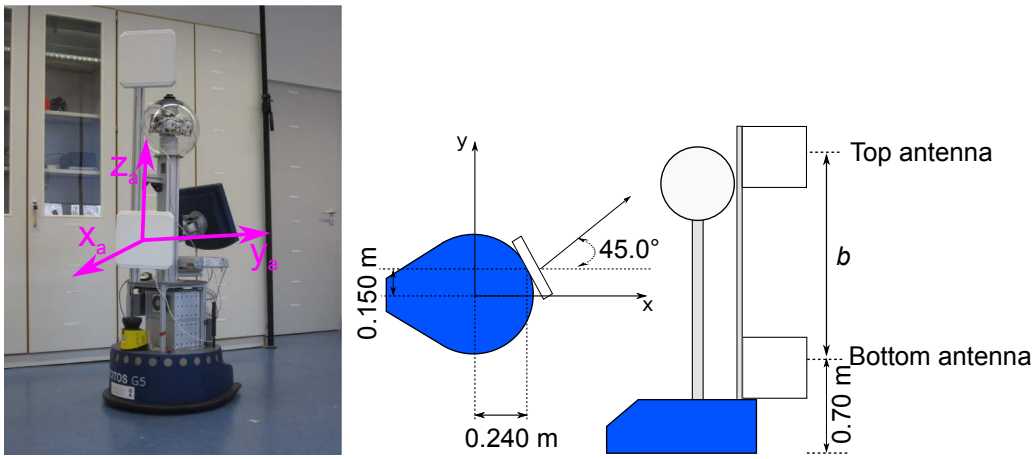

(a) Robot (b) Antenna setup

Figure 4.2: (a) The mobile robot used for our 3D mapping experiments and the annotation of the bottom antenna's coordinate system (marked with pink). The *xy*-plane is parallel to the ground plane and the *z*-axis is perpendicular to the *xy*-plane. (b) Antenna setup of our Scitos G5 robot. Vertical (left) and side view (right).

approach them, and grasp them. All approaches proposed in the literature depend on the fusion of measurements from additional sensors, e.g. cameras and laser range finders, i.e. none of them addresses the problem of 3D pose estimation of tags solely based on RFID measurements.

The idea of estimating the 3D poses of tagged objects with a pair of antennas is similar to the idea of stereo vision. Stereo vision aims at extracting the 3D position of an object by comparing the images from two different views on a scene taken from two cameras (Mountney *et al.* (2010)). Two cameras are typically placed in a horizontal plane and are usually separated by a distance called baseline. The distance from the object to the camera system is inversely proportional to the disparity of the object which is computed by a stereo matching algorithm. In our stereo antennas setup, we place two antennas at different heights on the robots (see Figure 4.2) in order to determine the 3D position of a tag by integrating the measurements from both antennas.

4.3 Mapping RFID Tags in 3D

We derived the Bayesian framework for estimating the positions of RFID tags in 2D space given the measurements perceived by the robot in Section 3.3. Theoretically, Equation (3.3) also allows us to estimate the 3D positions of RFID tags by integrating several detections at different 3D positions. There are two aspects we want to point out for localizing a tag in 3D. First, since our mobile agent only moves in the *xy* plane and the antennas are fixed on the robot, it is impossible to determine the 3D position of an RFID

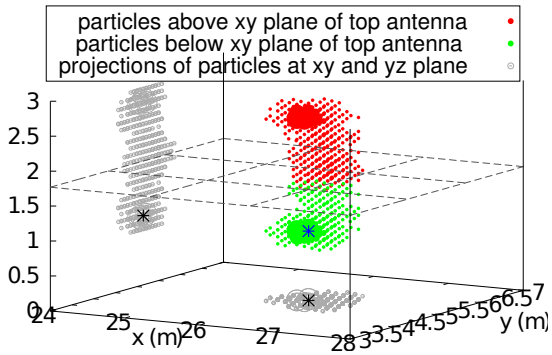

(a) After 20th update with only top antenna.

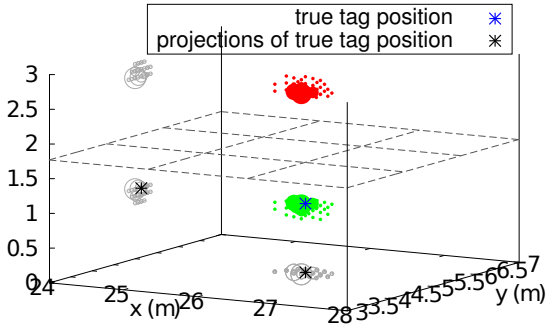

(b) After 30th update with only top antenna.

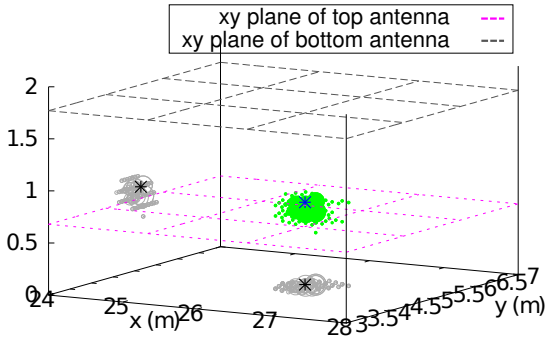

(c) After 30th update with our stereo setup.

Figure 4.3: Visualization of 3D mapping using only the top antenna and the stereo antennas setup. Particles with too small weights are neglected in our visualization. (a) After processing 20 detections with only the top antenna, there is high uncertainty about the position of the tag: the estimation of z is ambiguous, but the xy estimation is quite good, as can be seen from the projections of the particles. (b) After the 30th update, it is more clear that the particle filter converges to two regions that are symmetrical to the xy plane of the top antenna. (c) By integrating measurements from a pair of antennas, after 30 measurements, the particles converge to one region and the ambiguity is resolved.

tag by only a 2D sensor model. Second, we are not able to unambiguously determine the height of an RFID tag using a 3D sensor model if the mobile robot carries only one antenna or several antennas mounted at the same height. As shown in Figure 4.3, the posterior probability density representation over the height of an RFID tag obeys a bimodal distribution due to the symmetrical characteristics of the antenna. However, by integrating the measurements from a second antenna at a different height, this ambiguity can be resolved, as shown in Figure 4.3c. Particularly, we employ a pair of RFID antennas, which we call stereo antennas configuration in this chapter, since the two antennas only differ in the z-coordinate and span a distance of b (called baseline), as shown in Figure 4.2.

As in Section 3.4, we utilize a particle filter to estimate the 3D position of an RFID tag. Here each particle $\mathbf{x}^i$ consists of the three-dimensional coordinates of the tag, i.e. $\mathbf{x}^i = (x^i, y^i, z^i)$. For the initialization of the particle filter, the x and y coordinates are restricted by the maximum range of the RFID reader and the z coordinate is limited by the maximum height of the tags (e.g. 3 m) in the environment.

In our implementation, the positions and weights of particles are expressed as double values and kept in memory without compression. In the case of 2D pose estimation using 2D sensor models (see Chapter 3), we use $N = 1000$ particles, which takes approx. 1 ms for each measurement update (cf. Section 4.6.4), to achieve a good mapping accuracy. Therefore the algorithm can be run in real time in densely tagged-environments, where the RFID reader may receive hundreds of detections per second. Approx. 45.7 MB of memory are required to localize 2000 RFID tags in a store on-line. However, 3D position estimation requires a larger number of particles, due to the additional dimension. In order to get a good position estimation, we have to utilize a particle filter with 10000 samples. Hence, time complexity and memory consumption increase due to the increased number of particles. To reduce the running time of our mapping module, we utilize KLD-sampling to adapt the number of particles, as detailed in Section 4.4.

Since we assume the tags to be static in this chapter (i.e. tags do not change their positions while the robot traverses the environment), we used a grid-based Markov localization approach for mapping RFID tags, i.e. we neither utilize motion information to predict the movement of the particles nor execute resampling. This strategy is also deployed by Hähnel *et al.* (2004) and Rohweder *et al.* (2009). For a comparison and discussion of the particle filter related resampling/pertubation approaches, we refer to Chapter 3, Joho *et al.* (2009), and the dissertation of Vorst (2011).

4.4 Adapting the Number of Particles

Fox (2003) first used the KLD-sampling to adapt the particle size for robot localization. KLD-sampling is able to choose the number of particles dynamically with reference to the current state of approximation. At each update step, it determines the number of particles required for a good approximation, in order to guarantee that with a probability of

$1-\delta$ the error between the true posterior and the particle-based estimation is limited by a predefined threshold ε. More precisely, the desired number of particles n_χ is determined by:

$$n_\chi = \frac{1}{2\varepsilon}\chi^2_{k-1,1-\delta} \tag{4.1}$$

here $\chi^2_{k-1,1-\delta}$ is the $1-\delta$ quantile of the Chi-Square distribution with $k-1$ degrees of freedom. According to the Wilson-Hilferty transformation (see Johnson *et al.* (1995)), $\chi^2_{k-1,1-\delta}$ is approximated as:

$$\chi^2_{k-1,1-\delta} = (k-1)\left\{1 - \frac{2}{9(k-1)} + \sqrt{\frac{2}{9(k-1)}}z_{1-\delta}\right\}^3$$

here $z_{1-\delta}$ is the $1-\delta$ quantile of the standard normal distribution. Typical values of $z_{1-\delta}$ could be found at a prestored statistics table. k stores the number of support bins or non-empty bins which is tracked at each sampling step of the particle filter. For the implementation of the bins, one can use a fixed, multi-dimensional grid, or a more efficient tree structure (see Koller and Fratkina (1998) and Moore *et al.* (1997)). Details about the computation of $\chi^2_{k-1,1-\delta}$ can be found in Fox (2003) and Johnson *et al.* (1995).

We use a specialized version of the KLD-algorithm. In our application the tags are assumed to be static, and we therefore neglect resampling and prediction. As a result of this, the importance weights of the particles in the predictive distribution are not uniform after the application of updates. Therefore, after sampling a particle from the predictive belief, we keep tracking of the already chosen samples to not integrate them multiple times into the adapted distribution, which otherwise would lead to a corruption of the posterior. For that reason, the number of sampled particles n_χ differs from the actual number of particles k_χ that are selected for the adapted distribution, since duplicate particles are skipped. To keep the diversity in our distribution, we introduce another parameter $k_{\chi min}$ as a minimum threshold for the desired number of particles. As a result, we get a static Monte-Carlo based representation of our target domain, where particle numbers adapt to the current state of the estimation.

4.5 Utilizing Negative Information

Negative information has been successfully applied to object tracking (Koch (2007)) and localization (Hoffmann *et al.* (2005)) of mobile robots. Similar to Chapter 3, we treat non-detections as negative information for our stereo antennas configuration to improve 3D mapping accuracy.

As described in Section 3.7, non-detections are evidence that a tag is absent from a certain area, which may be useful to infer the potential location of the tag. However, it is difficult to balance detections and non-detections in practice. This is because, on the

one hand, the particles often converge to a region with low detection likelihood due to false negatives of non-detections, which is shown by Vorst (2011); on the other hand, incorporating non-detections requires more computational time. To compensate for that, we only consider non-detections when the specific tag is detected by at least one antenna in our stereo antennas setup. Particularly, if antenna a^+ detects the tag while a^- does not, we additionally apply the non-detection sensor model for antenna a^-. The idea of this is straightforward. Applying negative information may devalue the particles with high likelihood due to false negatives, but by integrating the non-detection model only in case of a detection, we minimize the false negative count.

4.6 Experimental Results

4.6.1 Setup

We use a Scitos G5 mobile robot (see Figure 5.1a) as the experimental platform. Our stereo antennas configuration is shown in Figure 4.2b, which is different from the setup used in Chapter 3. The experiments were conducted in an indoor environment with an area of approx. $60\,\mathrm{m}^2$. We placed 64 UHF RFID tags (Alien Technology Squiggle) on the furniture and the walls of the lab at different heights, ranging from 0.2 to 2.5 meters. The positions of all tags were measured manually beforehand to provide the ground truth for our experiments.

We manually steered the robot at different trajectories through the lab with a maximum velocity of 0.2 m/s. The robot traveled around 1.5 km with a duration of approx. three hours and seven log files were recorded at the same time with a wide baseline stereo antennas configuration ($b = 1.1$ m). Each log file consists of at least 2000 RFID measurements and the associated true position of the robot. In total, approx. 438762 RFID detections were recorded for the wide baseline configuration. The mean mapping accuracy was averaged by validating one tag using the sensor model learned from the rest of the tags. In addition, we recorded three log files for a middle baseline configuration ($b = 0.7$ m) and another three for a small baseline configuration ($b = 0.3$ m) to compare the impact of various baselines on mapping accuracy. The three different configurations of baseline width were obtained by fixing the bottom antenna and only moving the top antenna, as visualized in Figure 4.2b.

4.6.2 Evaluation of 2D Mapping Accuracy

The 2D mapping accuracy using different sensor models was evaluated by the first series of experiments. We used a particle number of 1000 for 2D sensor models. These particles were spread uniformly in the xy plane with a fixed height z, e.g. $z = 1.0$ m. For 3D sensor models, we equally distributed 13000 particles at various heights ranging from 0 to 2.4 meters with an interval of 0.2 m. Thus, the experimental results under various

Table 4.1: Mean and standard deviation (mean $\pm$ std.dev) of 2D mapping errors (in centimeters) under the influence of different sensor models and various antenna setups.

Antenna setup	Model dim.	Detection likelihood model	Combined model
Bottom	2D	39.0 ± 20.8	35.7 ± 24.4
	3D	39.1 ± 21.8	33.1 ± 20.8
Top	2D	38.2 ± 18.6	40.1 ± 22.5
	3D	36.2 ± 17.2	35.3 ± 17.2
Both	2D	32.6 ± 13.9	26.2 ± 16.1
	3D	38.4 ± 18.6	23.4 ± 15.6

sensor models are considered to be comparable, since the *xy* density of particles for the 3D sensor model is identical to the 2D sensor model. We neither performed KLD-sampling nor incorporated negative information in the experiments. The results are listed in Table 4.1, in which we combined different sensor models and antenna configurations. Obviously, using both antennas achieves better results than only one antenna for both 2D and 3D sensor models. We also observed that for all experiments conducted with the combined model, the 3D sensor model clearly improves mapping accuracy. For example, with only the top antenna in use, the mean mapping error is reduced from 0.401 m to 0.353 m by applying the 3D sensor model. This gives us an improvement of 12.0 % compared to the 2D sensor model.

As a comparison, we evaluated the approach presented by Joho *et al.* (2009). In case of a single antenna, the mean mapping error (i.e. 0.357 m for bottom antenna only) is higher than the error (0.29 m) obtained by Joho *et al.* (2009). The reason is that in our work the tags are distributed at different heights, while the tags are located roughly at the same height in Joho *et al.* (2009). However, with a pair of antennas and the 3D sensor model, we achieve a mean error of 0.234 m for 2D pose estimation, which is equivalent or even slightly better than the results in Joho *et al.* (2009).

4.6.3 Influence of Negative Information

The influence of negative information on mapping accuracy was investigated in further experiments. The algorithm was tested using a fixed number of particles ($N = 13000$) without KLD-sampling. As can be seen in Figure 4.4a which visualizes the mapping results with and without integrating negative information, utilizing negative information improves the mapping accuracy. For example, the mean height error is reduced from 0.38 m to 0.28 m, which is an improvement of approx. 26.3 %. This is due to the fact that we can exploit the stereo setup of our antennas by incorporating negative information: if both antennas detect a tag, we can infer that the tag is probably between the two antennas; otherwise, if only the top antenna detects the tag, it is likely that the tag's location is in the region closer to the top antenna.

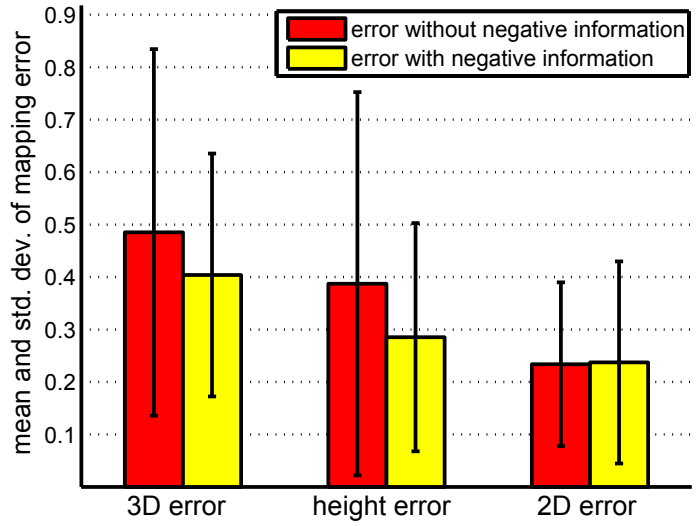

(a)

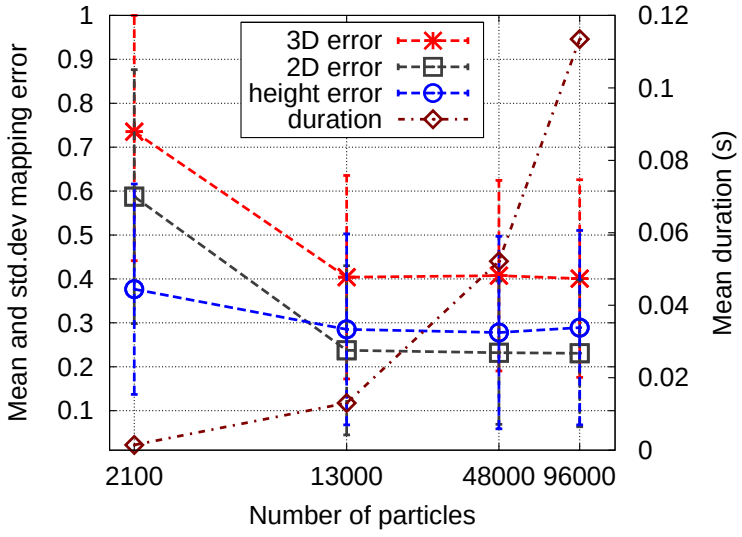

(b)

Figure 4.4: Performance evaluation under different parameters. (a) Mapping error with and without negative information; (b) Mean and standard deviation of absolute mapping error versus mean computational time of each detection event under different numbers of particles.

4.6.4 Evaluation of 3D Position Estimation

As a third series of experiments, we varied the number of particles N to evaluate the performance of 3D position estimation, as depicted in Figure 4.4b. We incorporated negative information in these experiments but did not perform KLD-sampling. Our algorithm was tested on an Intel Core i5-2410M @ 2.3 GHz CPU, with 4 GB RAM. As can be seen in Figure 4.4b, we obtain nearly the same mapping results for $N \geq 13000$, but at the same time the computational time increases drastically. With $N = 96000$, we obtain a mean absolute 3D mapping error of 0.40 m. As expected and shown in Figure 4.4b, the mapping errors increase for smaller N. Additionally, we noticed that the error in height estimation is usually larger than the error in the xy-plane in all experiments. For example, with $N = 13000$, the mean height error is approx. 0.28 m, which is much larger than the mean error of x or y: $\frac{0.23}{\sqrt{2}} \approx 0.16$ m. This can be explained as follows: x and y positions of the tags are estimated through various measurements collected by the mobile robot that moves in the xy plane, while z is only determined by the difference of two RFID antennas. Thus the deviation of measurements in xy direction is much higher than in the z direction. As a result, we do not get a good z-estimation due to the lack of distinct detection samples in the z-axis. We can also see in Figure 4.4b the computational time required for 3D mapping is quite high: we need approx. 52 ms (for $N = 48000$) to process one tag detection and thus it is impossible to run the algorithm in real time for densely tagged environments, where the robot may receive hundreds of RFID readings per second. However, as shown in Section 4.6.6, by applying KLD-sampling to adapt the number of particles, we are able to run our algorithm online, meeting the real-time requirements.

4.6.5 Influence of the Baseline of the Stereo Antennas System

In the next series of experiments, we examined the mapping accuracy under various baselines of our stereo antennas configuration. We did not perform KLD-sampling, but negative information was utilized in these experiments. Due to the physical and technical limitations of our robot, we are not able to set the baseline of the antennas wider than 1.1 m. As can be seen in Figure 4.5, wider baselines result in better mapping results. With small baselines, the mapping error is notably worse. For example, the mapping error of height with the smallest baseline (0.3 m) is nearly twice as high as the error of the widest baseline (1.1 m). This is because our stereo antennas setup degrades to a single antenna for small baselines, since the difference in the measurements is dominated by the characteristic noise from RF-propagation. In contrast, if the baseline is chosen too wide, there is no overlap between the two RF-fields, and the arrangement degrades to a simple antenna-array with two distinct (single) antennas. Since the possible height on the robot is limited, the second case is of no concern to us under the given configuration (i.e. full reader power level).

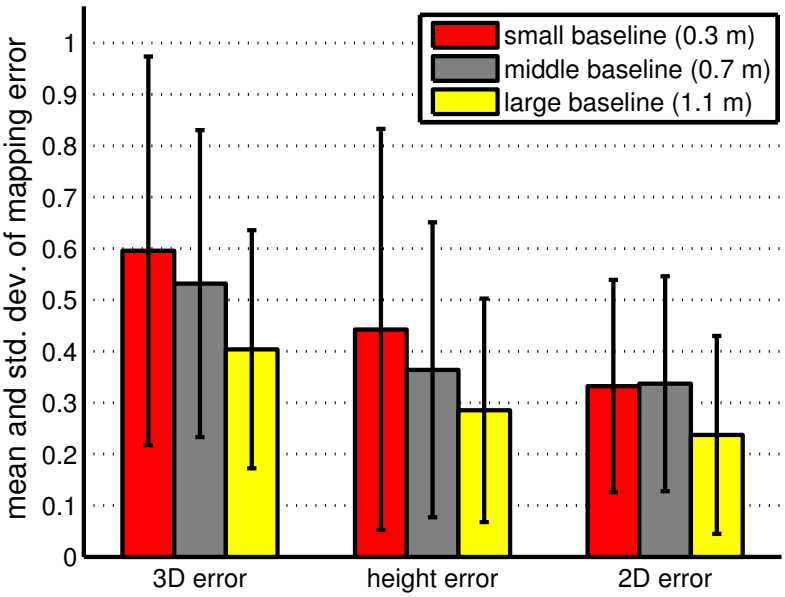

Figure 4.5: Mapping error under various baselines.

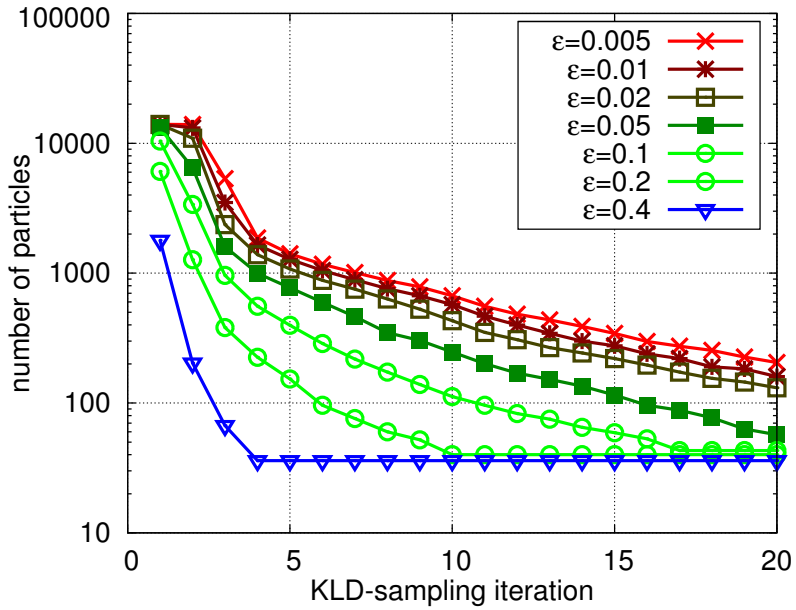

Figure 4.6: Number of samples required under various ε.

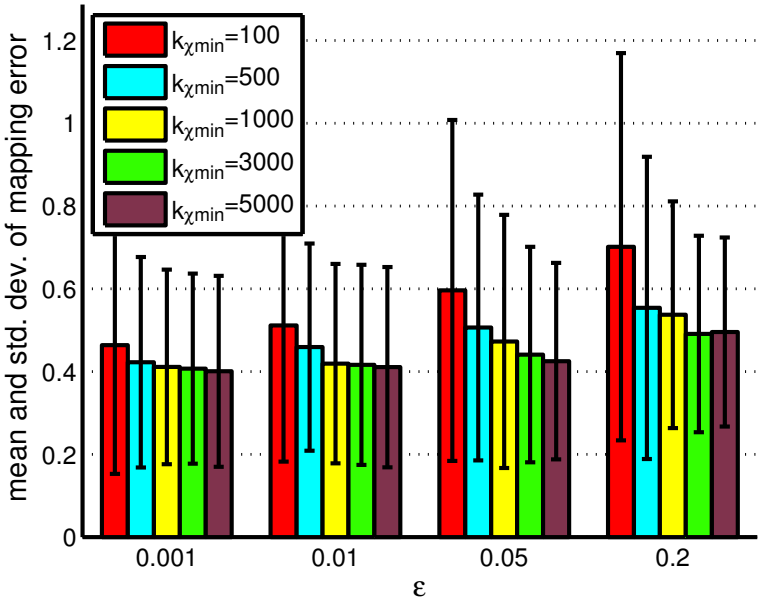

Figure 4.7: 3D Mapping error under various combinations of $k_{\chi min}$ and ε.

4.6.6 Performance Evaluation of KLD-sampling

To examine the performance of KLD-sampling, we conducted the last series of experiments by varying the values of ε and $k_{\chi min}$. This technique is also recommended by Fox (2003). We used a bin size of 0.5 m $\times$0.5 m$\times$0.5 m and fixed δ and $n_{\chi max}$ to 0.01 and 300000 respectively. Furthermore, we initialized the particle filters with $N = 13000$ and integrated negative information for all experiments. Figure 4.6 plots the number of particles as a function of KLD-sampling iterations and ε. As can be seen, the number of particles is reduced below $n_{\chi min}$ (e.g. 1000) after several updates of the measurements. Moreover, with a larger ε, the number of required particles drops faster than for a smaller ε. For our experiment, the number of particles is reduced below $k_{\chi min}$ (e.g. 1000) after several updates (e.g. five or ten) of the measurements.

Figure 4.7 illustrates the 3D mapping accuracy under various ε and $k_{\chi min}$. A smaller ε yields better results, while a larger ε leads to worse mapping accuracy. Moreover, it is obvious that a larger $k_{\chi min}$ leads to better results for all ε values. However in practice, we need to consider the trade-off between the time complexity and the mapping accuracy. Mapping with a larger $k_{\chi min}$ results in a good position approximation. On the contrary, utilizing too many particles requires more computational time. For example, the difference of 3D mapping error between $k_{\chi min} = 1000$ and $k_{\chi min} = 5000$ for $\varepsilon \leqq 0.01$ is less than two centimeters, which is relatively low as compared to the previous mean absolute mapping error of approx. 0.4 m, while the time consumption is doubled at the same time. Hence, it is reasonable for us to choose $k_{\chi min} = 1000$ rather than $k_{\chi min} = 5000$ for $\varepsilon \leqq 0.01$ considering the balance between efficiency and accuracy. In addition, for

$k_{\chi min} = 1000$ and $\varepsilon \leqq 0.01$, KLD-sampling only uses approx. 7 % of particles of the fixed sampling approach, but yields nearly the same good mapping accuracy.

4.7 Conclusions and Future Work

In this chapter, we presented a novel 3D sensor model, which considers both detection likelihood and signal strength for localizing UHF RFID tags with a mobile agent. The contributions of this chapter are summarized as follows:

- We pointed out that our 3D sensor model can be used to determine the 3D position of RFID tags by mounting two antennas at different heights on the robot.
- We demonstrated that 2D mapping accuracy can be improved by applying the 3D sensor model.
- We utilized the negative information to further improve the mapping accuracy and employed the KLD-sampling to perform the mapping task in real-time.

By using our stereo antennas setup and incorporating negative information, we are able to localize RFID tags with a mean absolute localization error of 0.24 m in 2D and 0.40 m in 3D with 0.28 m error for height. As compared to the existing 2D sensor model based approaches, our 3D sensor model improves the 2D mapping accuracy by approx. 12.0 % (from 0.401 m to 0.353 m). Additionally, utilization of negative information reduces the mean absolute mapping error by approx. 26.3 % (from 0.38 m to 0.28 m) for height. Moreover, with the KLD-sampling, we are able to save approx. 90 % computational time, while the mean mapping error increases by two or three centimeters.

There are several possible extensions of this work. First, due to the limitation of our hardware, we only used two antennas for our experiments, therefore it would be interesting to see if the 3D mapping accuracy can be improved by rotating our stereo antennas or installing more RFID antennas on the robot. Second, for 3D mapping of RFID tags, we only applied the grid-based approach; hence it is interesting to investigate if the same accuracy can be obtained by the particle filter based approach.

Chapter 5

Path Following with RFID Tags in Unknown Environments

In this chapter, we present a novel approach incorporating a combination of RFID and odometry information into the motion control of a mobile robot for the purpose of path following in unknown environments. Our method utilizes RFID measurements as landmarks and makes the robot autonomously follow a path that was previously recorded during a manual training phase. This chapter is organized as follows. After an introduction in Section 5.1, we review the related work in Section 5.2. Afterwards, we describe our path following approach in Section 5.3. Then, the details of the motion control algorithm are explained in Section 5.4. Finally, we present experimental results in Section 5.5 and draw conclusions in Section 5.6.

5.1 Introduction

Autonomous navigation of a mobile agent along a predefined path has many applications, such as environmental surveillance, service, and security. Traditional methods usually use a map or landmarks to represent the environment. The robot estimates its position by matching the sensor data with the map or the landmarks and determines its path to follow. This has been studied extensively for indoor robots with laser range finders by scan matching (Lu and Milios (1997), Surmann *et al.* (2003), and Hähnel *et al.* (2003)) or by comparing the similarities of visual features from the camera images (Furgale and Barfoot (2010) and Tang and Yuta (2002)). However, these methods require a significant amount of sensing and processing power.

Due to its simple, reliable, and contactless way of identifying products, RFID has become an emerging technology and thus has been used in many industrial environments, like warehouses, stores or libraries. Given the present infrastructures, RFID navigation features a cost-effective method if the robot is equipped with an RFID reader for inventory tasks. Therefore, we propose a new method employing a combination of RFID and odometry measurements for path following purpose.

In particular, we apply the teaching and playback scheme to perform this task, which has already been successfully used in different navigation systems with various sensors

(see Tang and Yuta (2002)). Precisely, during the teaching stage, the robot is manually controlled to move along a desired path. RFID measurements and the associated motion information are recorded in an online-fashion as reference data in this phase. In the second stage, the robot shall follow this path autonomously. Therefore, we compare the current RFID measurements to the previously recorded reference data to estimate the robot's relative position with respect to the reference path. As a result, motion control commands are generated by fusing the measured position and the reference motion data to steer the robot. Our approach needs no prior information about RFID sensor models, the distribution and positioning of the tags, and a map of the environment. Particularly, it is adaptive to different reader power levels and various tag densities, which have a major impact on the RFID performance. Extensive experiments with a Scitos G5 robot in different environments like a library, a supermarket, and hallways confirm the effectiveness of our approach.

This work was presented at the 2012 IEEE/RSJ International Conference on Intelligent Robots and Systems (IROS 2012) (Liu *et al.* (2012)). Furthermore, this work represents an extension of our previously published approach on path following using received signal strength (RSS) only (Liu *et al.* (2011)), which received the best paper award within the Symposium on RFID Technologies and Internet of Things at the 19th International Conference on Software, Telecommunications and Computer Networks (SoftCOM 2011). Through the integration of odometry data, the robot is able to navigate along more complex paths, as opposed to following a straight route in a hallway in Liu *et al.* (2011). Odometry, on the one hand, may be used to get quite accurate estimates of the change in position over short periods of time, but on the other hand, is very sensitive to accumulative error over long distances. Therefore, we utilize a combination of RFID as well as odometry information embedded into a particle filter to compensate for the errors of both and generate a new and reliable navigation system.

5.2 Related Work

Radio-based positioning systems have been widely researched in the literature. The global positioning system (GPS), which was developed in the 1970s, provides the position information of an object in outdoor environments with an accuracy of several meters. Other wireless devices, such as Bluetooth, Wifi, and RFID, are able to localize the objects inside buildings with an accuracy ranging from several meters to centimeters. For a comparison of different indoor positioning approaches, we refer to Vorst *et al.* (2008a).

Each RFID tag provides a unique identifier and thus can be used as the landmark for the robot localization as well as navigation. However, the RFID reader does not provide any information about the tag's pose, therefore a number of model-based or fingerprinting-based techniques have been proposed for the localization of mobile robots.

Radio frequency (RF) location fingerprinting approaches use the radio signal from RFID readers, WiFi access points, GSM (global system for mobile communications), or

(a)

(b)

Figure 5.1: (a) RFID-tagged library scenario; (b) High frequency (HF, red) and ultra high frequency (UHF, blue) tags attached to the books. Only the passive UHF tags are used throughout our experiments - more information on the environment as well as the project (AmbiSense) can be obtained from http://www.ambisense.org.

other RF-based sensors to represent the observations. The actual location of an agent is estimated by matching the current observations with the recorded measurements in a database. These approaches do not rely on an explicitly predicted model of the sensor's behavior. Instead, an a priori set of fingerprints, which expresses the sensor's output at sampled locations in the global frame, has to be recorded in advance. Fingerprinting-based approaches are therefore assumed to be more accurate and robust with regard to location-specific distortions; for this reason, we use fingerprints in our path-following approach.

5.2.1 Model-based Localization

Locating a mobile agent using a model-based approach is usually considered to be the inverse process of mapping, as described in Chapter 3 and Chapter 4. Hähnel *et al.* (2004) utilized a probabilistic sensor model, which describes the likelihood of a tag detection event, to localize mobile robots given the mapped tags. They also showed that a fusion of the RFID and the laser data makes the global localization of a robot faster than the laser data alone. The average positioning error reported by the authors is approx. 0.5 m. Joho *et al.* (2009) incorporated the signal strength into the sensor model to improve the localization accuracy of a mobile robot. The combined sensor model achieves an average localization accuracy of about 0.35 m, which is an improvement of 30% as compared to the previous tag detection model.

Miller *et al.* (2010) fused the RFID measurements with the LIDAR data into a Rao-Blackwellized particle filter to simultaneously localize the vehicle and map RFID tags attached to the assets. A combination of RFID and LIDAR measurements enables the

mobile robot to reliably localize itself in large and symmetric environments. To reduce the computational cost introduced by particle filters, Boccadoro *et al.* (2010) used Kalman filters for the localization of a mobile robot. Their experiments showed that, on the one hand, for the environment with low tag densities, the Kalman filter achieves the same localization accuracy as the particle filter, while the Kalman filter gives worse results in the environment with high tag densities; on the other hand, the computational time for the particle filter increases with the number of tags in the environment, whereas it is constant for the Kalman filter.

Some researchers employed RFID tags in a special scenario, called smart floor, for the localization and navigation of the mobile robot. A large number of RFID tags have to be installed under the floor to provide the position information of the robot. HF tags are usually chosen for this scene and in most case the tags must be assigned with some prior information about their global positions. Some representative works are done by Kämpke *et al.* (2008), Senta *et al.* (2010), Johansson and Saffiotti (2009), Kodaka *et al.* (2008), and Park and Hashimoto (2009).

Recent research also explores the application of UHF RFID for navigation and path following purposes using mobile robots. In most of the applications, a precise mapping of the RFID tags is not required. Kulyukin *et al.* (2006) used RFID labels as landmarks for the navigation of visually impaired people in structured indoor environments. The RFID tags are deployed in the environment and serve as topological nodes for the navigation of the robot. The robot is able to navigate itself based on the laser data and execute different actions (i.e. follow-hallway, make-u-turn, turn-left, and turn-right) according to the information stored in the tags. Gueaieb and Miah (2009) utilized the phase difference of RFID signals for the navigation task. The mobile agent is able to follow virtual paths that link the tags' orthogonal projections to the ground. Kim *et al.* (2007) developed an automated location sensing and docking system by estimating the direction of arrival signals via a dual directional RFID antenna.

5.2.2 Fingerprinting-based Localization

Radio fingerprinting-based approaches show a huge advantage over model-based approaches, since they are able to capture the unpredicted features in the existing radio infrastructures. In general, radio fingerprints represent a specific location by the signal strength information from multiple wireless sensors. The position estimation of the object is achieved by matching the observed measurement with the collected samples in the database. Fingerprinting technology is based on the fact that the radio signal propagation is hard to predict in practice due to the impact of many environmental factors. A thorough survey on radio fingerprinting techniques can be found at Kjærgaard (2007).

Bahl and Padmanabhan (2000) introduced a fingerprinting-based system (RADAR) to localize and track mobile agents. By observing the signal strength from several 802.11 access points, they are able to locate a laptop in an office building. They also evaluated the tracking accuracy between a fingerprinting-based approach and a propagation

model-based approach. They showed that the propagation model-based approach provides a cost-effective way to track objects, since it does not require any empirical measurements to generate the map of the fingerprints (i.e. the signal strength map). However, the fingerprinting-based approach achieves better tracking results than the propagation model-based approach, since it is able to characterize the location-dependent factors in the existing radio infrastructures.

Several distribution-based extensions have been proposed (e.g. Youssef *et al.* (2003) and Ladd *et al.* (2005)) to achieve a better localization accuracy of the object. For example, Youssef *et al.* (2003) improved the tracking accuracy by modeling the noisy features of the radio signals with probabilistic distributions. They reduced the computational cost by searching the radio map with a technique called joint clustering (JC). Ladd *et al.* (2005) used a sensor fusion approach embedded in a Bayesian framework to track a moving object (i.e. a robot or a laptop). They showed that they are able to track mobile devices reliably, with an error less than 1.5 meters, which is a significant improvement to the original RADAR system (with a mean tracking error of 2.5 meters). Otsason *et al.* (2005) utilized wide GSM-based signal strength as a representation of the fingerprint for indoor localization in large multi-floor buildings. They used k-nearest neighbors algorithm for the localization and achieved a median accuracy of 5 meters in their experiments.

In the field of RFID-based fingerprints, Lim and Zhang (2006) developed an indoor positioning system based on RFID fingerprints. In their approach, a set of measurements (i.e. samples of RFID reading patterns) are first collected at discrete locations in the environment by a mobile RFID reader. Afterwards, the location of a moving carrier (i.e. a human or a robot) is determined by a pattern recognition algorithm. The mean localization error is less than one meter. The proposed approach is expected to be able to solve the positioning problems of mobile devices in industrial environments where RFID tags are employed, since this approach does not rely on the tag distributions as well as the reader configurations.

The data recording process can be further automated using a mobile robot due to its autonomy and mobility. In this case, the fingerprints are annotated with the locations of the robot in the global world frame. Furthermore, the odometry provided by the robot can further facilitate the localization of the robot. This approach is comprehensively evaluated by Schneegans *et al.* (2007), Vorst and Zell (2010a), Vorst *et al.* (2011), and Vorst *et al.* (2011). They localized the robot with a particle filter by matching the current fingerprints with the pre-collected samples using vector space similarity measures and weighted k-nearest neighbors (WKNN). The experiments in a laboratory and a corridor environment with a total size of 125 m^2 showed that they are able to localize the robot with a mean error of about 0.2 m.

Gaussian processes, which work as a non-parametric approach for probabilistic modeling, have been widely used for modeling the signal strength in the context of radio-based localizations (Schwaighofer *et al.* (2004), Ferris *et al.* (2006), and Seco *et al.* (2010)). Among these works, Schwaighofer *et al.* (2004) presented an approach to estimate the

position of a mobile user using the signal strength obtained from a cellular network. They used a Gaussian process model, which represents the distribution of signal strength, for the position estimation. An advantage of the Gaussian process model is that it can be built up based on a small number of pre-collected measurements. The mean tracking accuracy reported in their experiments in a large hall environment with a size of 250 m$\times$180 m is 7.5 meters. Ferris *et al.* (2006) extended this work by using a Bayesian filter. More precisely, they constrained the motion of the user by modeling the environment with a mixed graph. The average tracking error in a three floors building with 54 rooms and 75 access points is about 2.1 meters. This approach is further implemented and evaluated by Seco *et al.* (2010) for the active RFID network. Their experiments with 71 tags in a building with an area of approx. 1600 m^2 achieved a median localization error of 1.5 m. They also showed that the Gaussian process model gives a better performance than parametric-based models.

5.3 Algorithm Overview

5.3.1 Data Recording During the Teaching Stage

During the teaching stage, the robot is manually controlled to move along a desired path in an RFID tagged environment. While traversing the environment, arrays of RSS values $\mathbf{f}_t$ of the detected tags (see Section 3.3 for more detail) as well as odometry observations $\mathbf{m}_t$ are gathered on the fly and stored as reference fingerprints $\mathbf{F}_t$ at each time step t: $\mathbf{F}_t = (\mathbf{f}_t, \mathbf{m}_t)$. Here $\mathbf{m}_t = (v_t, \omega_t)$, with v_t being the translational velocity and ω_t the rotational velocity respectively. The resulting set of fingerprints $M = (\mathbf{F}_1, \mathbf{F}_2, ...)$ expresses the desired path in the spatial domain as pairs of RFID and odometry observations. In our configuration, the robot has two antennas, so $A = 2$. The reference fingerprints are sorted ascending over time and each fingerprint has a unique index $i \in \{1, ..., I\}$, where I is the total number of reference fingerprints.

5.3.2 Navigation of the Robot in the Playback Stage

The goal of this stage is to make the robot autonomously follow a previously defined path represented by fingerprints only. Firstly, the robot's initial position shall not be constrained to the start position of the recording, and additionally, the mobile agent shall be able to compensate for small relative offsets to the recorded path. Using odometry only, an offset to the reference path would obviously lead to a bad result. Therefore, we utilize RSS as well as index differences between two antennas by comparing the current RFID observations with the reference fingerprints for position corrections, as detailed later (see Section 5.3.4 and Section 5.3.5). As a result, the robot can adjust its position and movement in this stage based on the RFID measurements and deal with the cumulative error of the odometry.

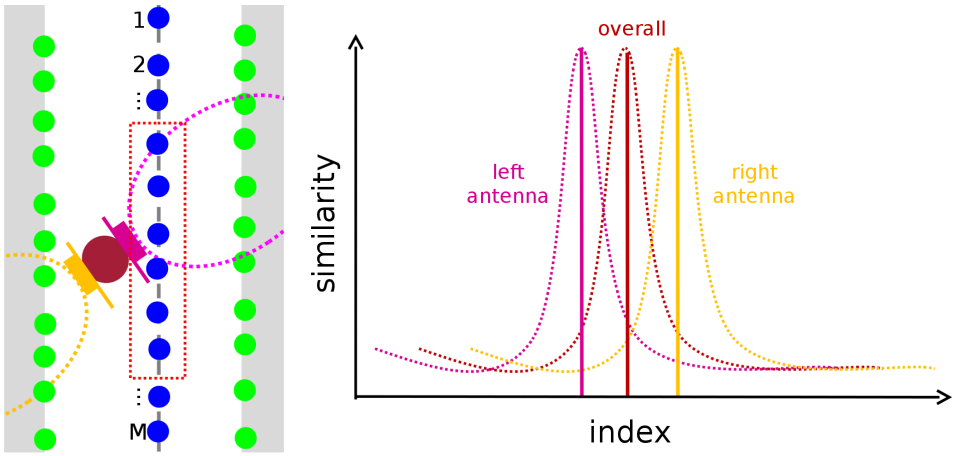

(a) (b)

Figure 5.2: Index estimation: (a) Robot following path with two antennas (orange, purple), RFID tags (green), reference fingerprints (blue), and the closest reference fingerprints (red box). (b) Respective similarities of left and right antenna, which are used to estimate the index difference as well as the overall weighted similarity.

5.3.3 Similarity Measures

The similarity function $sim(\mathbf{a},\mathbf{b})$ returns a positive scalar value, describing the similarity between two vectors $\mathbf{a}$ and $\mathbf{b}$. In our approach, we individually compute the similarities between the current RFID measurement $\mathbf{g}_t$ and the reference fingerprint $\mathbf{f}_j$ for each antenna $sim\left(\mathbf{g}_t^{(a)},\mathbf{f}_j^{(a)}\right)$. The overall similarity $sim(\mathbf{g}_t,\mathbf{f}_j)$ of the current observation to a reference fingerprint is calculated by weighting the individual similarities with the number of tags detected at the respective antennas.

$$sim(\mathbf{g}_t,\mathbf{f}_j) = \sum_{a=1}^{A} sim\left(\mathbf{g}_t^{(a)},\mathbf{f}_j^{(a)}\right) \frac{n\left(\mathbf{g}_t^{(a)},\mathbf{f}_j^{(a)}\right)}{\sum_{a=1}^{A} n\left(\mathbf{g}_t^{(a)},\mathbf{f}_j^{(a)}\right)} \tag{5.1}$$

Here, $n\left(\mathbf{g}_t^{(a)},\mathbf{f}_j^{(a)}\right)$ is the maximum number of detected tags in $\mathbf{g}_t^{(a)}$ as well as in $\mathbf{f}_j^{(a)}$. In our experiments, we use the cosine similarity (COS) which has also been utilized for trajectory estimation and localization purposes in Vorst and Zell (2009) as well as Vorst and Zell (2010a).

$$sim\left(\mathbf{g}_t^{(a)},\mathbf{f}_j^{(a)}\right) = \frac{\sum_{l=1}^{L} g_t^{(a,l)} f_j^{(a,l)}}{\sqrt{\sum_{l=1}^{L}\left(g_t^{(a,l)}\right)^2}\sqrt{\sum_{l=1}^{L}\left(f_j^{(a,l)}\right)^2}} \tag{5.2}$$

where $g_t^{(a,l)}$ and $f_j^{(a,l)}$ mean the measured values (signal strength in our case) of tag l in $\mathbf{g}_t^{(a)}$ and $\mathbf{f}_j^{(a)}$ respectively. For a comparison of different similarity measures, we refer to Vorst *et al.* (2011).

5.3.4 Orientation Estimation with Particle Filters

We approximate the angular deviation of the robot with respect to the expected path as the index difference between the left ($i_t^{(0)}$) and the right ($i_t^{(1)}$) antenna (see Figure 5.2):

$$e_{t,\theta} = i_t^{(0)} - i_t^{(1)} \tag{5.3}$$

An estimate for the index of the current fingerprint in the reference fingerprints can be calculated by a mean of the indices over both antennas:

$$i_t = \frac{i_t^{(0)} + i_t^{(1)}}{2} \tag{5.4}$$

Each antenna's index is estimated by using independent particle filters. More precisely, the state of each antenna is represented by N samples (particles), that are updated after receiving new RFID observations. Each particle consists of a hypothesis index $x_t^{(n,a)}$ and an appropriate weight $w_t^{(n,a)}$. The estimated index of the antenna is calculated by a weighted mean over all particles:

$$i_t^{(a)} = \sum_{n=1}^{N} x_t^{(n,a)} w_t^{(n,a)} \tag{5.5}$$

Particle filters perform three central steps iteratively:

1. *Prediction*: The position of each particle at time step t is predicted by its previous state and an uncertainty or noise model:

$$x_t^{(n,a)} = x_{t-1}^{(n,a)} + \mathcal{N}(\mu, \sigma^2) \tag{5.6}$$

   Here, $\mathcal{N}(\mu, \sigma^2)$ is Gaussian random noise added to the control input, with mean μ and standard deviation σ:

$$\mu = \frac{v_t}{v_{t,e}(K_f)}$$

   In our case, the particles' positions are actually expressed in the reference fingerprints' index-frame and represented by 1D scalar values (e.g. if a particle's position is between $\mathbf{f}_5$ and $\mathbf{f}_6$, $\mathbf{x}_t \in [5,6]$). μ is computed from the current velocity (based on the control input $\mathbf{m}_t$) and the estimated reference velocity (as explained in more detail in Section 5.4).

2. *Correction*: The weights of the particles are updated according to the observation model $p(\mathbf{g}|\mathbf{x},M)$, i.e. the likelihood of measurement $\mathbf{g}_t$ given the current sample set $\mathbf{x}_t$ and the M reference fingerprints:

$$w_t^{(n,a)} = \eta_t^{(a)} w_{t-1}^{(n,a)} p\left(\mathbf{g}_t^{(a)} | x_t^{(n,a)}, M\right) \tag{5.7}$$

Here $\eta_t^{(a)}$ is a normalizing factor which ensures that $\sum_{n=1}^{N} w_t^{(n,a)} = 1$ and M is the representation of the desired path (as explained in Section 5.3.1).

In our method, the observation model $p(\mathbf{g}_t|x_t^{(n,a)},M)$ represents the likelihood of observing the fingerprint $\mathbf{g}_t$ from the sample position $x_t^{(n,a)}$ given the M reference fingerprints and is computed individually for each antenna. Let $\mathbf{f}_{j_1},...,\mathbf{f}_{j_K}$ be the K most similar reference fingerprints compared to $\mathbf{g}_t$ (according to Equation (5.1)). We extract those by comparing the current measurement $\mathbf{g}_t$ to the $K+1$ reference fingerprints centered around $\mathbf{f}_{i_t}$, i.e. $\{\mathbf{f}_{j_1},...,\mathbf{f}_{j_K}\} \in [\mathbf{f}_{i_t-K},\mathbf{f}_{i_t+K}]$. This improves the robustness and reduces the computational cost if the number of reference fingerprints is large.

$$p(\mathbf{g}_t^{(a)}|x_t^{(n,a)},M) = \sum_{k=1}^{K} sim(\mathbf{g}_t^{(a)},\mathbf{f}_{j_k}) exp(-\frac{1}{2} d^2(x_t^{(n,a)},x_{j_k})) \tag{5.8}$$

where $d^2(\cdot)$ is a distance measure applied to the indices of the respective fingerprints $\mathbf{g}$ and $\mathbf{f}$

$$d^2(x_t^{(n,a)},x_{j_k}) = \frac{(x_t^{(n,a)} - x_{j_k})^2}{\delta_d} \tag{5.9}$$

and δ_d is the bandwidth parameter of the translational displacement component. As a result, the particles close to the similar reference fingerprints will get awarded by the observation model using Equation (5.8).

3. *Resampling*: If the effective sample size (ESS) falls below a predefined threshold, e.g. $N/2$, resampling is performed and all degenerated particles are replaced.

5.3.5 Estimation of the RSS Difference

The distance of the robot to the recorded path is expressed as the weighted average over the RSS differences between the current fingerprint and the K most similar reference fingerprints:

$$e_{t,d} = \frac{1}{\sum_{k=1}^{K} sim(\mathbf{g}_t,\mathbf{f}_{j_k})} \sum_{k=1}^{K} sim(\mathbf{g}_t,\mathbf{f}_{j_k}) d_t(\mathbf{g}_t,\mathbf{f}_{j_k}) \tag{5.10}$$

Where $d_t(\mathbf{g}_t, \mathbf{f}_{j_k})$ is the RSS difference of the fingerprints $\mathbf{g}_t$ and $\mathbf{f}_{j_k}$. The idea of using the K most similar reference fingerprints is to obtain a robust estimation of the RSS difference. We use this difference as an approximation for the distance of the robot to the reference path. Since in our setup (see Figure 5.1a) the two antennas span an angle of 180°, $d_t(\mathbf{g}_t, \mathbf{f}_{j_k})$ can be expressed as:

$$d_t(\mathbf{g}_t, \mathbf{f}_{j_k}) = \sum_{l=1}^{L} \sum_{a=1}^{A} (-1)^a (g_t^{(a,l)} - f_{j_k}^{(a,l)}) \tag{5.11}$$

5.4 Control Algorithm

Both the odometry and the RFID measurements are used for the navigation of the robot. The movement of the robot is divided into two independent components: translational (v) velocity and rotational velocity (ω). Let K_m and K_f be two manually set scalar parameters describing the number of the closest reference fingerprints taken for the estimation of v and ω, respectively. Then the estimated velocities $v_{t,e}$ and $\omega_{t,e}$ can be computed as the weighted average over the $K \in \{K_m, K_f\}$ closest reference fingerprints:

$$\omega_{t,e}(K) = \frac{1}{\sum_{k=i_t}^{i_t+K} sim(\mathbf{g}_t, \mathbf{f}_k)} \sum_{k=i_t}^{i_t+K} sim(\mathbf{g}_t, \mathbf{f}_k)\omega_k \tag{5.12}$$

$$v_{t,e}(K) = \frac{1}{\sum_{k=i_t}^{i_t+K} sim(\mathbf{g}_t, \mathbf{f}_k)} \sum_{k=i_t}^{i_t+K} sim(\mathbf{g}_t, \mathbf{f}_k)v_k \tag{5.13}$$

The parameter K_m is used to control the translational speed v_t. It reduces the current speed of the robot to prepare for a turn. The translational velocity v_t is computed as follows:

$$\begin{cases} v_t = v_{t,e}(K_m), & \omega_{t,e}(K_m) > \frac{\omega_{max}}{K_m} \\ v_t = v_{max}, & else \end{cases} \tag{5.14}$$

ω_{max} is the maximum rotation speed among all reference fingerprints. K_f determines whether the robot should rely on the RSS measurements during the navigation stage and determines the rotational speed ω_t. The rotational velocity ω_t is defined as:

$$\begin{cases} \omega_t = \omega_{t,e}(K_f), & \omega_{t,e}(K_f) > \frac{\omega_{max}}{K_f} \\ \omega_t = \omega_{t,f}, & else \end{cases} \tag{5.15}$$

$\omega_{t,f}$ is the PID controller component, that combines the orientation $e_{t,\theta}$ as well as the RSS difference $e_{t,d}$ to ensure that the robot follows the reference path. Precisely, we use two proportional coefficients ($P = [Ko, Kr]$), as shown in Equation (5.16), to combine the orientation and RSS difference together to make the robot follow the trajectory recorded

(a) (b)

Figure 5.3: The two experimental environments. (a) A library (9 m×20 m) with shelves (red boxes) of books tagged with RFID labels. (b) Hallway environment (50 m×80 m) which consists of an artificial supermarket laboratory (red box), a computer museum (green box), and corridors (orange boxes). Especially the corridor (dashed orange box) is used to evaluate the performance of our approach under different parameters like various tag densities.

at the teaching stage:

$$\omega_{t,f} = P \cdot [e_{t,\theta}, e_{t,d}]^T = Ko \cdot e_{t,\theta} + Kr \cdot e_{t,d} \tag{5.16}$$

Since in our case, the RFID sample frequency is 2 Hz and the robot needs a certain time to decelerate from a high speed, we constrain K_m to be larger than K_f, otherwise the robot would deviate from its tracking path. For further details we refer to our earlier work (Liu *et al.* (2011)).

Table 5.1: Description of the experimental data: ranges (min.-max.), mean values (∅)

Environment	Power Level (dBm)	Trajectory length (m)	Duration (s)	Number of Tags detected per inquiry	Number of unique tags detected
Library	30.0	50.76	538	10-144, ∅: 50.0	3313
Library	27.0	52.86	536	5-136, ∅: 33.6	2397
Library	24.0	53.12	533	3-70, ∅: 17.5	1363
Hallway	30.0	140.73	1455	0-210, ∅: 21.2	725

5.5 Experimental Results

5.5.1 Setup

The experiments were carried out with a Scitos G5 service robot from MetraLabs, as shown in Figure 5.1. The laser scanner is used throughout our experiments to provide the ground truth. RFID does not provide any obstacle information. To achieve obstacle avoidance, one needs to utilize other sensors, such as laser range finders, optical sensors, or sonar sensors. Note that the focus of this chapter is not obstacle avoidance, for which we employ a laser range finder. One may argue that if one already has a laser range finder installed on a mobile robot, it is unreasonable to use much less precise RFID measurements for path following. However, this chapter shows it is possible to use RFID fingerprints alone for path following in RFID tagged environments and this can be done without knowing a precise map of the environment. In our experimental setup, two antennas are installed with a height of 0.8 m and span an angle of 180°, which is different from the configurations used for mapping of RFID tags in Chapter 3 and Chapter 4.

We carried out our experiments in two kinds of environments: a library and a large indoor environment consisting of mainly hallways, as depicted in Figure 5.3. Firstly, we tested our approach in a single corridor environment under various tag densities to obtain an optimal set of parameters. In a final stage, we evaluated and verified the effectiveness and robustness of our method in a large hallway environment and a library environment (Figure 5.3b and Figure 5.3a).

The library contains about 7,000 books that are labeled with passive UHF RFID tags (Alien Technology Squiggle, ISO/IEC 18000-6C), as shown in Figure 5.1b. The books are distributed on the shelves at different heights reaching from 0.2 m to 3 m. We additionally placed tags on the walls of the adjacent corridors (at intervals of about 0.5 m and different heights) to ensure an appropriate tag density in the untagged areas. For the second environment, that was partly also used by Vorst *et al.* (2011) and Vorst *et al.* (2008b) (see Figure 5.3b), we additionally placed 250 tags on the walls of the long hallway part (see solid orange box in Figure 5.3b). These tags were distributed at different densities

to verify the robustness of our algorithm under various experimental setups.

For the teaching stage, we manually steered the robot in the corridor and recorded reference log files under four kinds of tag densities, namely highest (23.0 tags per inquiry), high (14.7 tags per inquiry), middle (7.8 tags per inquiry), and low (6.1 tags per inquiry). The true positions of the robot, computed with a laser-based Monte Carlo localization method, were recorded at the same time. For the purpose of comparing the performance of our approach under similar conditions, the recording of the references was performed on similar paths. The sample frequency of the RFID reader was set to 2 Hz and the maximum speed of the robot was limited to 0.1 m/s. In the library, three log files under different RFID power configurations were also recorded as reference data. As shown in Table 5.1, approx. 1100 measurements were recorded for each log file, with a distance traveled of about 50 m and a duration of about 10 minutes. In the hallway environment, the robot traveled around 140 m and the tag density was slightly lower.

The ideal parameters of the P-controller in our experiments depend on the RFID sample period and the maximum robot speed that the reference fingerprints were recorded at. We need several trials to adjust the control parameters (nearly 4 trials, which usually take 5 minutes) if the configurations of the experiment are different. In our experiments, the maximum robot speed and RFID sample period are fixed during the teaching phase. Therefore, we set $P = [0.008, -0.06]$.

5.5.2 Preliminary Results

Distance Estimation

We first did some experiments to observe how the RSS difference changes when the robot stays at different positions in the corridor. In these experiments, we manually controlled the robot moving like a cosine function through the corridor. In Figure 5.4, we plotted out the RSS difference with $K = 1$ (the case without smoothing, i.e. the original RSS difference) and $K = 5$ (the case of smoothed RSS difference) using Equation (5.10). It can be seen that the position of the robot and the corresponding RSS difference have some consistency. When the robot moves on the left side of the corridor (i.e. $y > 0$ in Figure 5.4a), the RSS difference is positive. Otherwise, when the robot travels on the right side of the corridor ($y < 0$ in Figure 5.4a), the RSS difference is negative. It can also be seen in Figure 5.4 that the RSS difference is nearly proportional to the distance between the robot and the expected trajectory. This property makes the later navigation feasible.

Robustness Against Disturbances

We examined the robustness of our approach in the next series of experiments. We started the robot at the center of the corridor with initial orientations of 45° and -45° to the expected trajectory. As shown in Figure 5.5, the robot is capable of navigating

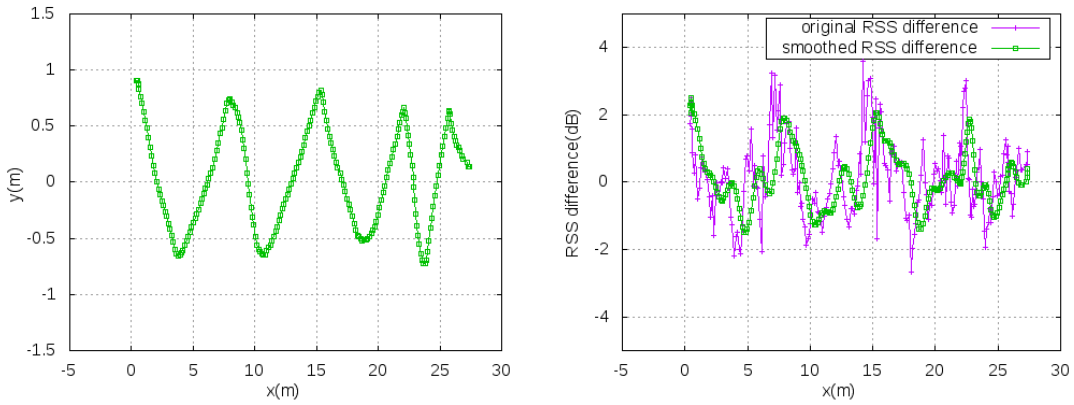

(a) (b)

Figure 5.4: Preliminary results indicate that RSS differences may be used to infer the relative position of the robot. (a) Actual trajectory of the robot. (b) Original and smoothed RSS differences.

through the corridor regardless of the initial angles of the robot. To further test the stability of our algorithm, we added some human disturbances while the robot navigated through the corridor (see in Figure 5.5). The orientation of the robot was altered with sudden disturbances at positions A, B, C, and D (nearly 40°). The results show that the robot is able to detect the changes of orientation quickly and adjust its heading back to the expected trajectory. Also, it can be seen that the navigation does not converge due to the noisy features of the RFID measurements (signal strength). Although a window filter and a particle filter are used to deal with the uncertainty, the noise still exists.

Different Reader Sampling Frequency

The influence of various RFID sample periods was investigated in the next experiments, as shown in Figure 5.6. In these experiments, the robot started at nearly the same pose and moved at a maximum speed of 0.3 m/s. We measured the mean and standard deviations of absolute tracking error (see Figure 5.6b). The results show that lower sample periods (i.e. higher sample frequencies) lead to smoother trajectories and lower absolute tracking errors than higher sample periods. This is obvious since the response of the controller at a lower sample period is faster. With a low sample period of 0.2 s, we achieved a mean absolute tracking error of 0.14 m, as shown in Figure 5.6b.

5.5.3 Impact of Particle Filters

The influence of the number of particles (N) on the tracking accuracy and the run-times of the navigation was examined in the next series of experiments. The algorithm was

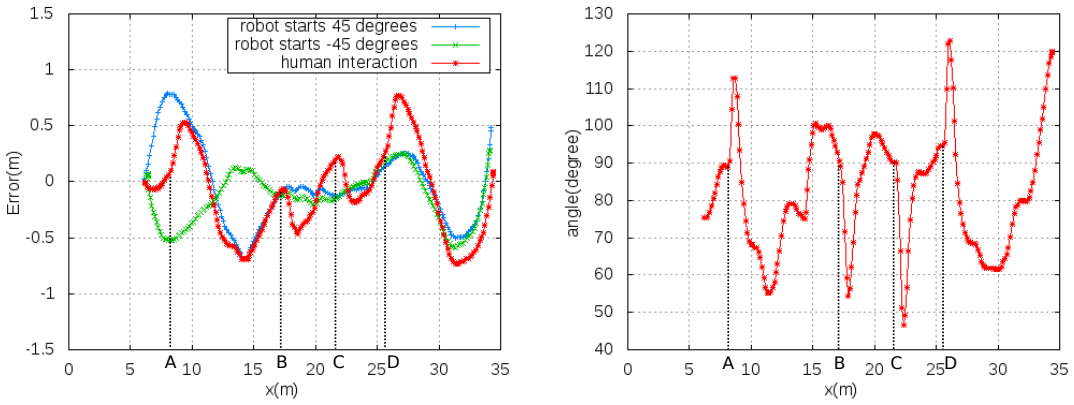

(a) (b)

Figure 5.5: Influence of different initial orientations on the navigation of the robot. (a) Tracking error. (b) Actual orientation of the robot under different disturbances.

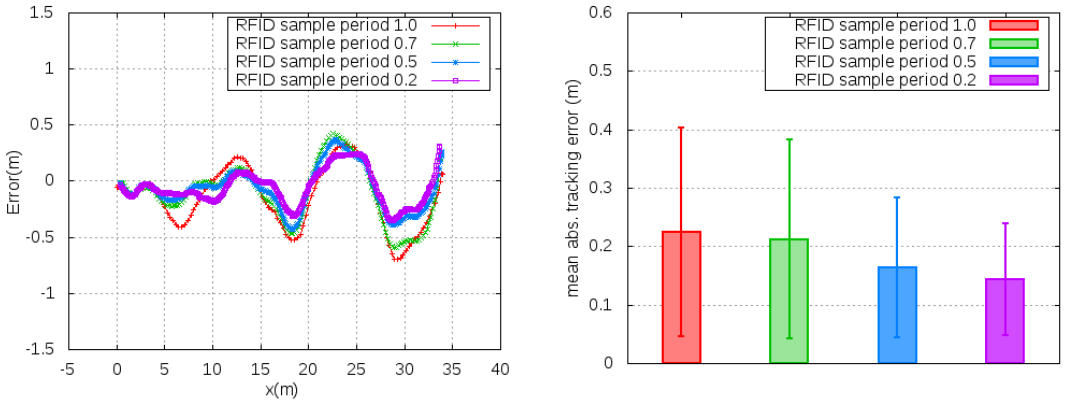

(a) (b)

Figure 5.6: Influence of different sample periods on the navigation of the robot. (a) Tracking error. (b) Mean and standard deviation of the tracking error.

Table 5.2: Tracking errors and average run-times for various number of particles in the hallway environment with a high tag density configuration.

Number of particles (N)	Mean $\pm$ std. dev. of tracking errors (m)	Max. tracking errors (m)	Run-times (s)
50	0.1094±0.0806	0.3486	0.010
100	0.0946±0.0530	0.4412	0.011
500	0.0659±0.0377	0.1748	0.015
1000	0.0577±0.0484	0.1917	0.029
2000	0.0660±0.0554	0.2287	0.041

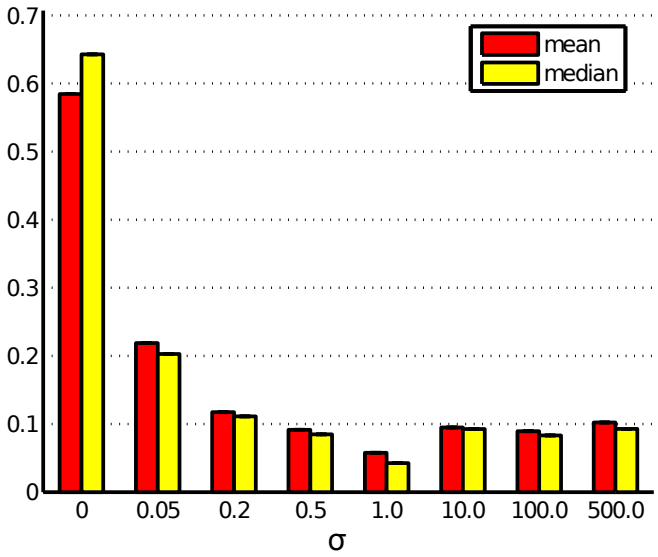

Figure 5.7: Mean and median tracking errors for various noise scales σ.

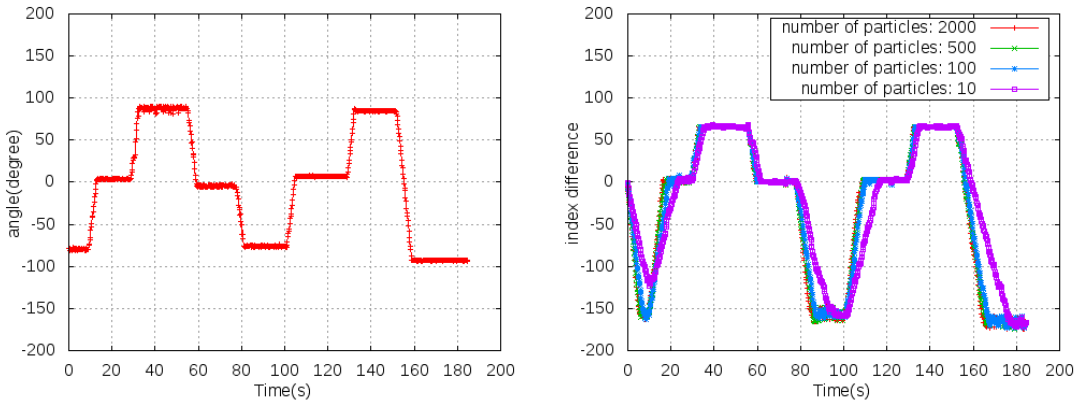

(a) (b)

Figure 5.8: Impact of the number of particles on the performance of the orientation tracking. (a) Actual orientation of the robot. (b) Index difference using various numbers of particles.

running on an Intel Core i5-2410M @ 2.3 GHz CPU, with 4 GB RAM. As shown in Table 5.2, the tracking results get worse with small N (e.g. N=50 or 100). We observed that the robot could not navigate with smaller N than 20. With $N > 100$, we achieved nearly the same navigation accuracy. On the other hand, for larger N, more computational time is required due to the increased number of particles.

Moreover, we investigate how the number of particles influences the performance of the orientation tracking in our algorithm. We remotely controlled the robot to rotate quickly for a certain angle and stopped it for several seconds. We repeated this several times. Finally, we applied a particle filter with different number of particles to observe the performance of our algorithm.

The index differences with different numbers of particles and the actual orientation of the robot are shown in Figure 5.8. It is obvious that the largest number of particles achieves the best tracking results. A large N is fast at tracking the orientation changes, but it also costs more run time. The tracking abilities of 100 particles, 500 particles, and 2000 particles do not have so much difference, but the run times increase rapidly (11 ms, 15 ms, and 41 ms for N=100, 500, and 2000 respectively as shown in Table 5.2).

In the next series of experiments, we investigated the stability of our approach for various noise-levels (σ) added to the odometry input, as shown in Figure 5.7. For a small σ (less than 0.2) the result is notably worse, whereas a large σ only decreases the tracking accuracy slightly. Obviously, too small σ values lead to an underestimation of the actual odometry error and thus give bad results. On the other hand, if the error is assumed to be too high, the particles are spread more and the overall particle density becomes lower. Still the estimation domain is completely sampled and covered with particles, whereas a lower particle density leads to slightly worse results due to the lower resolution. Finally,

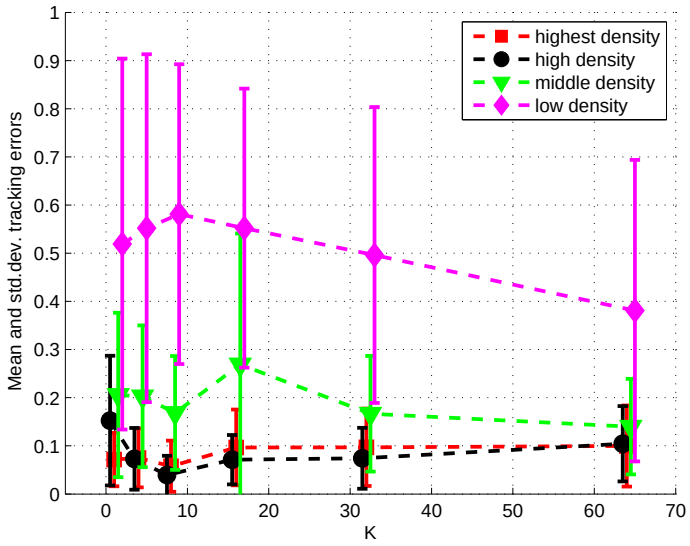

Figure 5.9: Mean and std. dev. of tracking error for various tag densities.

the best results regarding the experiments were achieved with $\sigma = 1.0$, which seems to give the best estimation of the control input's error.

5.5.4 Influence of Different Tag Densities

We fixed $N = 1000$ and $\sigma = 1$ and measured the effectiveness of our approach for various tag densities and different values of K (the closest reference fingerprints, see Section 5.4). The experiments were carried out in a corridor in front of the supermarket laboratory. The results are shown in Figure 5.9. As can be seen, higher tag densities lead to better results and increase the precision of our approach. For example, as compared to the environment with the lowest tag density, the environment with highest tag density improved the tracking accuracy by approx. 0.5 m (for $K = 8$). Moreover, we observed that the robot could not follow the path at a maximum speed greater than 0.2 m/s for environments providing low tag densities. In case of higher densities, the robot was able to track the path at a maximum speed of 0.7 m/s.

Generally, the choice of $K = 8$ produced the best results for high tag densities. Surprisingly, this is not the case if the environment features middle and low tag densities. It is difficult to explain the direct relationship between the tracking accuracy and K under middle and low tag densities. Still, an optimization of K generates an enhancement in navigation precision up to 0.13 m and 0.2 m for environments with middle and low tag densities respectively and thus has a major impact on the tracking accuracy.

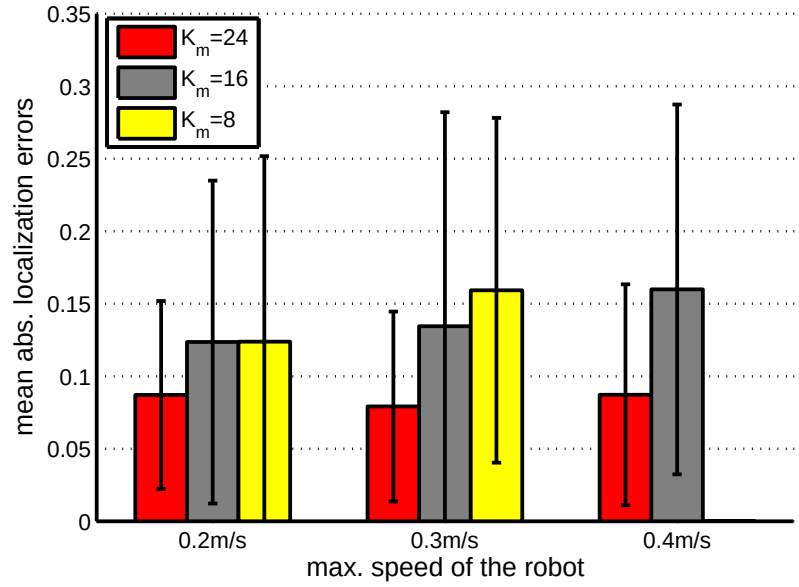

(a)

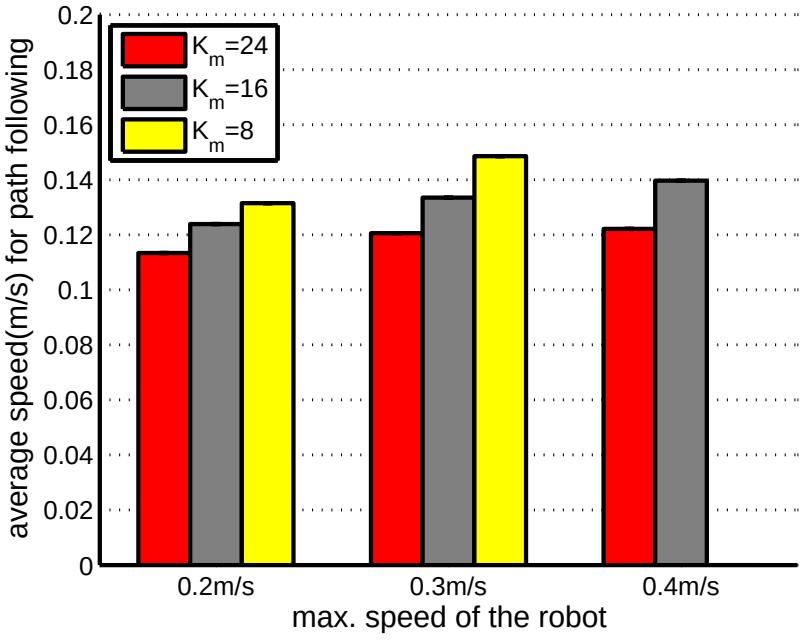

(b)

Figure 5.10: Speed vs. accuracy. (a) Tracking accuracy under different maximum speeds v_{max} and K_m; (b) Average navigation speed. For $K_m = 8$, the speed of 0.4 m/s was too high.

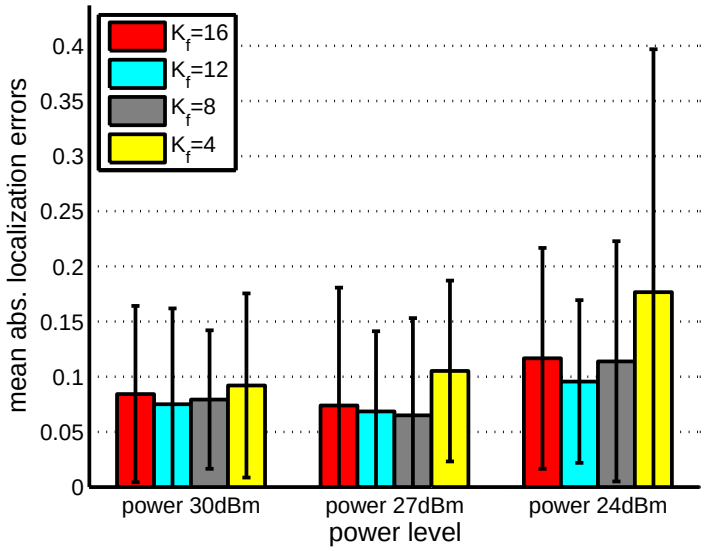

Figure 5.11: Impact of different reader power levels and K_f on the tracking error.

5.5.5 Parameter Evaluation

In the next experiments, we investigated the average speed that the robot can travel in the library under different maximum speeds v_{max} and K_m, as shown in Figure 5.10. We observed that speed and accuracy always conflict with each other. The largest K_m leads to the best precision, but the average speed slightly decreases. This is because the robot spends more time to move at a low speed while adjusting its position before making a turn. On the other hand, a smaller K_m results in a higher average speed but higher tracking errors. In our experiments, the robot lost the path it needed to follow for $K_m = 8$ and $v_{max} = 0.4$ m/s. Yet, in the library, the turning activity happens quite often (18 times), which amounts to 70% of the whole path and thus obviously limits the overall speed of the robot. In case of large environments with less curves, the average speed would be far higher.

The hallway environment achieved a slightly lower accuracy with a mean error of 0.2 m (cf. Figure 5.12b), which is due to the lower tag density. At some areas of the track, the RFID observations consisted of only one or even no tag detection at all. As a result, the tracking accuracy dropped to 0.6 m, since the measured RFID readings were not sufficient to compensate for the error that the robot deviated from the desired path.

5.5.6 Impact of the Reader Transmission Power

In the next experiments, we examined the influence of K_f under different power configurations in the library. The maximum navigation speed of the robot was set to 0.1 m/s and the particle filter was running with a fixed number of particles of $N = 1000$. As can be

seen in Figure 5.11, a too large or too small K_f obviously leads to higher tracking errors. The reason is that a large K_f gives the robot a higher belief in the odometry observations. Therefore, the robot relies too early on odometry at a turning place and thus wastes time to adjust its position through RFID observations. On the contrary, a small K_f makes the robot trust the RFID measurements too much and results in a delay for the robot to make a turn, since RFID observations are used to make up for the error of the odometry and not to make the robot to turn fast. Overall, $K_f = 8$ and $K_f = 12$ lead to roughly the same accuracy. At the full reader power level and $K_f = 8$, the robot achieves a mean navigation accuracy below 0.07 m with a standard deviation of approx. 0.08 m. An example of an actual trajectory under the full reader power with $K_f = 8$ is shown in Figure 5.12a. Compared with the mean error of 0.18 m for the raw odometry trajectory, our approach is more precise. Due to its cumulative characteristic, the localization accuracy of odometry will even get far worse for longer tracks. This can be seen in the hallway environment (Figure 5.12b), where the mean error of the odometry grows to 0.9 m.

Figure 5.11 also shows an interesting result for different reader power levels: the tracking accuracy remains the same or even improves if the power is reduced from full power (30 dBm) to 27 dBm. But, if the power is too low (24 dBm), the results get worse. By reducing the power, the reading range of the RFID reader becomes smaller and less tags are detected and thus the position uncertainty is lower. On the other hand, a higher transmission power will report more tags per inquiry and a larger band of RSS values. The additional observations seem to make up for the uncertainty introduced by the higher reading range.

5.6 Conclusions and Future Work

In this chapter, we presented a novel path following approach for mobile robots in RFID tagged environments by fusing RFID fingerprints and odometry. Our method is based on the teaching and playback scheme and does not rely on an explicit map of the environment. Particularly, during the teaching phase, a reference path is recorded by steering the robot manually through the environment. Afterwards, the robot is capable of navigating along that route autonomously. Key parameters were evaluated in a library environment with thousands of tags. The performance of our approach was validated in a large hallway environment with regard to different setups (e.g. the RFID tag density).

At a maximum speed of 0.3 m/s and an RFID sample frequency of 2 Hz, our method achieved a mean abs. tracking error of approx. 0.07 m in the library. Our algorithm provides a cost-effective and computationally inexpensive alternative for RFID-equipped environments utilizing mobile systems. In this chapter, the maximum speed of the robot is only 0.1 m/s during the teaching stage, which is slightly different to our previous work in Liu *et al.* (2011). There, the robot moved along a corridor at a maximum speed of 0.3 m/s during the teaching stage. However, the tag density (about 12 tags per inquiry) was far lower than the ones in the library, supermarket, and hallway scenarios and thus

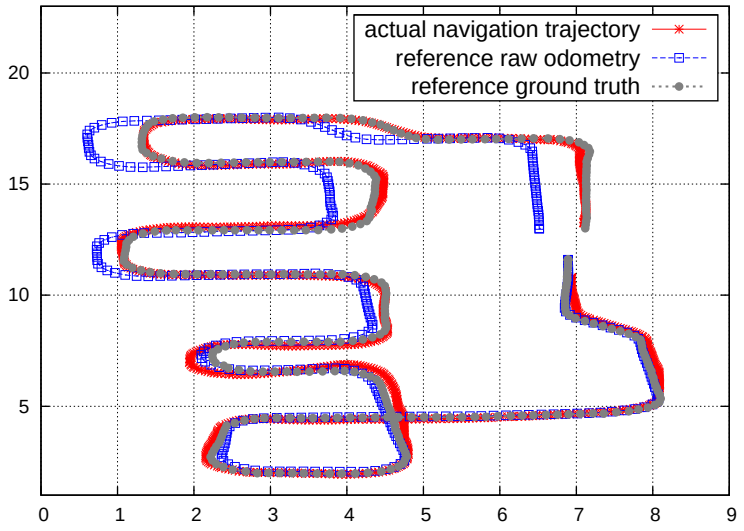

(a)

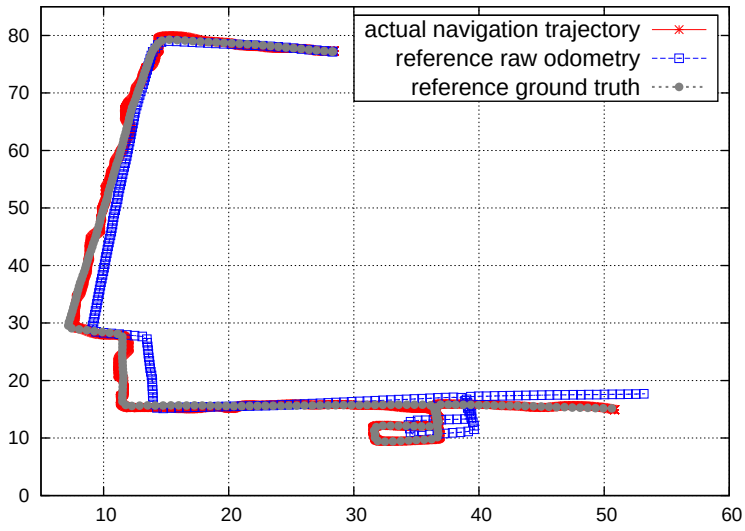

(b)

Figure 5.12: Ground truth, raw odometry data, and actual trajectory. (a) Navigation results in the library ($v_{max} = 0.1$ m/s, $K_f = 8$) with a mean tracking error of 0.064 m. (b) Navigation results in the hallway environment ($v_{max} = 0.2$ m/s, $K_f = 8$) with a mean tracking error of 0.2 m. For a speed of 0.3 m/s or higher, the robot lost its tracking path at areas with low tag densities.

the inquiry frequency was at 5 Hz. If the reader was able to report tags in high density environments more frequently, the recording speed of the robot could be improved.

In the future, we plan to investigate the impact of tag relocations on our approach. In addition, we are going to enhance the sample frequency of the RFID reader to improve the recording speed of the robot in order to minimize the efforts in the teaching stage. We also plan to investigate practical applications of the approach with regard to topological maps. There, paths between nodes could be used to connect distinct places through edges. A navigation from a starting node to a goal node could be achieved by traversing the appropriate edges represented by RFID fingerprints, which would enable the robot to reach arbitrary predefined places by graph-based path planning in large-scale environments.

Chapter 6

Active Perception for RFID Tags

Recent research deals more and more with the applications of UHF RFID on mobile robots. However, the sensing characteristics between the reader and the tag (i.e. tag detections and signal strength) are challenging to model due to the influence of environmental effects (e.g. tag density, reflection, diffraction, or absorption). In this chapter, we address the problem of tracking dynamic objects with a mobile agent using the signal strength from UHF RFID tags attached to objects. Our solution estimates the positions of RFID tags under a Bayesian framework. More precisely, we combine a two stage dynamic motion model with the dual particle filter to capture the dynamic motion of the object and quickly recover from failures in tracking. This approach is tested on a Scitos G5 mobile robot through various experiments.

The remainder of this chapter is organized as follows. After an introduction in Section 6.1, we review the related work in Section 6.2. Afterwards, we describe how the Bayesian framework is used to track RFID tags in Section 6.3. In Section 6.4 we present the combination of a two stage motion model and the dual particle filter. The whole searching, navigating, and sensing framework is described in Section 6.5. Finally, we present experimental results in Section 6.6 and draw conclusions in Section 6.7.

6.1 Introduction

For a mobile robot, the ability of object detection and tracking is a key issue to efficiently interact with its environment. Extensive research regarding object tracking has been done based on vision (Yilmaz *et al.* (2006)) or range-based sensors (Kluge *et al.* (2001)). The goal of object tracking is to acquire the trajectories of an object by localizing it at each sensor update, which usually has to solve the object detection and object tracking issues individually or jointly. Vision-based tracking is challenging, since it has to deal with occlusions, motion uncertainties, and appearance changes of the environment. As compared to vision, range-based sensors have longer reading range and are robust against illumination changes. Still, they have to face the difficulty of occlusions from the environment.

The usage of UHF RFID technology provides a way to overcome this difficulty, due to its automatic, contactless, and inexpensive way of identification. The UHF RFID tags

absorb, modulate, and backscatter the electromagnetic waves emitted from the reader and thus are able to respond up to a limited range (e.g. 7 m to 10 m). In the scope of this chapter, we focus on tracking dynamic objects with RFID tags using a mobile platform. As compared to the traditional vision-based or range-based sensors, passive UHF RFID features the following characteristics:

1. The RFID reader reports the IDs of the tags attached to objects directly, which does not require any additional algorithm for object detection. These IDs can be used as identities of the objects, which further simplify the recognition process involved in the traditional approaches.

2. The radio signal can pass through the objects as well as obstacles and thus can deal with occlusions that challenges the field of vision-based or range-based approaches. Moreover, the feature of communication without line of sight makes the RFID technology independent on the illumination of the environment, which is a big problem for vision-based approaches.

3. An RFID detection gives the coarse area about where the object should be. Although the RFID reader is not able to provide the position or the bearing of a tag directly, this information can be reasoned through a stream of RFID measurements in the history with a Bayesian filter, as shown in Chapter 3 and Chapter 4.

The new generation of RFID readers is additionally able to report the respective received signal strength (RSS). However, modeling the characteristics of radio signals is challenging, due to many influencing factors on the propagation of signals like multi-path effects, interferences, and occlusions.

In this chapter, an approach that uses radio signals from RFID tags to track dynamic objects is presented. We use a combination of a two stage dynamic motion model and a dual particle filter, also known as dual MCL (Monte Carlo localization), to deal with the uncertainty in the movement of the object and recover from the tracking failures, respectively. Our approach requires a sensor model to approximate the positions of the objects, which actually does not need to be too precise. The fast tracking of dynamic objects is achieved at a cost of the overall mapping accuracy. Low rate estimation from the RFID reader is used in a combination with the VFH+ (Vector Field Histogram), which serves as a local path planner for obstacle avoidance and navigation towards the target. VFH+ also has an integrated speed controller (both for the forward and angular velocity). This is used for test runs in several RFID-tagged scenarios, one of which is shown in Figure 6.1. We also compared our approach to the reactive controller in Deyle (2011), which does not need any explicit sensor models for approaching a tag that attached to an object. Additional experiments in different scenarios were conducted to show the effectiveness of our approach. This chapter represents an extended version of our paper accepted at IROS 2014 (Liu *et al.* (2014)).

For mapping of RFID tags, we want to obtain a high estimation accuracy of tag positions in a known environment, therefore a good localization accuracy of the antennas (i.e.

Figure 6.1: A scenario where our Scitos G5 robot is tracking a human carrying an RFID tag in a library.

the robot) is required. Unlike mapping of RFID tags, we do not need a precise position estimation of the robot in the context of tracking RFID tags, since the mapping error of RFID (e.g. around 0.3 m in ideal environments) is much higher than the accumulative error of the odometry (see Forster *et al.* (2013)) over a short distance. This means we can only rely on the odometry information for approaching a tag without precisely knowing the location of a robot in an environment. Therefore, we believe our approach can be extended to navigate mobile robots in unknown environments: the RFID tags can be easily installed on the walls or furnitures as landmarks (i.e. static nodes) for navigation. If two adjacent nodes are close enough (i.e. less than 6 meters), the robot can easily navigate itself between these nodes.

6.2 Related Work

The process of navigating a mobile robot towards a tagged-object is similar to the problems of source localization. In the field of source (e.g. gas) localization, the typical tasks that a mobile robot has to perform is to navigate towards an interested source or generate the concentration map of an environment. For an overview of the source localization approaches, we refer to Lilienthal *et al.* (2006). In the context of the radio-based navigation, on the one hand, the signal strength of the tag highly depends on the relative pose between the tag and antenna. This provides a useful measure of the position or the

bearing of a tag and thus can be used to navigate the mobile system towards a tagged object. On the other hand, besides the pose of the tag, many environmental factors (e.g. materials that the tag affixes to and interferences from the environment) also have significant impact on the signal strength of a tag. This makes the task of navigating a mobile robot using radio signals challenging. Although many researchers focus on the mapping of RFID tags, few of them concentrate on dynamic tags. Germa *et al.* (2010) fused visual data with RFID detections to allow a mobile robot to track people in a crowded environment. This chapter shows that we can rely on RFID alone for object tracking. According to the literature, the techniques of RFID-based navigation can be categorized into three classes: behavior-based approach, model-based approach, and sensor fusion-based approach.

6.2.1 Behavior-based Approach

For the behavior-based approach, the robot gradually corrects its actions according to the information obtained from the sensors without modeling the internal representation. In the context of RF-based navigation, Deyle (2011) presented an optimization-based approach based on a hybrid global-local search algorithm for perceiving RFID tags. For the global search, the robot has to move in the whole environment and perform a sparse sampling to obtain the best pose (i.e. the detection with the maximum signal strength), which serves as the initial pose for navigating towards the tag affixed to the object. For the local search, the robot is steered towards the object using the difference of the signal strength from two antennas. The robot stops searching once there are obstacles in front of it. Gueaieb and Miah (2009) used the phase difference of RFID signals, which allows the robot to follow the virtual paths that link the tags' orthogonal projections to the ground. They also addressed the problem of trajectory tracking for mobile robots using the radio signal from RFID tags (Miah and Gueaieb (2013)). However, their approach has to rely on the phase difference provided by a customized RFID system and the configurations of tags are fixed (i.e. the tags have to be installed on the ceiling of an indoor environment). Kim *et al.* (2007) developed an automated location sensing and docking system by utilizing a dual directional RFID antenna, which is able to estimate the direction of arrival (DOA) of the radio signal. However, the estimation of DOA is done with an active RFID system with loop antennas and currently it is not available in the market. Liu *et al.* (2012) used RFID tags as reference landmarks to let the robot follow a complex path based on the signal strength and the odometry in unknown environments (e.g. a library or a hallway environment). Since this approach has to rely on a fingerprinting-based approach for position estimation, a large number of tags have to be installed in the environment in order to get a good navigation accuracy.

6.2.2 Model-based Approach

In contrast to the behavior-based approach, the model-based approach usually uses well-calibrated models to localize the tags. The first work about how to localize passive RFID tags using a mobile system was presented by Hähnel *et al.* (2004). A model which characterizes the detection likelihood of a tag with reference to the antenna frame is used to determine the positions of the tags using a particle filter given several detection positions from a mobile robot. Vorst and Zell (2008) pointed out that this sensor model can be learned semi-autonomously during the normal navigation of the robot by placing several reference tags in the environment. Joho *et al.* (2009) incorporated the signal strength into the sensor model to improve the mapping accuracy of RFID tags. In our previous work (Liu *et al.* (2013)), we used a 3D sensor model and a pair of antennas to estimate the 3D positions of the RFID tags. There, we installed two antennas at different heights on the robot to solve the ambiguity problem of heights estimation that introduced by antennas placed at the same height. Kanda *et al.* (2007) obtained people trajectories with RFID tags attached to humans using a static reader setup, where 20 RFID readers are distributed in the entire science museum. The position of each person is estimated by fusing the detections from all readers using a Markov Chain Monte Carlo approach. As a result, they are able to recognize the visiting patterns of people and analyze how the space is used from these trajectories. Liu *et al.* (2006) investigated a mobile system, which is able to localize nomadic objects (i.e. objects that do move, but not frequently) with mobile RFID readers using conservative sensor models.

6.2.3 Fusing RFID with Other Sensors

Milella *et al.* (2009) estimated the bearings of RFID tags with a fuzzy antenna model. With a combination of visual landmarks, they are able to solve the kidnapped robot problem. Germa *et al.* (2010) combined RFID measurements with visual information to track people using a mobile robot in a crowded environment. In that case, the RFID system was used to determine the direction of the object and its readings have to be fused with a vision algorithm to get a better estimation of the position. They also designed a sensor-based controller to make the robot follow a tagged-person. Based on this work, Mekonnen *et al.* (2013) implemented a mobile system that is able to follow a person wearing an RFID tag and meanwhile avoid the passer-by by taking their dynamics into consideration. The trajectories of the passer-by and the tagged-person are estimated by the on-board sensors (i.e. an RFID reader, a camera, and a laser scanner) from the robot and two cameras mounted on the walls. Rohweder *et al.* (2009) used the information about the structure of an environment to improve the position estimation of RFID tags. Based on the assumption that tags are attached to objects, they fused the pose estimation of an RFID tag with a 2D occupancy map and showed an improvement of 10%, as compared to no fusion. Deyle *et al.* (2009) presented an approach that generated the RSS image of a tagged-object for manipulation tasks of mobile robots. They constructed this image by

rotating (i.e. panning and tilting) a mobile antenna and recorded the signal strength at the same time. The RSS image was then fused with the image from a camera and the point cloud from a 3D laser scanner to locate the tag in 3D. This approach was demonstrated on a mobile platform for finding, approaching, and grasping objects equipped with RFID tags. Schulz *et al.* (2003) proposed an approach that integrates anonymous sensors (i.e. laser range finders) and ID sensors (i.e. infrared or ultrasound badge sensors) using a Rao-Blackwellised particle filter to track people in an environment with a network of sensors. They are able to accurately track people and determine their identities owing to the advantages of both sensors.

6.3 Tracking RFID Tags

To estimate the tag position l_{jt} at time t, we need to know the posterior probability $p(\mathrm{l}_{jt}|\mathbf{f}_{1:t},\mathbf{x}_{1:t})$. According to Bayesian theory and the Markov assumption, $p(\mathrm{l}_{jt}|\mathbf{f}_{1:t},\mathbf{x}_{1:t})$ can be factorized into:

$$\begin{aligned} p(\mathrm{l}_{jt}|\mathbf{f}_{1:t},\mathbf{x}_{1:t}) &= \eta \cdot p(\mathbf{f}_t|\mathrm{l}_{jt},\mathbf{x}_{1:t}) \\ &\quad \cdot p(\mathrm{l}_{jt}|\mathrm{l}_{jt-1}) \cdot p(\mathrm{l}_{jt-1}|\mathbf{f}_{1:t-1},\mathbf{x}_{1:t-1}), \end{aligned} \tag{6.1}$$

where l_{jt} is the 2D position of the tag j that we want to estimate and $\mathbf{f}_{1:t}$ are the measurements gathered by the robot until time t, as detailed in Section 3. $p(\mathbf{f}_t|\mathrm{l}_{jt},\mathbf{x}_t)$ is the sensor model or the observation model. We refer the reader to Chapter 3 for more details about the variables in the above equations. In this chapter, only the 2D relative position of the antenna and the tag is relevant to our sensor model. Similar to Chapter 3 and Hähnel *et al.* (2004), we apply a particle filter (PF) to track the position of each RFID tag. Each PF consists of N samples at the 2D position hypotheses $\mathbf{x}^i = \{x^i, y^i\}_{1\leq i\leq N}$ and the associated weight w^i. In general, the particle filter is performed recursively with the following three steps:

1. *Prediction*: generate particles based on the motion model $p(\mathrm{l}_{jt}|\mathrm{l}_{jt-1})$, which is represented by a random walk with different scales of noise, as detailed in Section 6.4.

2. *Correction*: the weight w_t^i of each particle $\mathbf{x}_t^i$ is adjusted based on the measurement $\mathbf{f}_t$.

3. *Resampling*: a set of new samples is drawn with probabilities proportional to the weights.

Following Liu and West (2001), we consider the perturbation after resampling. The details about the perturbation can be found in Section 3.5.

6.4 Dynamic Motion Model and the Dual Particle Filter

In the field of tracking, a robust and fast estimation of the object position is very important, in order to let the robot react quickly to the movements of the objects. Particle filter-based trackers need to solve the problem of motion uncertainty (e.g. abrupt and fast motions of the objects). A poor motion model may place a small number of particles (or no particles at all) around the true pose of the tracked target, which leads to tracking failures. However, it is almost impossible to build up an accurate motion model due to the dynamics of the objects. To deal with this challenge, we utilize a two stage dynamic motion model, which is similar to the ideas in Kwon and Lee (2010) and Kristan *et al.* (2010). Specifically, this model integrates two basic motion models: a slow motion model and fast motion model, both of which are modeled as a Gaussian with different standard deviations, namely σ_s and σ_f for slow and fast motion respectively.

Moreover, the pose estimation accuracy of an RFID tag highly depends on the poses of the robot and the influence from the environment, as shown by Deyle (2011). The regular particle filters place a few or no particles around the true position of the tag and has the problem to recover from the kidnapped robot problem. In regard to this issue, Lenser and Veloso (2000) showed that this problem can be solved by sensor resetting, i.e. adding new samples, which are generated according to the current measurement. A better way to determine the number of particles that need to be added is to utilize two smoothed estimations of the likelihood (see Gutmann and Fox (2002) for more details). The generated new samples may cause an inconsistency to the current probability density function. We solve this problem (i.e. kidnapped robot problem) by using the dual particle filter (Thrun *et al.* (2000)), which draws particles from the observations and weighs them according to the current probability estimation.

In particular, we determine the importance weights of new particles by reconstructing the belief using kernel density estimation (KDE) (see Thrun *et al.* (2000) for more information) based on the current estimation. In our application, it is straightforward to draw particles based on the current observation, since we have built up a precise sensor model for the measurements (see Section 2.4). Similar to Gutmann and Fox (2002), these samples are generated by a 2D grid with a resolution of 20 cm. So, we draw α particles according to the dual particle filter based on the current measurement, β particles with a fast motion parameter σ_f, and the rest of the particles with a slow motion parameter σ_s ($0 \leq \alpha, \beta \leq 1$):

$$\mathrm{l}_{jt+1} \sim \alpha \cdot \frac{p(\mathbf{f}_t|\mathrm{l}_{jt}, \mathbf{x}_t)}{\pi(\mathbf{f}_t, \mathrm{l}_{jt}, \mathbf{x}_t)} + \beta \cdot \mathcal{N}(\mathrm{l}_{jt}, \sigma_f^2) + (1 - \alpha - \beta) \cdot \mathcal{N}(\mathrm{l}_{jt}, \sigma_s^2), \tag{6.2}$$

$$\text{where } \pi(\mathbf{f}_t, \mathrm{l}_{jt}, \mathbf{x}_t) = \int p(\mathbf{f}_t|\mathrm{l}_{jt}, \mathbf{x}_t) \mathrm{dl}_{jt}. \tag{6.3}$$

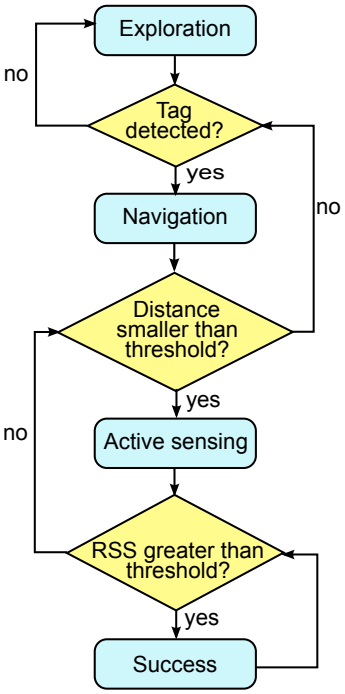

Figure 6.2: Flowchart representing the whole searching and tracking behavior.

6.5 Active Perception

By integrating the state estimator into a local path planner, we are able to track objects carrying RFID tags and simultaneously avoid obstacles. The chosen local path planner is VFH+ (Ulrich and Borenstein (1998)), which was implemented in the Orca-Robotics project[1]. It fuses the following behaviors: avoiding obstacles, tracking a target, and controlling both the forward and the angular velocity. This is then integrated into a framework, which allows the robot to search for a tag, follow it, and maintain the distance between them.

The whole searching and tracking behavior is explained as follows (also shown in Figure 6.2):

1. *Exploration*: the robot searches for a specific RFID tag with a predefined path until the tag is detected. To explore the environment, the robot simply follows several way-points on the map, which are given by hand.

2. *Navigation*: the robot navigates towards the tagged target using VFH+ based on the estimation of the target, while the distance between the target and the robot is smaller than a threshold, i.e. 0.5 m.

[1] http://orca-robotics.sf.net/

3. *Active sensing*: the robot rotates for a certain angle (e.g. $\pm 45^{\circ}$) to check if the RSS of the tag is higher than a threshold (e.g. -47 dBm).

4. *Success*: the robot approaches the tag successfully and switches into the *active-sensing* state, once the RSS value is smaller than the RSS threshold.

6.6 Experimental Results

To validate our approach, we implemented the presented system on a Scitos G5 service robot (see Section 1.4.2). We equipped the robot with a laser range finder for obstacle avoidance. We configured the RFID reader at the full power level and used the sensor model generated in Section 2.4.4. The frequency of the reader is set to 2 Hz.

6.6.1 Influence of Various Motion Parameters in the Particle Filter

We did some preliminary experiments to see the influence of different motion parameters on the estimation accuracy. We set the number of particles N to 200 for all experiments. The mixture ratio α of the dual particle filter was fixed to 0.1 for all experiments, as suggested in Thrun *et al.* (2000). The small motion parameter σ_s was set to 0.05 and the fast motion parameter σ_f was fixed to $10\sigma_s$. The robot was static and the tag was moved backward and forward in front of the robot several times. Figure 6.3a shows the true distance between the robot and the tag obtained by the laser scanner and also the estimated distance using various values of β. For different values of β, we get a similar tracking performance if the tag moves towards the robot, as can be seen in the drops of the curves in Figure 6.3a, which have the same descending rate. But when the object moves away from the robot, there is a certain delay of the estimation, as can be seen from the rise of the curves in Figure 6.3a. This can be explained as follows. The dual particle filter evaluates the weights of the samples drawn from the observation, in a way to make them consistent with the belief. If the object is far from the robot, which usually means high uncertainty in the belief, and is moving closer to the robot, newly drawn particles will be weighted with higher values, because they coincide with the belief. If the object is closer to the robot, so that the uncertainty of the belief is small (i.e. we have a strong belief), and it is moving away from the robot, the newly drawn particles will be weighted with small values, to preserve the belief. These weights gradually change with new measurements, which can lead to a certain lag, represented by a slow rise of the curves in Figure 6.3a. A larger β gives faster tracking as the tag moves away from the robot, as can be seen in the rise of the curves in Figure 6.3a: those with the larger β rise faster than ones with the smaller β. However, a larger β introduces more noise into the motion model, which usually does not give a robust estimation, and leads to a worse tracking result, as shown in the following experiments.

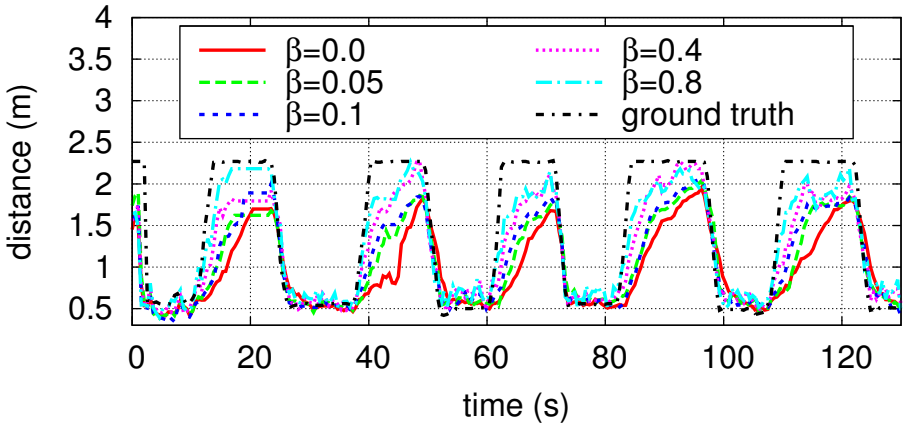

(a)

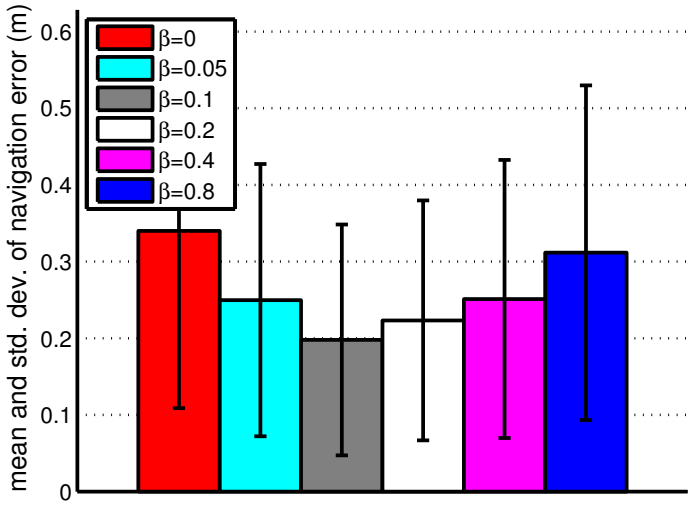

(b)

Figure 6.3: Impact of parameter β on the tracking accuracy. (a) Ground truth and the estimated distance from the robot to the tag with different values of β; (b) Mean and standard deviation of the tracking error under different values of β.

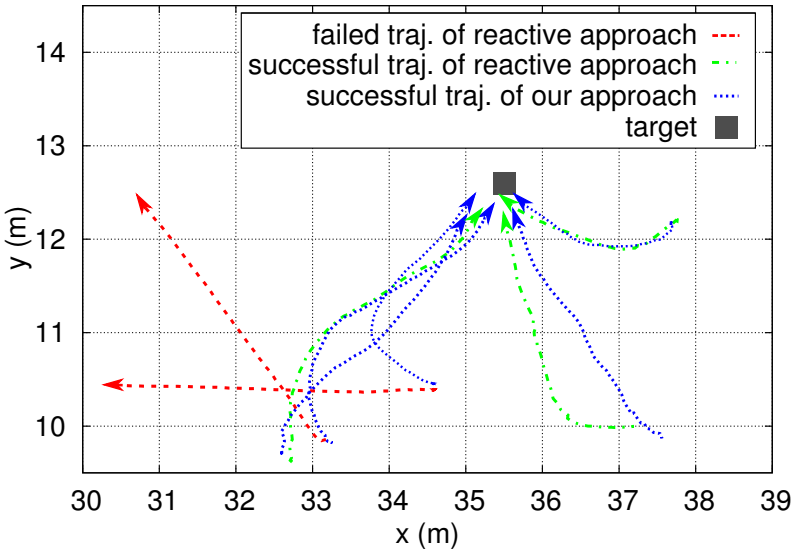

Figure 6.4: Trajectories of the reactive approach and our approach.

To show the overall influence on the tracking performance with different parameters β, we performed experiments in a hallway environment. In all trials, a person carrying a tag was moving along the central line of a hallway of $4.5 \times 28\,\mathrm{m}^2$, at a low speed. If the robot lost its track, the person waited for the recovery. For the local path planning, VFH+ was used with a maximum forward velocity of 0.3 m/s. Different values of β were tested and each configuration was repeated six times. The resulting mean and standard deviation of the tracking error (i.e. the difference between the path of the robot and the central line in the hallway) is shown in Figure 6.3b. As can be seen in Figure 6.3b, the choice of $\beta = 0.1$ gives the best results. A too large or too small β obviously leads to a worse result. For example, as compared to $\beta = 0.0$ and $\beta = 0.8$, $\beta = 0.1$ gives an improvement of 42.9% (from 0.34 m to 0.19 m) and 37.7% (from 0.31 m to 0.19 m), respectively. This happens, because if β is too small, the robot is not able to react quickly enough to the changes, while a large β results in an unstable estimation and thus gives a bad performance, as explained in the first part of this section. Therefore, we chose $\beta = 0.1$ for the rest of experiments.

In Figure 6.5, the mapping error of the robot navigating towards the tag using our approach is shown. As can be seen in Figure 6.5, the error of the estimation is reduced gradually during the navigation towards the tag, i.e. the mapping error highly depends on the distance between the tag and the robot. Figure 6.5 also shows the change of the uncertainty, which is represented by the covariance of the particles here: the uncertainty of the estimation is reduced when the robot is approaching the tag, since the signal strength in that case becomes greater. The signal strength at far distances is usually very low (see the mean signal strength in Figure 2.9) and the sensor model of low signal strength is wider than the one with higher signal strength, as can be seen from the sensor models with a

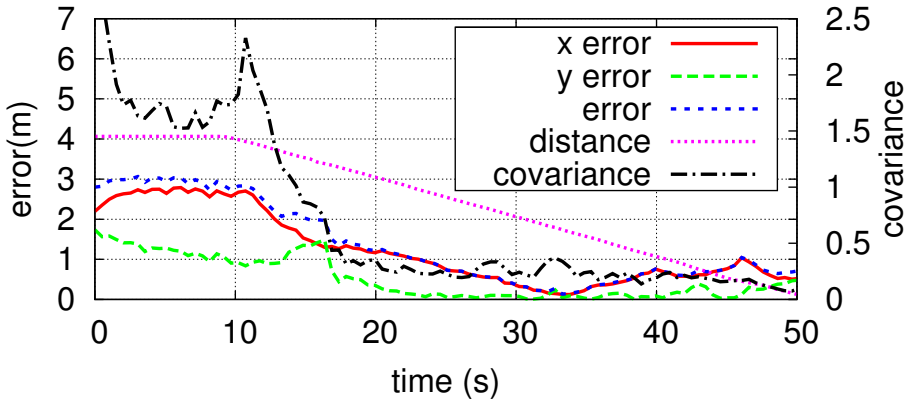

Figure 6.5: Mapping error and the covariance of the particle set during the approaching of a tag.

low signal strength (s=-62 dBm in Figure 2.10f) and a high signal strength (s=-50 dBm in Figure 2.10c).

6.6.2 Comparison with the Reactive Controller

A simple and a fast way to navigate a robot towards RFID tags is presented in Deyle (2011). This approach uses the RSS difference between two RFID antennas and calculates the angular velocity according to that difference. Forward velocity in this case is constant (it may also be controlled e.g. proportional to RSS). This approach will be referred to as the reactive controller. To justify the usage of our approach, we compared it to the reactive controller. The Impinj RFID reader, which we used for the experiments, gives RSS values from -72 dBm to -38 dBm. If there are no detections, RSS is set to -70 dBm.

In the implementation of the reactive controller, the forward velocity is fixed to 0.1 m/s and the proportional factor for the angular velocity control is set to 0.02 rad/dBm·s. In the implementation of our approach in this case, the forward velocity is also fixed to 0.1 m/s and the estimated position of the target is used to calculate the angle between the robot and the target. This angle is then used as an error in a proportional controller, with the proportional gain of 0.4 rad/rad·s. For both approaches, the robot was programmed to stop in the case of obstacles nearby.

The experiments were conducted for approaching static objects in our laboratory of a size of $5 \times 8\,\mathrm{m}^2$. The robot was placed at different poses and started to move towards the object, as soon as the tag was detected. Figure 6.4 shows the successful and failed trajectories during the navigation of the robot in several trials. For the reactive controller, the robot sometimes faced failures (see red dotted lines in Figure 6.4), since the difference of RSS was so small that the robot couldn't make a fast turn towards the object. This weakness was also pointed out in Deyle (2011). In all cases when the reactive controller

failed, our approach succeeded, since it always had the estimated pose of the object at its disposal. If the tag is in a good view of the antennas, both approaches show good results. This experiment is supposed to show the advantages of our approach even in this special case by setting the conditions for both approaches similar (fixed forward velocity, proportional control of the angular velocity, and no obstacle avoidance). But usually, our approach can use both angular and forward velocity control, and also obstacle avoidance.

As mentioned before, another advantage of our approach is an easier integration of the obstacle avoidance strategy. To our knowledge, in the applications so far, the reactive controller doesn't use any obstacle avoidance method. It only stops the robot, if there is an obstacle very close. Also, one of the biggest advantages of our approach is the recovery from losing the tag. If a robot is tracking a target carrying a tag, and if the target suddenly gets out of the RFID antennas range, the reactive controller is not able to recover, since there is no signal strength anymore. On the other hand, our approach has the last estimated position, which is, in most cases, enough to recover from the loss.

6.6.3 Impact of Different Antenna and Tag Configurations

In the experiments presented in this section, we evaluated the influence of different antenna configurations and different heights of the tag during the object tracking. Different angles between the antennas (at the tag height of 0.8 m) were 45°, 90°, and 135°. Different tag heights were chosen to be 0.8 m, 0.3 m, and 1.8 m. The experiments were conducted in the same way as the ones presented in Section 6.6.1. As it can be seen from the tracking performance in Figure 6.6a, the best configuration of the antennas is 90°. A larger spanning angle between the antennas leads to a worse tracking accuracy. As an example, the tracking error with a spanning angle of 135° is two times larger than the one with 90°. A small spanning angle slightly decreases the tracking error (from 0.23 m to 0.19 m, as compared with the spanning angle of 45° and 90°). The reason for this is that our antenna configuration deteriorates into a single antenna setup, which is good at distance estimation but weak at determining the orientation of the object. In contrast, a wide spanning angle leads to little or no overlapping area between two antennas, such that it is not able to get a good distance estimation of the object. Moreover, as can be seen in Figure 6.6b, the heights of the tag also have influence on the tracking accuracy (0.19 ± 0.15 m for a height of 0.8 m, as compared with 0.27 ± 0.17 m for a height of 0.3 m and 0.38 ± 0.17 m for a height of 1.8 m), due to the variance between the characteristics of the tags at different heights pointed out by our previous work (Liu *et al.* (2013)).

6.6.4 Influence of Different Materials

As we mentioned before, the radio signal is highly influenced by the environmental factors. The RFID reader has very poor readability when water or metal are present, or when the tag is occluded. In this experiment, several placements of the tag were chosen:

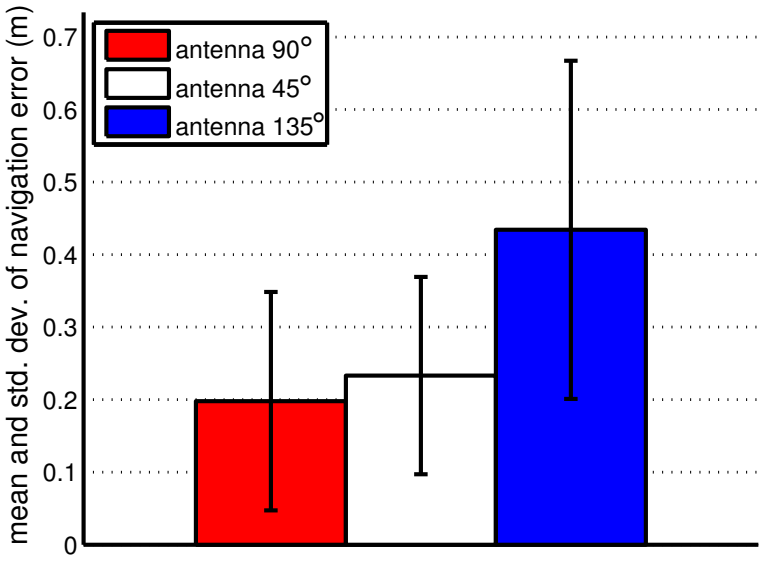

(a)

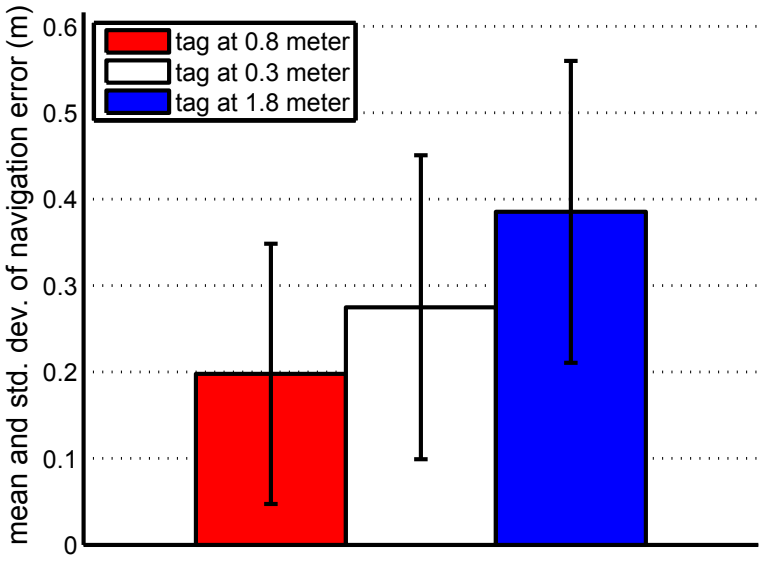

(b)

Figure 6.6: Mean and standard deviation of the tracking error under the influence of different antenna setups and tag heights. (a) Tracking accuracy under the influence of different antenna setups; (b) Tracking accuracy under the influence of different tag heights.

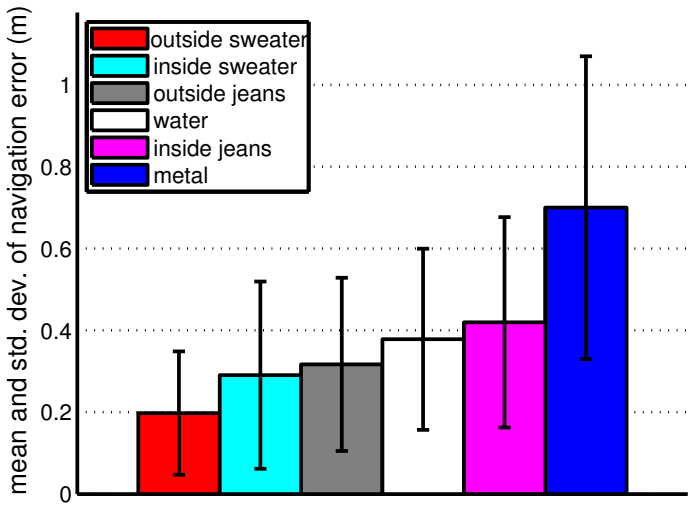

Figure 6.7: Mean and standard deviation of the tracking error under different materials the tag attached to.

attached to a bottle full of water, on an iron object, inside and outside jeans, outside and inside a sweater as a name tag attached to a person at a height of 0.8 m.

For the cases when the tag was attached to the jeans, the robot had to follow the person from behind. The idea of attaching the tags to jeans is motivated by the fact that more and more clothing stores will attach permanent tags to the clothes in the future. Again we conducted experiments in the same way as Section 6.6.1 and showed the mean and standard deviation of the tracking accuracy in Figure 6.7. We found that the robot lost the person one or two times during the tracking of the tag attached to a bottle of water and inside jeans (i.e. the case of heavy occlusion). We observed that the robot was not able to track a tag attached to a metal object, which can be seen from the high tracking error (0.7 m) due to many circles that the robot made during the tracking. On the other hand, water has less influence on the tracking accuracy than metal, as can be seen in Figure 6.7.

6.6.5 Test in a Library and a Hallway Scenario

We finally tested our approach for person following under two different environments: a library and a hallway environment. The hallway environment mainly consists of one lecture room, several corridors, and a robot lab. Approximately 400 products with RFID tags are placed on a metal shelf in the middle of the robot lab. There are a small number of tags at the corridor adjacent to the robot lab and no tags in the lecture room and other corridors. The robot has to enter and go out of the lecture room and the robot lab during

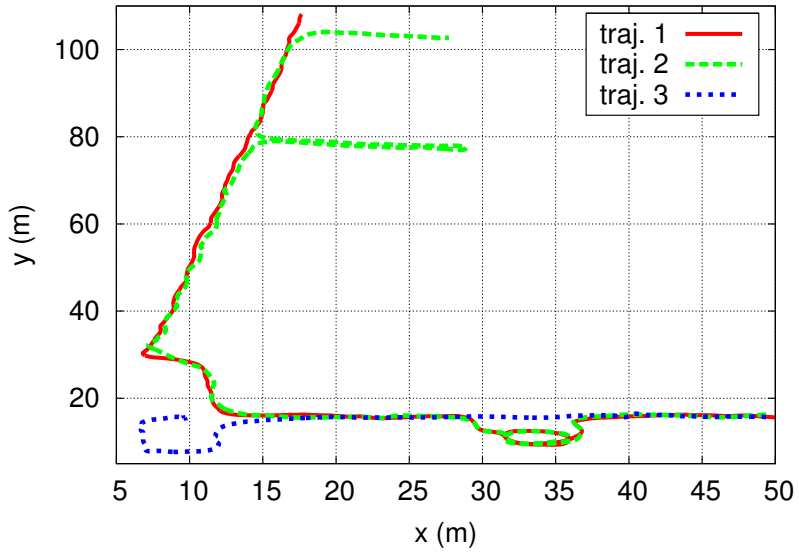

(a)

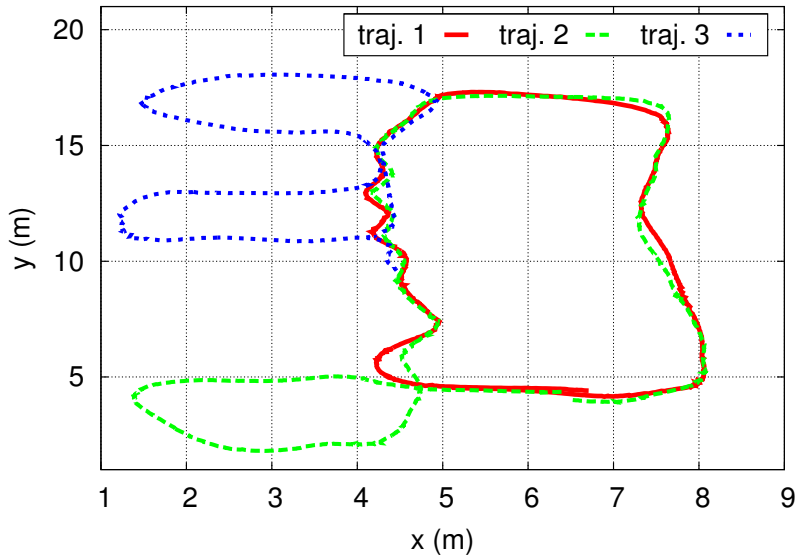

(b)

Figure 6.8: Trajectories of our Scitos robot autonomously following a person in a hallway (top) and a library environment (bottom).

Table 6.1: Analysis of the running time (in milliseconds) under the impact of different number of particles (N).

Number of particles	100	200	500	1000	5000
Running time [ms]	0.52	0.73	1.58	2.95	14.58

the driving in the hallway environment. In contrast, the library is considered to be a densely tagged environment, where approx. 7000 books are equipped with UHF and HF RFID tags and placed at different heights on the shelves, as described in Section 1.4.1. During the tracking, the robot has to use VFH+ to avoid obstacles (e.g. walls, shelves, tables, and chairs) in the environments. In total, the robot drove a distance of 417.5 m in 1502.8 seconds in the hallway and 102.1 m in 465.2 seconds in the library, as shown in Figure 6.8. In the library, the robot lost tracking three times during the test, which all happened when it faced a sharp turn into one 1.1 m wide corridor, since the robot was not able to detect the tracking tag in time due to the influence of other tags. We did not see any failures during the tracking in the hallway environment, although the robot had to enter the door of the robot lab which is only 1.0 m wide.

6.6.6 Performance Analysis

The mean running time of processing each tag detection is measured by processing six log files that were recorded in the library and the hallway environment, as listed in Table 6.1. Both parameters α and β were set to 0.1. All of the tests were performed on an Intel Core i5-2410M@2.3 GHz CPU, with 4 GB RAM. As can be seen in Table 6.1, processing one detection with N=200 only requires 0.73 ms, which satisfies the requirement of real time processing. Yet, this time can be ignored as compared to the frequency that the RFID reader works at (i.e. 2 Hz in our case).

6.7 Conclusions and Future Work

This chapter addressed the problem of tracking dynamic objects with UHF RFID tags using a Bayesian framework with a mobile robot. We used a two stage dynamic motion model and the dual particle filter, which is able to capture the dynamic motion of the object and quickly recover from tracking failures. Integrated into a local path planner, the robot is able to track moving objects and avoid obstacles at the same time, using only two UHF RFID antennas and a laser scanner. For dynamic objects tracking with RFID, it is also possible to choose the approach which uses only the signal strength difference between the antennas, which we referred to as the reactive controller. This approach is simple and fast. But the ability of tracking dynamic objects while avoiding obstacles, even with the low signal strength and the ability of recovery after losing an object, clearly gives the advantage to our approach. We performed extensive experiments with a Scitos

G5 service robot to validate the effectiveness of our approach. A video demonstrating our work can be found at `www.cogsys.cs.uni-tuebingen.de/mitarb/liuran/videos/object_tracking.mp4`.

There are several directions into which this work can be extended. First, improving the tracking performance through a combination of RFID with other sensors would be promising in the future. A combination with a laser scanner would be especially interesting. Second, heuristic control algorithms need to be investigated to quickly capture the potential movements of the objects and obtain the maximum information gain at the same time when the robot approaches the tagged objects.

Chapter 7

Conclusions

7.1 Summary

In order to effectively interact with the surroundings, service robots with mobility and autonomy have to deal with various types of objects. RFID technology, which achieves the communication between the reader and the RFID tags without line of sight, provides a new way of object identification. Furthermore, each tag carries a unique ID, which can serve as the landmark for the robot localization or navigation.

In Chapter 2, we introduced the background of RFID technology as well as the fundamental theory used in this thesis. Then, in the rest of this thesis (i.e. Chapter 3, Chapter 4, Chapter 5, and Chapter 6), we addressed some fundamental problems in the field of mobile robots using RFID technology, which consist of mapping, path following, and tracking. To be precise, the contributions of this thesis are summarized as follows:

- **Mapping:** Chapter 3 focused on the mapping of RFID tags, which aims at inferring the positions of RFID tags by integrating the measurements from the on-board RFID reader equipped on the robot. The traditional particle filters face the issue of mapping failures due to the noisy measurements from the RFID reader. In order to recover from mapping failures of RFID tags, we presented the adaptive particle filter in Chapter 3. Compared to the traditional particle filters, the adaptive particle filter improves the mapping accuracy by 6.3 % without further examination of negative information. Moreover, the adaptive particle filter is able to relocalize non-static RFID tags.

  We further examined the usefulness of negative information for RFID-based mapping. We showed that, the integration of negative information gives an improvement of the mapping accuracy and helps to recover from mapping failures and relocalize non-static RFID tags. By examining negative information, we are able to improve the mapping accuracy by 3.5 %. We finally compared the particle filter-based approach to our previous grid-based Markov localization approach. As compared to the grid-based Markov localization approach, we are able to save a large amount of computational cost and memory storage, while the mean mapping accuracy is only reduced by two centimeters.

- **Mapping with 3D Sensor Models:** In Chapter 4, we presented a novel 3D probabilistic sensor model, which characterizes both tag detection events as well as the received signal strength. Compared to the 2D-based sensor models, the 3D sensor model achieves a higher mapping accuracy for 2D position estimation. In our experiments, the 3D sensor model improves the 2D mapping accuracy by approx. 12.0%, as compared to the 2D sensor model. Especially, with this sensor model, we are able to determine the 3D position of a tag using a stereo antennas configuration, i.e. two antennas mounted at different heights on the robot. We additionally integrated the negative information (i.e. non-detections) to improve the mapping accuracy in our special antenna configuration. To summarize, by using our stereo antennas setup and incorporating negative information, we are able to localize the RFID tags with a mean absolute localization error of 0.24 m in 2D and 0.40 m in 3D as well as 0.28 m for height. The negative information gives an additional improvement of approx. 26.3% for the height estimation. In all experiments, the mapping error for the height is much larger than the error in the x and y direction. The reason for this can be explained as follows: the height of the tag is only estimated by the difference of two RFID antennas, while x and y positions are determined through various measurements perceived by the mobile robot that moves in the xy plane. As a result, the deviation of measurements in x and y direction is much higher than in the z direction. Therefore, we do not get a good z-estimation due to the lack of distinct detection samples in the z-axis. Finally, in order to enable our algorithm to perform online, we utilized the KLD-sampling to reduce the number of particles.

- **Path Following:** In Chapter 5, we addressed the problem of path following of a mobile robot using the signal strength from RFID tags in unknown environments. To be precise, our method utilizes RFID measurements as fingerprints (i.e. landmarks) and makes the mobile robot to autonomously follow a path that was previously recorded during a manual training phase. The relative position of the robot to the desired path is estimated by comparing the current RFID measurements to the reference measurements. As a result, the robot is steered by the control commands generated by fusing the position estimation and the reference odometry data.

  The proposed approach needs neither an explicit sensor model of RFID nor the knowledge about the environment (e.g. the distribution of the tags and the map of the environment). We evaluated the performance of our approach in two different environments, namely a library and a large hallway environment. Our approach provides a cost-effective and computationally inexpensive alternative to other navigation approaches for mobile systems in RFID-equipped environments.

  Tag density is one factor that has high impact on the accuracy of our approach. In general, higher tag densities lead to better tracking results. In one of our experiments in the hallway environment with a high tag density configuration, the robot

was able to navigate along the path at a maximum speed of 0.7 m/s in spite of the low frequency control commands (i.e. 2 Hz) generated from the RFID reader. Compared to the library environment, the hallway environment achieved a slightly lower tracking accuracy due to the low tag density. Sometimes the RFID fingerprint consisted of only one or even no tag detection at all. As a result, the tracking errors at these positions were increased over 0.6 m, since the RFID measurement in that case was not sufficient to steer the robot to follow the desired path.

Another factor which plays an important role in our approach, is the power configuration of the RFID reader. The tracking accuracy remains the same or even gets improved if the reader power is slightly reduced, while a too low reader power obviously gives a worse tracking result. The reason for this can be explained as follows. On the one hand, a low reader power leads to a short reading range and thus a low uncertainty about the position of the tag. On the other hand, a higher reader power provides a larger reading range and a wider band of the received signal strength. The additional tag detections are able to make up for the uncertainty introduced by the increased reading range.

Odometry is quite accurate to estimate the change in position over short period of time. Whereas the odometry has cumulative errors for longer tracks. The path following approach proposed in this thesis is able to compensate for the error from the odometry by utilizing RFID fingerprints as landmarks.

- **Tracking:** The robot has to deal with a large number of dynamic objects during the interaction with its environment. Since RFID tags can be attached to any objects, we addressed the problem of dynamic objects tracking with a mobile agent using the signal strength emitted from RFID tags. Our solution estimates the position of an RFID tag under a Bayesian framework. More precisely, we combine a two stage dynamic motion model with the dual particle filter to capture the dynamic motion of the object and quickly recover from failures in tracking. The state estimation is then integrated into a local path planner, which allows the robot to track moving objects and avoid obstacles at the same time using only two UHF RFID antennas and a laser scanner.

  A simple way to track moving objects is a reactive controller, which steers the robot based on the difference of the signal strength from two antennas. Compared to the reactive controller, our approach has two main advantages. First, our approach successfully deals with the situations when the reactive controller fails. Second, it is easier to integrate the obstacle avoidance into our approach. The reactive controller implemented so far does not have any obstacle avoidance strategy and only stops the robot, if there are obstacles nearby.

  The tracking performance was examined by affixing the RFID tags to objects with different materials. We observed that the robot lost the object one or two times during the tracking in cases when the tag was placed on a water bottle and inside

jeans due to the absorption of the water or the occlusion of the jeans. Moreover, the metal has more influence on the tracking accuracy than the water, since in our experiment the robot was not able to track a tag attached to a metal object.

We implemented and extensively evaluated our approaches with a service robot in different environments. Several mechanisms were proposed and thoroughly validated to improve the mapping accuracy and efficiency of RFID tags. The path following approach proposed in this thesis has been proven to be an efficient and cost-effective solution for the navigation of mobile robots in RFID-equipped environments. Furthermore, the tracking solution presented in this thesis enables the mobile agent to track any dynamic objects equipped with RFID tags, which provides an alternative to the state-of-the-art object tracking approaches if RFID technology is employed for the sensation of the robot.

7.2 Future Work

Although we presented a cost-effective approach for path following and an efficient solution for tracking dynamic objects as well as some mechanisms to improve the mapping accuracy, there are a number of possible extensions of this thesis. One promising direction is the investigation of an outlier-removal approach to improve the mapping accuracy by removing the ghost detections of RFID tags caused by environmental effects, since the ghost detections bring a large amount of uncertainty to the state estimation and lead to mapping failures.

Due to the hardware limitations, only two RFID antennas are utilized for localizing the 3D positions of RFID tags throughout this thesis. In all experiments, the antennas are fixed on the robot during the operation. Due to the lack of distinct measurements, the error of height estimation is usually larger than the estimations in x and y directions. Therefore, it would be interesting to see if the 3D mapping accuracy can be improved by fusing the measurements from multiple antennas installed at different heights on the robot.

The RFID reader only provides a coarse measurement about the position of the tag. Therefore, the obvious extension of this thesis is the fusion with the metric measurements obtained from other sensors equipped on the robot, such as cameras or laser range finders, to improve the mapping accuracy. In this case, the object detection or recognition process can be further facilitated by taking advantages of both techniques.

For the path following, we assume a static configuration of the environment, i.e. the RFID tags are affixed to the immobile items or the walls. In practice, the items are not always static and may be relocated or removed by people. In this context, we plan to test our path following approach in dynamic environments.

Furthermore, one could combine the work described in Chapter 5 and Chapter 6 for the navigation of a robot with regard to a topological map in large unknown environments. The nodes in the topological graph can be represented by a single RFID tag

or the RFID fingerprint. The tracking solution presented in this thesis allows the robot to navigate towards static RFID tags as well as dynamic ones and the path following approach we proposed enables the robot to travel along the path defined by RFID fingerprints autonomously. Both approaches have their weaknesses and advantages. The advantage of the tracking solution is the capability of coping with dynamic tags and an easier integration with obstacle avoidance, but suffers from the uncertainty of the tag position estimation caused by many environmental factors. By means of fingerprints, the path following approach does not rely on the distribution of the tags and is shown to be robust against the location-specific distortions that challenge our tracking approach, but the obstacle avoidance is not yet addressed. Therefore, it is interesting to combine these two techniques in order to achieve a robust and efficient navigation approach.

Our current strategy chooses the shortest path to the goal, while the robot moves towards the target during the tracking in this thesis. Therefore, an extension of this thesis is to use heuristic control algorithms in order to quickly move towards the object and meanwhile obtain the maximum information gain (i.e. best reading rate of the tag attached to the object).

Obviously, the applications of our approaches are not limited to the fields mentioned in this thesis. Recently, manipulation capabilities of a mobile system have been widely addressed in industrial environments and everyday life. Moreover, low-cost embedded mobile RFID devices are popular in the market and the industry nowadays. Therefore, we believe that the approaches proposed in this thesis can be applied in a broad area of applications.

Bibliography

Alghamdi, S. and van Schyndel, R. (2012). Accurate positioning based on a combination of power attenuation and a signal strength indicator using active RFID technology. In *Third International Conference on Indoor Positioning and Indoor Navigation*, pages 1–4, Sydney, Australia.

Alghamdi, S., van Schyndel, R., and Khalil, I. (2013). Accurate positioning using long range active RFID technology to assist visually impaired people. *Journal of Network and Computer Applications*.

Alippi, C., Cogliati, D., and Vanini, G. (2006). A statistical approach to localize passive RFIDs. In *2006 IEEE International Symposium on Circuits and Systems (ISCAS 2006)*, pages 843–846, Island of Kos, Greece.

Arulampalam, M., Maskell, S., Gordon, N., and Clapp, T. (2002). A tutorial on particle filters for online nonlinear/non-gaussian Bayesian tracking. *Signal Processing, IEEE Transactions on*, **50**(2), 174–188.

Azzouzi, S., Cremer, M., Dettmar, U., Knie, T., and Kronberger, R. (2011a). Improved AoA based localization of UHF RFID tags using spatial diversity. In *2011 IEEE International Conference on RFID-Technologies and Applications (RFID-TA)*, pages 174–180.

Azzouzi, S., Cremer, M., Dettmar, U., Kronberger, R., and Knie, T. (2011b). New measurement results for the localization of UHF RFID transponders using an angle of arrival (AoA) approach. In *2011 IEEE International Conference on RFID*, pages 91–97.

Bahl, P. and Padmanabhan, V. (2000). Radar: An in-building RF-based user location and tracking system. In *Proc. of the Nineteenth Annual Joint Conf. of the IEEE Computer and Communications Societies (INFOCOM 2000)*, volume 2, pages 775–784, Tel Aviv, Israel.

Balanis, C. A. (2005). *Antenna Theory: Analysis and Design*. John Wiley & Sons, Inc.

Boccadoro, M., Martinelli, F., and Pagnottelli, S. (2010). Constrained and quantized Kalman filtering for an RFID robot localization problem. *Autonomous Robots*, **29**(3-4), 235–251.

Borenstein, J., Feng, L., and Borenstein, C. J. (1996). Measurement and correction of systematic odometry errors in mobile robots. *IEEE Transactions on Robotics and Automation*, **12**, 869–880.

Burgard, W., Fox, D., and Hennig, D. (1997). Fast grid-based position tracking for mobile robots. In *In Proc. of the 21th German Conference on Artificial Intelligence*, pages 289–300. Springer Verlag.

Burgard, W., Derr, A., Fox, D., and Cremers, A. (1998). Integrating global position estimation and position tracking for mobile robots: the dynamic Markov localization approach. In *Proc. of the IEEE/RSJ International Conference on Intelligent Robots and Systems*.

Chawla, K., Robins, G., and Zhang, L. (2010). Object localization using RFID. In *the 5th IEEE International Symposium on Wireless Pervasive Computing (ISWPC 2010)*, pages 301–306, Modena, Italy.

Chawla, K., McFarland, C., Robins, G., and Shope, C. (2013). Real-time RFID localization using RSS. In *Proc. of the 2013 International Conference on Localization and GNSS (ICL-GNSS 2013)*, pages 1–6, Turin, Italy.

Choi, J. S., Lee, H., Engels, D., and Elmasri, R. (2012). Passive UHF RFID-based localization using detection of tag interference on smart shelf. *Systems, Man, and Cybernetics, Part C: Applications and Reviews, IEEE Transactions on*, **42**(2), 268–275.

Cover, T. M. and Thomas, J. A. (1991). *Elements of Information Theory*. Wiley-Interscience, New York, NY, USA.

Deyle, T. (2011). *Ultra High Frequency (UHF) Radio-Frequency Identification (RFID) for Robot Perception and Mobile Manipulation*. Ph.D. thesis, Georgia Institute of Technology.

Deyle, T., Anderson, C., Kemp, C. C., and Reynolds, M. S. (2008a). A foveated passive UHF RFID system for mobile manipulation. In *2008 IEEE/RSJ International Conference on Intelligent Robots and Systems (IROS 2008)*, pages 3711–3716. IEEE.

Deyle, T., Kemp, C., and Reynolds, M. (2008b). Probabilistic UHF RFID tag pose estimation with multiple antennas and a multipath RF propagation model. In *Proc. of the 2008 IEEE/RSJ Int. Conf. on Intelligent Robots and Systems (IROS 2008)*, pages 1379–1384, Nice, France.

Deyle, T., Nguyen, H., Reynolds, M., and Kemp, C. (2009). Rf vision: RFID receive signal strength indicator (RSSI) images for sensor fusion and mobile manipulation. In *Proc. of the 2009 IEEE/RSJ Int. Conf. on Intelligent Robots and Systems (IROS 2009)*, pages 5553–5560, St. Louis, MO.

Douc, R. and Cappe, O. (2005). Comparison of resampling schemes for particle filtering. In *Image and Signal Processing and Analysis, 2005. ISPA 2005. Proceedings of the 4th International Symposium on*, pages 64–69.

Doucet, A., Godsill, S., and Andrieu, C. (2000). On sequential monte carlo sampling methods for Bayesian filtering. *STATISTICS AND COMPUTING*, **10**(3), 197–208.

Dudek, G. and Jenkin, M. (2000). *Computational Principles of Mobile Robotics*. Cambridge University Press, New York, NY, USA.

Ehrenberg, I., Floerkemeier, C., and Sarma, S. (2007). Inventory management with an RFID-equipped mobile robot. In *Proc. of the 2007 IEEE Int. Conf. on Automation Science and Engineering (CASE 2007)*, pages 1020–1026, Scottsdale, Arizona, U.S.A.

Eliazar, A. I. and Parr, R. (2004). Learning probabilistic motion models for mobile robots. In *Proceedings of the Twenty-first International Conference on Machine Learning*, ICML'04, pages 32–40, New York, NY, USA. ACM.

EPCglobal (2013). UHF Class 1 Gen 2 Standard v.2.0.0. Available on line: http://www.gs1.org/gsmp/kc/epcglobal/uhfc1g2.

Ferris, B., Hhnel, D., and Fox, D. (2006). Gaussian processes for signal strength-based location estimation. In *In Proc. of Robotics Science and Systems*.

Finkenzeller, K. (2003). *RFID Handbook: Fundamentals and Applications in Contactless Smart Cards and Identification*. John Wiley & Sons, Inc., New York, NY, USA, 2 edition.

Forster, C., Sabatta, D., Siegwart, R., and Scaramuzza, D. (2013). RFID-based hybrid metric-topological SLAM for GPS-denied environments. In *Robotics and Automation (ICRA), 2013 IEEE International Conference on*, pages 5228–5234.

Fox, D. (2003). Adapting the sample size in particle filters through KLD-sampling. *International Journal of Robotics Research*, **22**(12), 985–1004.

Fox, D., Burgard, W., and Thrun, S. (1999). Markov localization for mobile robots in dynamic environments. *Journal of Artificial Intelligence Research*, **11**, 391–427.

Friedman, N., Murphy, K., and Russell, S. (1998). Learning the structure of dynamic probabilistic networks. In *Proceedings of the Fourteenth Conference on Uncertainty in Artificial Intelligence (UAI 1998)*, pages 139–147, San Francisco, CA, USA. Morgan Kaufmann Publishers Inc.

Furgale, P. and Barfoot, T. (2010). Visual teach and repeat for long-range rover autonomy. *Journal of Field Robotics*, **27**(5), 534–560.

Germa, T., Lerasle, F., Ouadah, N., and Cadenat, V. (2010). Vision and RFID data fusion for tracking people in crowds by a mobile robot. *Computer Vision Image Understanding*, **114**(6), 641–651.

Gerold, K. (2007). *Radio-frequency signal strength based localisation in unstructured outdoor environments*. Thesis, The University of Sydney, Australia.

Grisetti, G., Stachniss, C., and Burgard, W. (2005). Improving grid-based SLAM with Rao-Blackwellized particle filters by adaptive proposals and selective resampling. In *IEEE International Conference on Robotics and Automation (ICRA 2005)*, pages 2443–2448, Barcelona, Spain.

Gueaieb, W. and Miah, M. (2009). A modular cost-effective mobile robot navigation system using RFID technology. *Journal of Communications*, **4**(2), 89–95.

Gutmann, J.-S. and Fox, D. (2002). An experimental comparison of localization methods continued. In *Proc. of the 2002 IEEE/RSJ Int. Conf. of Intelligent Robots and Systems (IROS 2002)*, pages 454–459, EPFL, Switzerland.

Haeberlen, A., Flannery, E., Ladd, A. M., Rudys, A., Wallach, D. S., and Kavraki, L. E. (2004). Practical robust localization over large-scale 802.11 wireless networks. In *Proceedings of the 10th Annual International Conference on Mobile Computing and Networking (MobiCom 2004)*, pages 70–84, New York, USA.

Hähnel, D., Burgard, W., and Thrun, S. (2003). Learning compact 3D models of indoor and outdoor environments with a mobile robot. *Robotics and Autonomous Systems*, **44**(1), 15–27.

Hähnel, D., Burgard, W., Fox, D., Fishkin, K., and Philipose, M. (2004). Mapping and localization with RFID technology. In *Proc. of 2004 IEEE Int. Conf. on Robotics and Automation (ICRA 2004)*, pages 1015–1020, USA. IEEE.

Hightower, J., Want, R., and Borriello, G. (2000). SpotON: An indoor 3D location sensing technology based on RF signal strength. Uw cse, University of Washington, Department of Computer Science and Engineering, Seattle, USA.

Hodges, S., Thorne, A., Mallinson, H., and Floerkemeier, C. (2007). Assessing and optimizing the range of UHF RFID to enable real-world pervasive computing applications. In A. LaMarca, M. Langheinrich, and K. Truong, editors, *Pervasive Computing*, volume 4480 of *Lecture Notes in Computer Science*, pages 280–297. Springer Berlin Heidelberg.

Hoffmann, J., Spranger, M., Ghring, D., and Jngel, M. (2005). Making use of what you dont see: Negative information in markov localization. In *Proc. of the 2005 IEEE/RSJ Int. Conf. of Intelligent Robots and Systems (IROS 2005)*, pages 2947–2952.

Hori, T., Wda, T., Ota, Y., Uchitomi, N., Mutsuura, K., and Okada, H. (2008). A multi-sensing-range method for position estimation of passive RFID tags. In *2008 IEEE International Conference on Wireless and Mobile Computing, Networking and Communications (WIMOB 2008)*, pages 208–213, Avignon, France.

Johansson, R. and Saffiotti, A. (2009). Navigating by stigmergy: A realization on an RFID floor for minimalistic robots. In *Proc. of the IEEE Int. Conf. on Robotics and Automation (ICRA)*, pages 245–252, Kobe, Japan.

Johnson, N. L., Kotz, S., and Balakrishnan, N. (1995). *Continuous Univariate Distributions*, volume 1. John Wiley & Sons, New York, NY.

Joho, D., Plagemann, C., and Burgard, W. (2009). Modeling RFID signal strength and tag detection for localization and mapping. In *Proc. of 2009 IEEE Int. Conf. on Robotics and Automation (ICRA 2009)*, pages 3160–3165, Kobe, Japan.

Julier, S. J. and Uhlmann, J. K. (1997). A new extension of the Kalman filter to nonlinear systems. *Int. symp. aerospace/defense sensing, simul. and controls*, **3**(26).

Kalman, R. E. (1960). A new approach to linear filtering and prediction problems. *Journal of Fluids Engineering*, **82**, 35–48.

Kämpke, T., Kluge, B., Prassler, E., and Strobel, M. (2008). Robot position estimation on a RFID-tagged smart floor. In C. Laugier and R. Siegwart, editors, *Field and Service Robotics*, volume 42 of *Springer Tracts in Advanced Robotics*, pages 201–211. Springer Berlin Heidelberg.

Kanda, T., Shiomi, M., Perrin, L., Nomura, T., Ishiguro, H., and Hagita, N. (2007). Analysis of people trajectories with ubiquitous sensors in a science museum. In *Proc. of 2007 IEEE Int. Conf. on Robotics and Automation (ICRA 2007)*, pages 4846–4853, Roma, Italy.

Kantor, G. A. and Singh, S. (2002). Preliminary results in range-only localization and mapping. In *Proceedings of the IEEE Conference on Robotics and Automation (ICRA 2002)*, pages 1818–1823, Washington, USA.

Karmakar, N. C. (2011). Handbook of smart antennas for RFID systems.

Kim, M., Kim, H., and Chong, N. (2007). Automated robot docking using direction sensing RFID. In *Proc. of the 2007 IEEE Int. Conf. on Robotics and Automation (ICRA 2007)*, pages 4588–4593, Italy.

Kjærgaard, M. B. (2007). A taxonomy for radio location fingerprinting. In *Location-and Context-Awareness*, pages 139–156. Springer Berlin Heidelberg.

Kleiner, A., Kleiner, E., Prediger, J., and Nebel, B. (2006). RFID technology-based exploration and SLAM for search and rescue. In *In Proc. of the IEEE/RSJ Int. Conf. on Intelligent Robots and Systems (IROS*, pages 4054–4059, Beijing, China.

Kleiner, A., Dornhege, C., and Dali, S. (2007). Mapping disaster areas jointly: RFID-coordinated SLAM by humans and robots. In *2007 IEEE International Workshop on Safety, Security, and Rescue Robotics (SSRR 2007)*, pages 1–6, Rome, Italy.

Kloos, G., Guivant, J., Nebot, E., and Masson, F. (2006). Range based localisation using RF and the application to mining safety. In *2006 IEEE/RSJ International Conference on Intelligent Robots and Systems*, pages 1304–1311, Beijing, China.

Kluge, B., Kohler, C., and Prassler, E. (2001). Fast and robust tracking of multiple moving objects with a laser range finder. In *Proc. of 2001 IEEE Int. Conf. on Robotics and Automation (ICRA 2001)*, pages 1683–1688, Seoul, Korea.

Koch, W. (2007). On exploiting negative sensor evidence for target tracking and sensor data fusion. *Information Fusion*, **8**(1), 28–39.

Kodaka, K., Niwa, H., Sakamoto, Y., Otake, M., Kanemori, Y., and Sugano, S. (2008). Pose estimation of a mobile robot on a lattice of RFID tags. In *2008 IEEE/RSJ International Conference on Intelligent Robots and Systems (IROS 2008)*, pages 1385–1390.

Koller, D. and Fratkina, R. (1998). Using learning for approximation in stochastic processes. In *In Proceedings of the 1998 International Conference on Machine Learning (ICML*, pages 287–295, Madison, Wisconsin, USA.

Kristan, M., Kovacic, S., Leonardis, A., and Pers, J. (2010). A two-stage dynamic model for visual tracking. *IEEE Transactions on Systems, Man, and Cybernetics, Part B: Cybernetics*, **40**(6), 1505–1520.

Kulyukin, V., Gharpure, C., Nicholson, J., and Pavithran, S. (2004). RFID in robot-assisted indoor navigation for the visually impaired. In *Proc. of the 2004 IEEE/RSJ Int. Conf. on Intelligent Robots and Systems (IROS 2004)*, pages 1979–1984.

Kulyukin, V., Gharpure, C., Nicholson, J., and Osborne, G. (2006). Robot-assisted wayfinding for the visually impaired in structured indoor environments. *Autonomous Robots*, **21**(1), 29–41.

Kwon, J. and Lee, K. M. (2010). Visual tracking decomposition. In *The Twenty-Third IEEE Conference on Computer Vision and Pattern Recognition (CVPR 2010)*, pages 1269–1276, San Francisco, CA, USA.

Ladd, A., Bekris, K., Rudys, A., Kavraki, L., and Wallach, D. (2005). Robotics-based location sensing using wireless ethernet. *Wireless Networks*, **11**(1-2), 189–204.

Lau, P.-Y., Yung, K.-O., and Yung, E.-N. (2008). A smart bookshelf for library RFID system. In *The 2008 Asia-Pacific Microwave Conference (APMC 2008)*, pages 1–4, Hong Kong, China.

Lee, S., Min, B.-C., Kim, D., Yoon, J., and Kim, D. (2013). Passive RFID positioning system using RF power control. In J.-H. Kim, E. T. Matson, H. Myung, and P. Xu, editors, *Robot Intelligence Technology and Applications 2012*, volume 208 of *Advances in Intelligent Systems and Computing*, pages 845–853. Springer Berlin Heidelberg.

Lehpamer, H. (2007). *RFID Design Principles*. Artech House, Inc., Norwood, MA, USA.

Lenser, S. and Veloso, M. (2000). Sensor resetting localization for poorly modelled mobile robots. In *Proc. of the 2000 IEEE Int. Conf. on Robotics and Automation (ICRA 2000*, pages 1225–1232, San Francisco, CA, USA.

Levis, C. A. (2001). *Friis Free-Space Transmission Formula*. John Wiley & Sons, Inc.

Lilienthal, A. J., Loutfi, A., and Duckett, T. (2006). Airborne chemical sensing with mobile robots. *Sensors*, **6**(11), 1616–1678.

Lim, A. and Zhang, K. (2006). A robust RFID-based method for precise indoor positioning. *Advances in Applied Artificial Intelligence*, pages 1189–1199.

Liu, J. and West, M. (2001). *Combined Parameter and State Estimation in Simulation-Based Filtering*. Statistics for Engineering and Information Science. Springer New York.

Liu, J. S. (1996). Metropolized independent sampling with comparisons to rejection sampling and importance sampling. *Statistics and Computing*, **6**, 113–119. 10.1007/BF00162521.

Liu, R. and Zell, A. (2014). Towards Localizing Both Static and Non-static RFID Tags with a Mobile Robot. In *International Conference on Intelligent Autonomous Systems (IAS-13)*, Padova, Italy.

Liu, R., Vorst, P., Koch, A., and Zell, A. (2011). Path following for indoor robots with RFID received signal strength. In *Proc. of the 19th Int. Conf. on Software, Telecommunications and Computer Networks (SoftCOM 2011)*, Croatia.

Liu, R., Koch, A., and Zell, A. (2012). Path following with passive UHF RFID received signal strength in unknown environments. In *Porc. of the 2012 IEEE/RSJ Int. Conf. on Intelligent Robots and Systems (IROS 2012)*, pages 2250–2255, Vilamoura, Algarve, Portugal.

Liu, R., Koch, A., and Zell, A. (2013). Mapping UHF RFID Tags with a Mobile Robot using 3D Sensor Model. In *IEEE/RSJ International Conference on Intelligent Robots and Systems (IROS 2013)*, pages 1589–1594, Big Sight, Tokyo, Japan.

Liu, R., Huskić, G., and Zell, A. (2014). Dynamic Objects Tracking with a Mobile Robot using Passive UHF RFID Tags. In *IEEE/RSJ International Conference on Intelligent Robots and Systems (IROS 2014)*, Chicago, Illinois, USA.

Liu, X., Corner, M. D., and Shenoy, P. (2006). Ferret: RFID localization for pervasive multimedia. In *Proc. of the 8th Int. Conf. on Ubiquitous Computing (UbiComp 2006)*, pages 422–440, Orange County, CA, USA.

Lu, F. and Milios, E. (1997). Robot pose estimation in unknown environments by matching 2D range scans. *Journal of Intelligent & Robotic Systems*, **18**(3), 249–275.

Maguire, Y. and Pappu, R. (2009). An Optimal Q-Algorithm for the ISO 18000-6C RFID Protocol. *IEEE Transactions on Automation Science and Engineering*, **6**(1), 16–24.

Mallinson, H., Hodges, S., and Thorne, A. (2006). Determining a better metric for RFID performance in environments with varying noise levels. In *12th IEEE International Conference on Methods and Models in Automation and Robotics (MMAR 2006)*, pages 39–48. Miedzyzdroje, Poland.

Medeiros, C., Costa, J., and Fernandes, C. (2008). RFID smart shelf with confined detection volume at UHF. *Antennas and Wireless Propagation Letters, IEEE*, **7**, 773–776.

Mehmood, M. A., Kulik, L., and Tanin, E. (2008). Autonomous navigation of mobile agents using RFID-enabled space partitions. In *Proceedings of the 16th ACM SIGSPATIAL International Conference on Advances in Geographic Information Systems*, GIS '08, pages 1–21.

Mekonnen, A. A., Lerasle, F., and Herbulot, A. (2013). Cooperative passers-by tracking with a mobile robot and external cameras. *Comput. Vis. Image Underst.*, **117**(10), 1229–1244.

Miah, M. S. and Gueaieb, W. (2013). Mobile robot trajectory tracking using noisy RSS measurements: An RFID approach. *ISA Transactions: The Journal of Automation, Elsevier*.

Milella, A., Cicirelli, G., and Distante, A. (2008). RFID-assisted mobile robot system for mapping and surveillance of indoor environments. *Industrial Robot: An International Journal*, **35**(3), 143–152.

Milella, A., Di Paola, D., Cicirelli, G., and D'Orazio, T. (2009). RFID tag bearing estimation for mobile robot localization. In *Proc. of the 2009 International Conference on Advanced Robotics (ICAR 2009)*, pages 1–6, Munich, Germany.

Miller, T., Stolfo, D., and Spletzer, J. (2010). An automated asset locating system (AALS) with applications to inventory management. In A. Howard, K. Iagnemma, and A. Kelly, editors, *Field and Service Robotics*, volume 62 of *Springer Tracts in Advanced Robotics*, pages 163–172. Springer Berlin Heidelberg.

Montemerlo, M., Roy, N., and Thrun, S. (2003). Perspectives on standardization in mobile robot programming: The carnegie mellon navigation (CARMEN) toolkit. In *In Proc. of the IEEE/RSJ Int. Conf. on Intelligent Robots and Systems (IROS*, pages 2436–2441, Las Vegas, Nevada, USA.

Moore, A. W., Schneider, J., and Deng, K. (1997). Efficient locally weighted polynomial regression predictions. In *In Proceedings of the 1997 International Machine Learning Conference (ICML)*, pages 236–244, Nashville, Tennessee, USA.

Mountney, P., Stoyanov, D., and Yang, G.-Z. (2010). Three-dimensional tissue deformation recovery and tracking: Introducing techniques based on laparoscopic or endoscopic images. *IEEE Signal Processing Magazine*, **27**(4), 14–24.

Nemmaluri, A., Corner, M. D., and Shenoy, P. (2008). Sherlock: Automatically locating objects for humans. In *Proceedings of the 6th International Conference on Mobile Systems, Applications, and Services*, MobiSys '08, pages 187–198, New York, NY, USA. ACM.

Ni, L., Liu, Y., Lau, Y. C., and Patil, A. (2003). LANDMARC: indoor location sensing using active RFID. In *Proc. of the 2003 IEEE Int. Conf. on Pervasive Computing and Communications (PerCom 2003)*, pages 407–415, USA.

Ota, Y., Hori, T., Onishi, T., Wada, T., Mutsuura, K., and Okada, H. (2008). An adaptive likelihood distribution algorithm for the localization of passive RFID tags. *IEICE Transactions A: IEICE Transactions on Fundamentals of Electronics, Communications and Computer Sciences*, **E91-A**(7), 1666–1675.

Otsason, V., Varshavsky, A., LaMarca, A., and De Lara, E. (2005). Accurate GSM indoor localization. *UbiComp 2005: Ubiquitous Computing*, pages 141–158.

Park, S. and Hashimoto, S. (2009). An approach for mobile robot navigation under randomly distributed passive RFID environment. In *2009 IEEE International Conference on Mechatronics (ICM 2009)*, pages 1–6.

Patil, A., Munson, J., Wood, D., and Cole, A. (2005). BlueBot: asset tracking via robotic location crawling. In *Pervasive Services, 2005. ICPS '05. Proceedings. International Conference on*, pages 117–126.

Pitt, M. K. and Shephard, N. (1999). Filtering via simulation: Auxiliary particle filters. *Journal of the American Statistical Association*, **94**(446), 590–599.

Ramadurai, V. and Sichitiu, M. L. (2003). Localization in wireless sensor networks: A probabilistic approach.

Raoui, Y., Goller, M., Devy, M., Kerscher, T., Zollner, J.-M., Dillmann, R., and Coustou, A. (2009). RFID-based topological and metrical self-localization in a structured environment. In *International Conference on Advanced Robotics (ICAR 2009)*, pages 1–6, Munich, Germany.

Roewekaemper, J., Sprunk, C., Tipaldi, G., Stachniss, C., Pfaff, P., and Burgard, W. (2012). On the position accuracy of mobile robot localization based on particle filters combined with scan matching. In *Proc. of the IEEE/RSJ International Conference on Intelligent Robots and Systems (IROS)*.

Rohweder, K., Vorst, P., and Zell, A. (2009). Improved mapping of RFID tags by fusion with spatial structure. In *Proc. of the 4th European Conf. on Mobile Robots (ECMR 2009)*, pages 247–252, Mlini/Dubrovnik, Croatia.

Roy, N. and Thrun, S. (1999). Online self-calibration for mobile robots. In *the 1999 IEEE International Conference on Robotics and Automation (ICRA 1999)*, pages 2292–2297, Detroit, Michigan.

Russell, S. J. and Norvig, P. (2003). *Artificial Intelligence: A Modern Approach*. Pearson Education, 2 edition.

Schairer, T., Weiss, C., Vorst, P., Sommer, J., Hoene, C., Rosenstiel, W., Straer, W., Zell, A., Carle, G., Schneider, P., and Weisbecker, A. (2008). Integrated scenario for machine-aided inventory using ambient sensors. In *4th European Workshop on RFID Systems and Technologies (RFID SysTech 2008)*, number 209 in ITG-Fachbericht, Freiburg, Germany. VDE Verlag.

Schmid, J., Beutler, F., Noack, B., Hanebeck, U., and Mller-Glaser, K. (2011). An experimental evaluation of position estimation methods for person localization in wireless sensor networks. In P. Marrn and K. Whitehouse, editors, *Wireless Sensor Networks*, volume 6567 of *Lecture Notes in Computer Science*, pages 147–162. Springer-Verlag, Berlin Heidelberg.

Schneegans, S., Vorst, P., and Zell, A. (2007). Using RFID snapshots for mobile robot self-localization. In *Proceedings of the 3rd European Conference on Mobile Robots (ECMR 2007)*, pages 241–246, Freiburg, Germany.

Schulz, D., Fox, D., and Hightower, J. (2003). People tracking with anonymous and ID-sensors using Rao-Blackwellised particle filters. In *Proceedings of the 18th International Joint Conference on Artificial Intelligence (IJCAI 2003)*, pages 921–926, San Francisco, CA, USA. Morgan Kaufmann Publishers Inc.

Schwaighofer, A., Grigoras, M., Tresp, V., and Hoffmann, C. (2004). GPPS: A Gaussian process positioning system for cellular networks. In *IN NIPS*. MIT Press.

Seco, F., Plagemann, C., Jimenez, A., and Burgard, W. (2010). Improving RFID-based indoor positioning accuracy using Gaussian processes. In *Indoor Positioning and Indoor Navigation (IPIN), 2010 International Conference on*, pages 1–8, Zurich, Switzerland.

Senta, Y., Kimuro, Y., Takarabe, S., and Hasegawa, T. (2010). Self-localization for mobile robots using RFID tags without layout information. *Electrical Engineering in Japan*, **172**(4), 19–30.

Shirehjini, A., Yassine, A., and Shirmohammadi, S. (2012). Equipment location in hospitals using RFID-based positioning system. *Information Technology in Biomedicine, IEEE Transactions on*, **16**(6), 1058–1069.

Sprunk, C., Roewekaemper, J., Parent, G., Spinello, L., Tipaldi, G., Burgard, W., and Jalobeanu, M. (2014). An experimental protocol for benchmarking robotic indoor navigation. In *Proc. of the International Symposium on Experimental Robotics (ISER)*, Marrakech/Essaouira, Morocco.

Stachniss, C., Grisetti, G., and Burgard, W. (2005). Information gain-based exploration using Rao-Blackwellized particle filters. In *Proc. of Robotics: Science and Systems (RSS)*, pages 65–72, Cambridge, MA, USA.

Surmann, H., Nüchter, A., and Hertzberg, J. (2003). An autonomous mobile robot with a 3D laser range finder for 3D exploration and digitalization of indoor environments. *Robotics and Autonomous Systems*, **45**(3), 181–198.

Tang, L. and Yuta, S. (2002). Indoor navigation for mobile robots using memorized omni-directional images and robot's motion. In *Proc. of the 2002 IEEE/RSJ Int. Conf. on Intelligent Robots and Systems (IROS 2002)*, pages 269–274, Switzerland.

Thrun, S. (2003). Exploring artificial intelligence in the new millennium. chapter Robotic Mapping: A Survey, pages 1–35. Morgan Kaufmann Publishers Inc., San Francisco, CA, USA.

Thrun, S., Fox, D., and Burgard, W. (2000). Monte Carlo localization with mixture proposal distribution. In *Proc. of the 17th National Conf. on Artificial Intelligence (AAAI-2000)*, pages 859–865, Austin, Texas. MIT Press.

Thrun, S., Burgard, W., and Fox, D. (2005). *Probabilistic Robotics (Intelligent Robotics and Autonomous Agents)*. The MIT Press.

Ulrich, I. and Borenstein, J. (1998). VFH+: reliable obstacle avoidance for fast mobile robots. In *Proc. of the 1998 IEEE Int. Conf. on Robotics and Automation (ICRA 1998)*, pages 1572–1577, Leuven, Belgium.

Vorst, P. (2011). *Mapping, Localization, and Trajectory Estimation with Mobile Robots Using Long-Range Passive RFID*. Ph.D. thesis, University of Tübingen, Tübingen, Germany.

Vorst, P. and Zell, A. (2008). Semi-autonomous learning of an RFID sensor model for mobile robot self-localization. In *European Robotics Symposium 2008*, volume 44/2008 of *Springer Tracts in Advanced Robotics*, pages 273–282. Springer Berlin/Heidelberg.

Vorst, P. and Zell, A. (2009). Particle filter-based trajectory estimation with passive UHF RFID fingerprints in unknown environments. In *Proc. of the 2009 IEEE/RSJ Int. Conf. on Intelligent Robots and Systems (IROS 2009)*, pages 395–401, USA.

Vorst, P. and Zell, A. (2010a). A comparison of similarity measures for localization with passive RFID fingerprints. In *Proc. of the joint Conf. of 41st Int. Symposium on Robotics and 6th German Conf. on Robotics*, pages 354–361, Munich, Germany.

Vorst, P. and Zell, A. (2010b). Fully autonomous trajectory estimation with long-range passive RFID. In *2010 IEEE International Conference on Robotics and Automation (ICRA)*, pages 1867–1872, Anchorage, Alaska, USA. IEEE.

Vorst, P., Sommer, J., Hoene, C., Schneider, P., Weiss, C., Schairer, T., Rosenstiel, W., Zell, A., and Carle, G. (2008a). Indoor positioning via three different RF technologies. In *4th European Workshop on RFID Systems and Technologies (RFID SysTech 2008)*, number 209 in ITG-Fachbericht, Freiburg, Germany. VDE Verlag.

Vorst, P., Schneegans, S., Yang, B., and Zell, A. (2008b). Self-localization with RFID snapshots in densely tagged environments. In *Proc. of the 2008 IEEE/RSJ Int. Conf. on Intelligent Robots and Systems (IROS 2008)*, pages 1353–1358, Nice, France.

Vorst, P., Yang, B., and Zell, A. (2009). Loop closure and trajectory estimation with long-range passive RFID in densely tagged environments. In *14th International Conference on Advanced Robotics (ICAR 2009)*, pages 1–6, Munich, Germany.

Vorst, P., Koch, A., and Zell, A. (2011). Efficient self-adjusting, similarity-based location fingerprinting with passive UHF RFID. In *Proc. of IEEE Int. Conf. on RFID-Technology and Applications (RFID-TA 2011)*, pages 160–167, Spain.

Wan, E. and Van der Merwe, R. (2000). The unscented Kalman filter for nonlinear estimation. In *IEEE Symposium on Adaptive Systems for Signal Processing, Communication and Control*, Lake Louise, Alberta, Canada.

Want, R. (2006). An introduction to RFID technology. *IEEE Pervasive Computing*, **5**(1), 25–33.

Weis, S. A. (2007). RFID (radio frequency identification): principles and applications.

Welch, G. and Bishop, G. (1995). An introduction to the Kalman filter. Technical report, Chapel Hill, NC, USA.

Whitehouse, K., Karlof, C., and Culler, D. (2006). A practical evaluation of radio signal strength for ranging-based localization. *ACM Mobile Computing and Communications Review (MC2R), Special Issue on Localization Technologies and Algorithms*.

Yilmaz, A., Javed, O., and Shah, M. (2006). Object tracking: A survey. *ACM Comput. Surv.*, **38**(4).

Youssef, M., Agrawala, A., and Udaya Shankar, A. (2003). WLAN location determination via clustering and probability distributions. In *Proc. of the IEEE Int. Conf. on Pervasive Computing and Communications (PerCom 2003)*, pages 143–150, USA.

Zhang, Y., Amin, M. G., and Kaushik, S. (2007). Localization and tracking of passive RFID tags based on direction estimation. *International Journal of Antennas and Propagation*, **2007**, 1–9.